Lawrence Berkeley National Laboratory

Title
VIBRATIONAL RELAXATION OF MATRIX ISOLATED CH3F AND HC1

Permalink
https://escholarship.org/uc/item/1dv5q4q8

Author
Young, L.

Publication Date
1981-08-01

Peer reviewed

Lawrence Berkeley Laboratory
UNIVERSITY OF CALIFORNIA

Materials & Molecular Research Division

MA. TER

VIBRATIONAL RELAXATION OF MATRIX-ISOLATED CH_3F AND HCl

Linda Young
(Ph.D. thesis)

August 1981

LBL--13440

DE82 007768

VIBRATIONAL RELAXATION OF MATRIX-ISOLATED CH$_3$F AND HCl

Linda Young

Ph.D. Thesis

August 1981

Materials and Molecular Research Division
Lawrence Berkeley Laboratory
University of California
Berkeley, CA 94720

VIBRATIONAL RELAXATION OF MATRIX ISOLATED
CH_3F AND HCL

Linda Young

Abstract

Kinetic and spectroscopic studies have been performed
on CH_3F and HCl as a function of host matrix and tempera-
ture. Temporally and spectrally resolved infrared fluore-
scence was used to monitor the populations of both the
initially excited state and the lower lying levels which
participate in the relaxation process.

For CH_3F, relaxation from any of the levels near 3.5 μ,
i.e. the CH stretching fundamentals or bend overtones, occurs
via rapid (<5 ns) V → V transfer to $2v_3$ with subsequent
relaxation of the v_3 (CF stretch) manifold. Lifetimes
of $2v_3$ and v_3 were determined through overtone, $\Delta v=2$,
and fundamental fluorescence. These lifetimes show a dra-
matic dependence on host lattice, an increase of two orders
of magnitude in going from Xe to Ar matices. Lifetimes
depend only weakly on temperature. The relaxation of $2v_3$
and v_3 is consistent with a model in which production
of a highly rotationally excited guest via collisions with
the repulsive wall of the host is the rate limiting step.

For HCl, lifetimes of $v=1,2,3$ have been determined.
In all hosts, the relaxation is non-radiative. For a given
vibrational state, v, the relaxation rate increases in the
series $k(Ar)<k(Kr)<k(Xe)$. The dependence of the relaxation

rate on v is superlinear in all matrices, the deviation from linearity increasing in the order Ar<Kr<Xe. The relaxation rates become more strongly temperature dependent with increasing vibrational excitation. The results are consistent with a mechanism in which complex formation introduces the anisotropy necessary to induce a near resonant V → R transition in the rate limiting step.

Dedicated to my parents

ACKNOWLEDGEMENTS

I have profitted greatly from studying under the
guidance of Brad Moore. His attitude of conducting
research aimed at solving a fundamental question, rather
than being a "wandering apparatus in search of a prob-
lem", is one which I will carry away. In addition, I
hope to inherit his unique ability to clearly and imme-
diately grasp the relevant factors in any given problem.

Regarding experimental techniques, special credit
goes to Jay Wiesenfeld, Andy Kung, Jim Chao and Michael
Diegelmann for skillful instruction in matrix isolation
techniques, lasers, microcomputers and electronics,
respectively. Floyd Hovis, Hai-lung Dai, Alison Abbate
and Chi-ke Cheng have loyally fought on my side against
malfunctioning equipment. In addition, the help of the
Strauss group and Heinz Frei in FTIR moving/alignment is
gratefully acknowledged.

Despite claims to the contrary, thesis writing need
not be, and in my case, was not, an agonizing chore. For
this I must thank the entire Moore group, whose support
I will recall long after memories of sleepless nights
have faded. In particular, I am grateful for the help
of Wes Natzle and Joan Frisoli, both of whom almost
seemed willing to write the dissertation. I will also
always remember Jackie Denney's much needed encourage-
ment at seemingly bleak moments. Perhaps most important
was the constant long range source of motivation and

inspiration provided by Steve Sibener.

Finally, I would like to thank my parents for their continual faith and support in my endeavors.

TABLE OF CONTENTS

INTRODUCTION

With the advent of tunable narrow band sources the
prospect of mode selective excitation and subsequent reac-
ti n has become more than just an experimentalist's dream.
Studies of the influence of vibrational excitation on re-
actions occuring on the ground potential surface are
generally free from complications due to near lying elec-
tronic states. When carried out in a cryogenic environment,
translational and rotational excitation can be made negli-
gible with respect to vibrational excitation. Thus, the
relative efficiencies of various types of vibrational ex-
citation can be readily evaluated. However, attempts at
infrared laser induced chemistry in matrices have met with
only a modicum of success. Turner et.al. report isomeri-
zation of $Fe(CO)_4$, induced by one vibrational quantum in
a CO ligand, to be not only isotopically and sterec se-
lective, but also site and orientationally selective (1-3).
A recent study by Frei et.al. of $NO \cdot O_3$ pairs in matrices
shows excitation of NO causes reaction whereas that of the
ν_3 mode of O_3 does not, despite the fact that both exci-
tation frequencies exceed the accepted gas phase activation
energy (4). However, numerous other systems have been
tested by Turner with a singular lack of success. A better
understanding of the competition between reaction and
relaxation is needed in order to be able to design reaction

systems with reasonable chances of success.

With this in mind, these studies are aimed at elucidat-
ing the fundamental processes involved in the dissipation
of vibrational energy of small molecules isolated in inert
gas matrices. Systematic studies of non-radiative relaxa-
tion in matrix isolated molecules have begun fairly re-
cently, leading to qualitative correlations between guest/
host properties and the relative propensities of the various
decay channels (5,6). The vibrational energy of a matrix
isolated molecule may be lost in a variety of ways, namely:
1) The molecular vibration may be directly coupled to the
lattice, leading to the creation of many bulk phonons upon
loss of a vibrational quantum. 2) The vibrational energy
may decay into modes localized at the guest site, i.e. guest
rotation or translation. 3) The vibrational quantum may
be resonantly transferred by long range dipole-dipole coup-
ling to another guest. 4) The vibrational energy may be
non-resonantly transferred to a chemically different guest
species. 5) Polyatomic molecules may lose vibrational
energy by intramolecular V-V processes. 6) The molecular
vibrations may decay radiatively. All of the above pro-
cesses have been observed (5).

For isolated diatomics the following trends are begin-
ning to emerge. First, low moment of inertia hydrides tend
to relax their vibrational energy by coupling initially to
a localized rotational motion of the guest. Therefore,
vibrationally excited molecules such as HCl (7), NH (8,9),

OH (10) and their deuterated analogs, predominantly decay by
production of a highly rotationally excited species in the
next lower v level. On the other hand, the relative impor-
tance of the rotational channel is reduced in heavy molecules
with large moments of inertia and closely spaced rotational
levels. Thus, the molecules $S_2(B^3\Sigma^-)$ (6) and $C_2^-(B^3\Sigma^-)$ (11)
relax their vibrational energy via a multiphonon mechanism,
involving either bulk or local phonons.

    In polyatomics, the situation is more complex due
to the added decay channels of intramolecular V-V transfer.
Studies of the lowest lying vibrational levels of CH_3F and
CD_3F (13,14) show that their behavior is similar to that of
diatomics. That is, relaxation is thought to proceed through
high rotational levels of these low moment of inertia guests.
However intramolecular V-V processes are still poorly under-
stood. Intermode V-V transfer is much less efficient in ClCF
(12) than CNN and NCO (13,14). The different behavior is
attributed to the Fermi resonance between the bending over-
tones and stretching fundamentals of CNN and NCO. Due to the
lack of data on polyatomics propensity rules can only be
suggested on the basis of gas phase V → V transfer data.

    Even after the deactivation pathway for a particular
guest-host system is determined, the fundamental question
remains of what forces are responsible for relaxation.
Indeed, an isolated small molecule cannot decay non-
radiatively, thus relaxation is a sensitive function of
the guest-host interaction potential, although empirically

determined correlations neglect this (5) and concentrate on isolated guest and host properties. Similarly, the observed spectroscopic shift from gas phase is extremely sensitive to this potential. An interesting question is whether or not forces determined spectroscopically can be used to predict relaxation behavior. In other words, is the potential sampled spectroscopically that responsible for relaxation as is commonly assumed in theoretical treatments (15-18). A useful test of this is the variation of host for a particular guest molecule.

In this thesis, experiments determining the vibrational relaxation mechanisms for the ground electronic states of CH_3F and HCl isolated in inert gas matrices will be described. Chapter II is a brief description of experimental techniques; Chapter III kinetic and spectroscopic results for CH_3F in Ar, Kr and Xe; and Chapter IV, kinetics and spectroscopy of HCl, $v=1,2,3$ in Ar, Kr and Xe matrices.

REFERENCES

1. B. Davies, A. McNeish, M. Poliakoff and J. J. Turner, J. Am. Chem. Soc. 99, 7573 (1977).

2. B. Davies, A. McNeish, M. Poliakoff, M. Tranquille and J. J. Turner, Chem. Phys. Lett. 52, 477 (1977).

3. M. Poliakoff, N. Breedon, B. Davies, A. McNeish and J. J. Turner, Chem. Phys. Lett. 56, 474 (1978).

4. H. Frei, L. Fredin, G. C. Pimentel, J. Chem. Phys. 74, 397 (1981).

5. F. Legay in Chemical and Biological Applications of Lasers, Vol. II, Academic Press, New York (1977).

6. V. Bondybey in Photoselective Chemistry, Part II, John Wiley & Sons Inc., New York (1981).

7. J. M. Wiesenfeld and C. B. Moore, J. Chem. Phys. 70, 930 (1979).

8. L. E. Brus and V. E. Bondybey, J. Chem. Phys. 63, 794, (1975).

9. V. E. Bondybey and J. H. English, J. Chem. Phys. 73, 87, (1980)

10. L. E. Brus and V. E. Bondybey, J. Chem. Phys. 63, 786, (1975).

11. V. E. Bondybey and L. E. Brus, J. Chem. Phys. 63, 2223, (1975).

12. V. E. Bondybey, J. Chem. Phys. 66, 4237 (1977).

13. V. E. Bondybey and J. H. English, J. Chem. Phys. 67, 664 (1977).

14. V. E. Bondybey and J. H. English, J. Chem. Phys. 67, 2868 (1977).

15. K. B. Freed and H. Metiu, Chem. Phys. Lett. 48, 262, (1977).

16. M. Berkowitz and R. B. Gerber, Chem. Phys. 37, 369(1979).

17. D. J. Diestler, E. W. Knapp and H. D. Ladouceur, J. Chem. Phys. 68, 4056 (1978).

18. D. J. Diestler and H. D. Ladouceur, Chem. Phys. Lett. 70, 287 (1980).

CHAPTER II

EXPERIMENTAL

A. Matrix preparation

Matrices were prepared by deposition of high pressure pulses (50-150 torr, 12 cm^3, 4/min) of a premixed gaseous sample onto a target mounted in an Air Products Inc. Model CSA 202 closed cycle helium refrigerator. The spray-on orifice consists of 1/4 in. OD stainless steel tubing terminated 3/4 in. from the target. The uniformity of the matrices is strongly dependent on the temperature of the target during deposition. Too high a temperature results in poor isolation, whereas too low a temperature yields matrices which are highly scattering. For Ar, Kr and Xe hosts, the deposition temperatures used were 9, 20 and 25 K respectively. The target temperature could be raised from a minimum temperature of ca. 9 K to 300 K by increasing the effective heat load. This was accomplished by passing DC current through a nichrome wire wrapped around the copper block into which the target holder was screwed. The temperature was monitored by a KP vs. Au 0.07 at% Fe thermocouple sandwiched between the target and its holder. The thermocouple was referenced to an ice-water bath and the output read on a microvoltmeter. Temperature stability ranged from ±0.3 K at the lowest temperature to ±0.1 K at 40 K. An equilibration time of 20 minutes at the deposition temperature was found to be necessary to prevent "crown" formation due to a thermal gradient between the

center and edges of the substrate causing a preferential
accumulation at the cooler substrate edges for the heavier
gases.

The gases used were HCl (Matheson Electronic Grade,
>99.99%), CH_3F (Matheson >99.0%), Ar (Matheson Ultra-high
Purity, >99.9995%), Kr (Airco, >99.995%), Xe (Airco,
>99.995%). HCl and CH_3F were purified by fractional dis-
tillation from 135 K (isopentane/n-pentane slush) to 77 K.
Kr and Xe were subjected to two freeze-pump-thaw cycles
before use. Pressures were measured using a mercury
triple McLeod gauge and mercury manometer to better than
two percent. Matrix concentrations were assumed to be
identical to those of the gaseous mixture, as sticking
coefficients for the components are estimated to be unity.
A more detailed description of the gas handling system,
cryostat and temperature controlling apparatus can be
found in Ref. 1.

The purity, hence suitability for relaxation experi-
ments, of each matrix was determined by infrared absorption
spectroscopy using either a Nicolet 7199 FTIR or, in ear-
lier experiments, a Beckman IR-12. The major contaminant
is air, which is readily identified by strong H_2O or
H_2O-HCl absorptions. Typically, the deposition was inter-
rupted once to take a preliminary spectrum of the sample
to determine whether or not continued deposition was
worthwhile.

B. Spectroscopy

High resolution spectroscopy of the fundamental and
first overtone regions of HCl and $CH_3F/Ar,Kr,Xe$ is now
routinely possible using a Nicclet 7199 FTIR. It is
necessary to suspend the cryostat and its interconnecting
hoses independently of the optics bench of the FTIR in
order to prevent disturbance of the travel of the moving
mirror by cryostat vibration. Such coupling leads to an
erroneous and noisy spectrum. A detailed description of
the principles and operating procedures can be found in
Ref. 2.

Various detector, beamsplitter and source combinations
can be used to optimize S/N in a given spectral region. For
the $4000-400$ cm^{-1} region, the most commonly used combination
was a HgCdTe detector, KBr beamsplitter and Globar source.
In the $6000 - 3200$ cm^{-1} region an InAs detector, KBr beam-
splitter and tungsten halogen source were used. This com-
bination was found to be optimal for observing the 5600 cm^{-1}
region of the first overtone of HCl, both in terms of S/N
and ease of interchangeability with mid-IR optics.

C. Fluorescence

1. Excitation Sources

a) $1.4 - 4.0$ μ

For absorption frequencies between 1.4 and 4.0 μ, the
angle-tuned Nd:YAG-pumped optical parametric oscillator was
used as the excitation source. The 1.06 μ pump beam was
produced by a Raytheon SS404 Nd:YAG oscillator-amplifier

system. This system is described in detail elsewhere (3).
Design details of the optical parametric oscillator can be
found in Ref. 4. The theory of optical parametric oscilla-
tion is described in a number of review articles (5,6).

There is a problem with optical damage occuring on the
output face of the $LiNbO_3$ crystal. Since the damage thres-
hold of $LiNbO_3$ is roughly 200 MW/cm^2 ($2J/cm^2/10ns$), the
spatial mode quality of the pump beam is of crucial impor
tance. Hot spots in the beam which do not exceed the da-
mage threshold will nevertheless increase walk-off effects
in the phase matching process, leading to decreased con-
version efficiency. The 1.06 μ spatial mode can be quan-
titatively observed using a conventional closed circuit
TV camera (Hitachi CCTV, HV-62U) equipped with a 10 mm
extender. The camera is focussed on a dispersing screen,
i.e. a ground glass slide, located approximately two inches
away, upon which a small fraction of the pump beam is in-
cident. The output of the camera is in horizontal raster
scan format (525 lines/frame, 15.75 KHz sweep) such that
the vertical profile is viewed on an oscilloscope as the
envelope of the individual horizontal profiles. The hori-
zontal profile is readily observed with an appropriate
trigger delay and time scale. In practice this is only
necessary after complete realignment of the Nj:YAG pump
system. Routinely, the spatial mode of the 1.06 μ pump
is observed either as a burn spot on photographic paper or
in the visible after doubling in Type I KDP. Continuous,

damage-free operation is possible at pump energies up to 180 mJ/pulse when the 1.06 μ pump beam is of good quality and the crystal is free of surface and bulk defects. Typical operating parameters are shown in Table I and Fig. 1.

b) 1.2 μ sources

The initial source of 1.2 μ radiation consisted of a second $LiNbO_3$ crystal used to double the output idler beam from the OPO. The vertically polarized signal (1.9 μ) and idler (2.4 μ) beams were focussed by a 25 cm quartz lens placed 20 cm from the OPO output coupler into the second $LiNbO_3$ crystal, located 30 cm from the lens. Rotation of the z axis about a horizontal lab axis brings the second crystal in to the phase matching condition, $n_e(2\omega)(\theta_m)$ = $n_o(\omega)$. The 1.2 μ output can be monitored visually with the aid of an IR phosphor card. Directly after the doubling $LiNbO_3$ crystal a KDP crystal was placed to act as a filter for the unwanted radiation (2.4 μ, 1.9 μ). Using KDP as a filter had 'the added advantage of doubling the desired 1.2 μ output 0.6 μ, thus facilitating further alignment. Typical operating parameters were OPO output (1.9+2.4 μ) = 10-25 mJ/pulse, 1.2 μ output = 0.4-1.0 mJ/pulse, 1.2 μ linewidth (with etalon in OPO cavity) = 0.5 cm^{-1}.

A more powerful source of 1.2 μ was ultimately used for most of the experiments. The output of a Quanta-Ray Model DCR Nd:YAG laser, HG-1 Harmonic Generator and PDL-1 pulsed dye laser was used to stimulate Raman shifted emission from a high pressure gas. The theory of stimulated

Raman scattering is well documented in Refs. 6,7 and 8. The high pressure gas cell was 1 m in length, fitted with 1/2 in thick x 1 in diameter suprasil windows, a 0-1500 psi pressure gauge and standard Hoke valves. Focussing of the pulsed dye laser output to the center of the Raman cell using a 50 cm quartz lens can produce usable output up to the fifth antistokes and down to the third stokes line. The focussing geometry and pressure of the scattering medium can be varied to optimize the output of the forward scattered wavelength of interest. In general, higher pressures are found to enhance the first stokes output in accordance with the equation for gain

$$g_S = \frac{4 \; \lambda_S^2 N \; (d\sigma/d\Omega) \; I_p}{n_S \; \hbar \; \omega_p \; \Delta\omega_R} \tag{1}$$

$$P_S(l) = P_S(0) \; \exp(g_S l) \tag{2}$$

where N = population density of scatterer (e.g. H_2)
    $\Delta\omega_R$ = FWHM Raman linewidth
    $d\sigma/d\Omega$ = spontaneous Raman cross section
    λ_S = stokes wavelength
    l = length
    I_p = pump intensity.

    At high intensities of the first stokes line, a four wave mixing process generates radiation at the second stokes and first anti-stokes frequencies, which act as sources for the generation of higher order stokes and anti-stokes lines. In practice, the desired output at the second stokes frequency howed a monatonic increase to an upper pressure of 425 psi. A further increase of pressure tended to decrease

the higher order anti-stokes output due to the increased
dispersion at the higher frequencies. Again, spatial mode
quality of the input beam was of crucial importance as the
threshold defined as the gain required to achieve an output
power at the Stokes field comparable to the pump input can
be quite high. For SRS initiated from the initial sponta-
neous Raman noise level, $P_s(0) \simeq h\nu_s \approx 10^{-10}$ W, in the
visible, the gain required to reach 1 MW is $g_s l$
= $\ln(P_s(1)/P_s(0))$ = $\ln(10^6/10^{-10})$ = 36. For l = 100 cm,
g_s/I = 1.5 cm/GW (H_2 Q(1) @ λ_p = 514.5 nm) this implies
I_p = 240 MW/cm^2. Focussable energy therefore is the key
ingredient for efficient conversion. Typically, Rhodamine
640 is pumped with 200 mJ of 532 nm to give 50 mJ @ 600 nm
with a linewidth of <1.0 cm^{-1}. This in turn yields 2-3
mJ of output at the second stokes line in H_2 at 400 psi,
measured after a Corning filter 7-56 (70% T @ 1.2 μ).
The frequency profile of the second stokes output was
measured on a 3/4 m SPEX monochromator and is shown in
Fig. 1.

2. Detectors

The theory and operation of photoconductive infrared detectors has been amply discussed elsewhere (9,10,11). Hg:Ge and Cu:Ge detectors were used for the HCl and CH_3F experiments, respectively. As these two experiments probed vastly different time regimes and spectral regions, the post detector electronics and pre-detector spectral filters were matched accordingly.

The conditions under which the two detectors were operated are summarized in Table II. Post-detection electronics were modified to ensure that electronic distortion of the signal was minimized. The preamp circuit used to impedance match the detector, essentially a high output impedance current source, to the 50 Ω input impedance wideband amplifier is shown in Fig. 2. The high and low frequency responses of this circuit can be determined by varying the parameters R_1, C_c and R_p. They are given by

$$\tau_{high} = (C_s + C_d) \times (R_L \parallel R_d \parallel R_p) \tag{3}$$

$$\tau_{low} = C_c (R_L \parallel R_d + R_p) \tag{4}$$

Note that R_L and R_p can be interchanged with no effect on the high frequency response of the system. Also note that with this interchange, the low frequency response can still be set arbitrarily by varying C_c.

The high frequency response of the detectors was determined by scattering 3.5 μ OPO radiation (FWHM 8 ns) onto the

detector element. The resulting waveforms were digitized and analyzed using a Tektronix 7912AD transient digitizer and LSI-11 microcomputer, as shown in Fig. 3. It was of interest to operate the Cu:Ge detector used in the CH_3F studies at the highest speed possible. Though doped germanium detectors have been reported to have intrinsic recombination times of less than 2.2 ns (12), this particular element exhibited an intrinsic response of 15 ns. This was determined by fitting the tail of the deconvolved response to a single exponential decay. Deconvolution of the detector response from the input signal to yield the impulse response was done by standard Fourier transform techniques.

$$x(t) \rightarrow h(t) \rightarrow y(t) \qquad (5)$$

$$X(\omega)H(\omega) = Y(\omega) \qquad (6)$$

$$h(t) = \int_0^\infty \exp(i\omega t) \ H(\omega) \ d\omega \qquad (7)$$

where (t) = input signal
    h(t) = impulse response, calculated from Eqns.(6)
          and (7)
    y(t) = output signal

The results for a 511 Ω load are shown in Fig. 4. The expontial tail does not change appreciably upon deconvolution although the pulse width is decreased by 15%. Digital high frequency filtering is responsible for the finite rise and oscillatory behavior of the deconvolved response. Decreasing the filtering leads to an extremely noisy deconvolved response which limits the usefulness of the technique.

Decreasing the load to 50 Ω had no effect, implying that the intrinsic recombination time of electron-hole pairs had been reached.

The low frequency time constants of the systems were measured by chopping a heat lamp at ca. 5 Hz and observing the decay from the initial sharp rise of a square wave. The results were 2 ms and 50 ms for the Cu:Ge and Hg:Ge detectors, respectively.

Undisorted transmission to the 50 Ω input impedance wideband amplifier (RMS noise = 60 μV, 10cps-100 mega-cycles referred to input) is possible by matching the output impedance of the LH0033 (output noise = 180 μV rms, $I_{out} \gtrsim$ 6 Ω) to 50 Ω using the 13 Ω resistor in series after the output as shown in Fig. 2. This drops the effective signal by almost a factor of 2, hence should be used only under conditions of high S/N.

D. Experimental Set Up

1. Vibrational relaxation

The overall experimental set up is shown in Fig. 5. The excitation sources, described in the previous section, were focussed to a diameter of roughly 8 mm at the matrix. f/1 focussing of the fluorescence onto the 3x10 mm detector element gives a collection efficiency of roughly 1%. Samples were excited on either the front or rear surface. In general, the rear surface excitation geometry facilitated alignment, but had the undesirable effect of attenuating emission at optically thick fundamental frequencies. This

can be quite serious when both the excited and emitting
states are strongly absorbing.

Signal averaging was necessary to enhance the single
shot S/N. Data acquisition was performed on one of two
systems: (1) Biomation 8100 transient digitizer + Northern
575 Signal Analyzer (10ns - 10s channel, maximum sensiti-
vity 100 mv/8 bits), (2) Tektronix 7912AD ÷ LSI-11 micro-
computer (9.8 ps - 19.5 μs/channel, 100 mv/9 bits).

2. Fluorescence Excitation Spectroscopy

Fluorescence excitation spectra of the matrix isolated
species were taken by monitoring the fluorescence intensity
while scanning the excitation frequency. For low resolution
(ca. 0.5 cm^{-1}) experiments involving the Quanta Ray PDL-1,
stepping the grating suffices to tune the dye, and hence the
Raman-shifted, output. This is done under computer control
as is averaging of the broadband fluorescence signal on the
7912AD. Interfacing details can be found in Ref. 13. The
scanning program can be found in App. I. The general ar-
chitecture of the program follows. First a reference trace
is acquired and stored. After setting the grating at the
starting wavelength, a suitable number of shots is averaged
(ca. 64), the reference trace subtracted, the resultant
waveform integrated and the integral stored in memory
before stepping to the next wavelength. Upon completion
of the scan the spectrum can be stored on floppy disc.

E. Data Analysis

Fluorescence traces were analyzed by computer as the sum of exponentials by least squares fit of a theoretical function to the experimental data. Data acquired on the Biomation/Northern 575 or 575A systems were transferred to the floppy via magnetic tape, using the programs included in App. I. It should be noted that both the data output rate and format differ for the Northern 575 (9600 baud) and 575A (2400 baud) ⌐   ⁻ ⁻ ⁻ ⁻ ⁻ ⁻⁻⁻⁻⁻ ⁻ ⁻   ⁻⁻⁻⁻ ⁻⁻ ⁻⁻⁻ program CTXFER.FOR.

The fitting method is quite general and can be used on any functional form. Details and a sample program are given in App. II.

REFERENCES

1. J.M. Wiesenfeld, Thesis, University of California, Berkeley (1977).

2. Technical Manual, Nicolet 7199 FTIR

3. M. Zughul, Thesis, University of California, Berkeley (1978).

4. H.L. Dai, Thesis, University of California, Berkeley (1981).

5. R. Byer and R.L. Herbst, Non-linear Infrared Generation, edited by Y.R. Shen (Springer-Verlag New York, 1977).

6. A. Yariv, Quantum Electronics (J. Wiley & Sons, New York, 1975).

7. N. Bloembergen, American Journal of Physics 35, 989 (1967).

8. J. Paisner, R.S. Hargrove "Tunable Coherent UV to Near IR Generation using High Order Stimulated Raman Scattering".

9. P. Kruse, Optical and Infrared Detectors, edited by R.J. Keyes (Springer-Verlag New York, 1980).

10. J. Finzi, Thesis, University of California, Berkeley (1972).

11. F. Arams, Infrared-to-Millimeter Wavelength Detectors, (Artech House, Inc. Dedham, MA, 1973).

12. J. T. Yardley, C.B. Moore, Appl. Phys Lett. 7, 311 (1965).

13. Quanta-Ray PDL Manual.

TABLE I. Typical operating parameters for Nd:YAG pumped OPO

1.06 μ characteristics

    Energy   120-150 mJ/pulse

    Linewidth 0.1 cm^{-1}

    Pulse duration (FWHM)   ~ 15 ns

    Diameter at input   ~ 4 mm

    Energy density   120 MW/cm^2

    Divergence   1 mrad

OPO output characteristics

    Signal Energy   8 mJ

    Idler Energy (w/o etalon)   1.5 mJ

    Idler linewidth (FWHM)

        grating only 2.0 cm^{-1}

        grating + etalon 0.2 cm^{-1}

    Pulse duration (FWHM)   8 ns

    Divergence   10 mrad

TABLE II. Typical operating parameters for IR detectors

|	3x10 mm Cu:Ge	3x10 mm Hg:Ge
Bias	-45 V	-45 V
R_L	28.9 kΩ (511 Ω)	12 kΩ
SCNC	2.5×10^{-12} amp/√hz	7.3×10^{-12} amp/√hz
	$Q \sim 10^{18}$ $sec^{-1}cm^{-2}$ (0-16 μ,BaF_2)	$Q \sim 1.2 \times 10^{16}$ (3-5 μ filter)
τ_{high}	150 ns (15ns)	75 ns
τ_{low}	2 ms	50 ms
C_c	0.02 μF	0.56 μF
$B=1/2\pi\tau$	1.06 MHz (10.6MHz)	2.1 MHz
T_{op}	4 K	4 K

$SCNC = N_D/[R_L(\pi B/2)^{1/2}]$
  N_D = detector noise
  B = upper 3db frequency

Q = background flux in photons/sec cm^2.

Fig. 1: (a) Frequency profile of OPO with grating in
             cavity.
         (b) Frequency profile of OPO with grating and
             etalon (1 mm quartz, finesse = 7) in
             cavity.
         (c) Frequency profile of Raman shifted dye.

         All determined on 3/4 m SPEX monochromator with
         0.1 cm^{-1} resolution, PbSe or PbS detector.

22
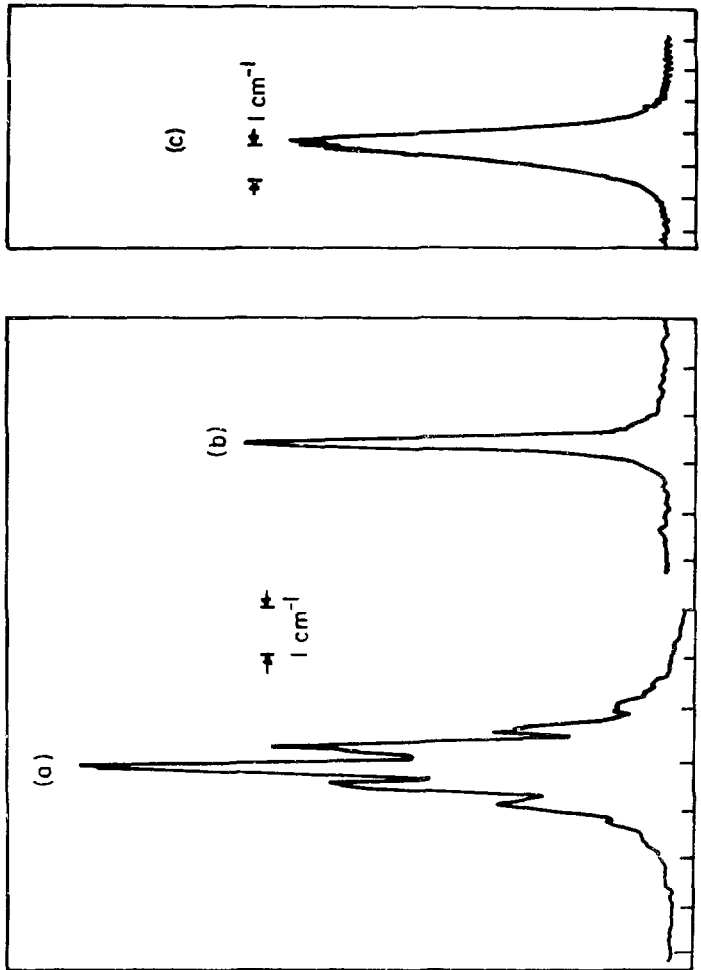
XBL 817-10767

Fig. 2: Preamp circuit used in Cu:Ge detector.
Capacitances in µF unless specified.
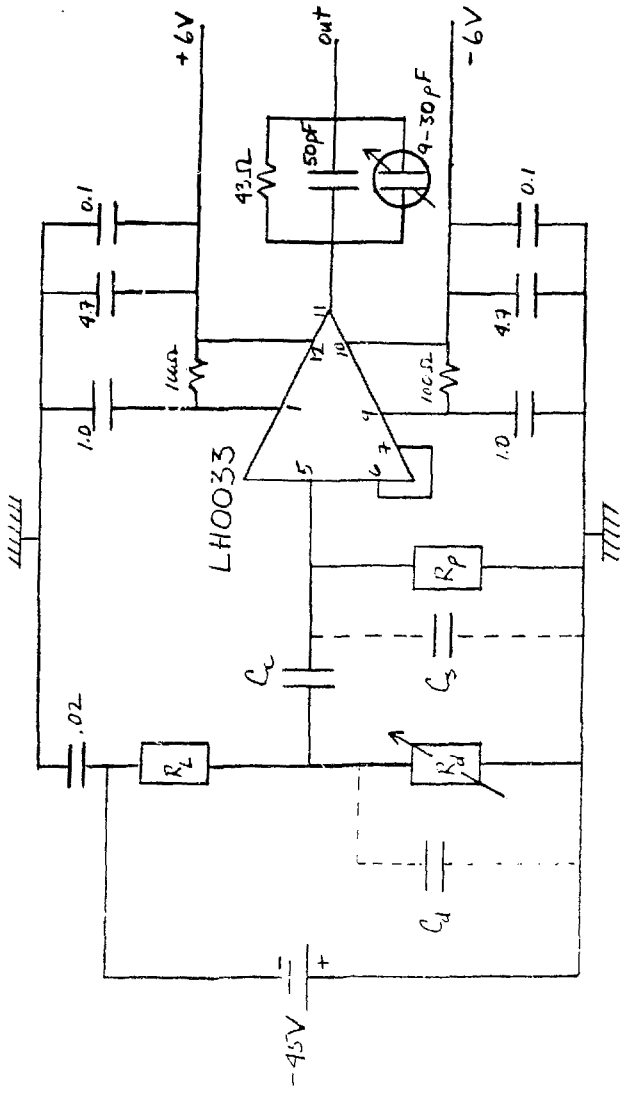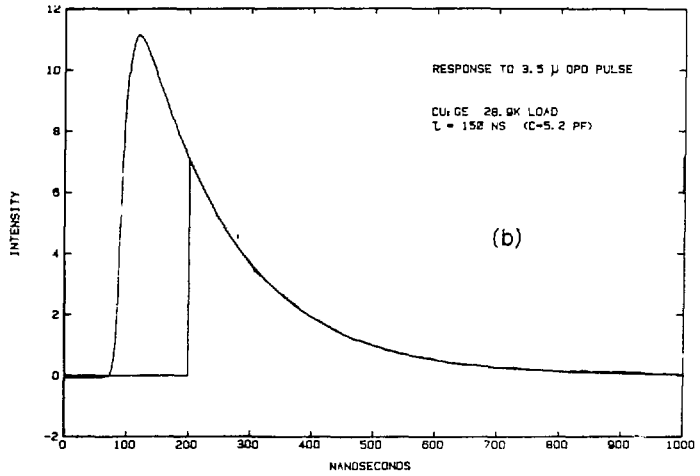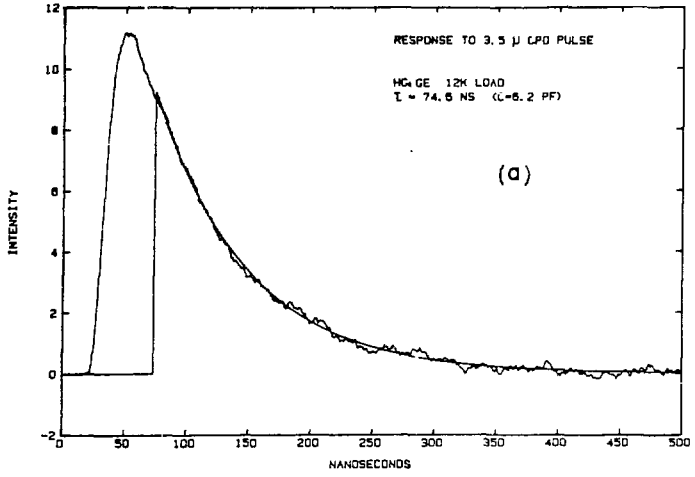Dotted lines indicate inherent or stray
capacitances.

Fig. 3: (a) High frequency time constant of Hg:Ge detector.
         (b) High frequency time constant of Cu:Ge detector.

RESPONSE TO 3.5 μ CPO PULSE

HG: GE   12K LOAD
$\Upsilon = 74.6$ NS   (C=6.2 PF)

(a)

NANOSECONDS

RESPONSE TO 3.5 μ OPO PULSE

CU: GE   28.9K LOAD
$\Upsilon = 150$ NS   (C=5.2 PF)

(b)

NANOSECONDS

Fig. 4: (a) Temporal profile of 3.5 μ OPO pulse = x(t).
        (b) Response to 3.5 μ OPO pulse of Cu:Ge detector
            with 511 Ω load = y(t).
        (c) Deconvolved response to 3.5 μ OPO pulse = h(t).
        (d) Response to 3.5 μ OPO pulse, Cu:Ge detector,
            50 Ω load, τ = 15 ns.
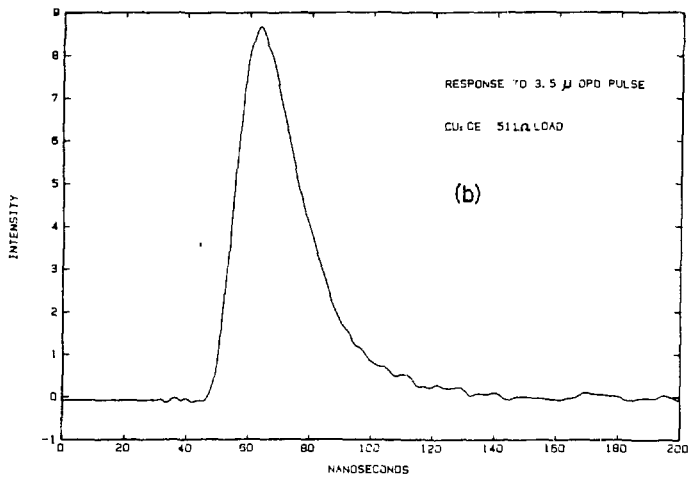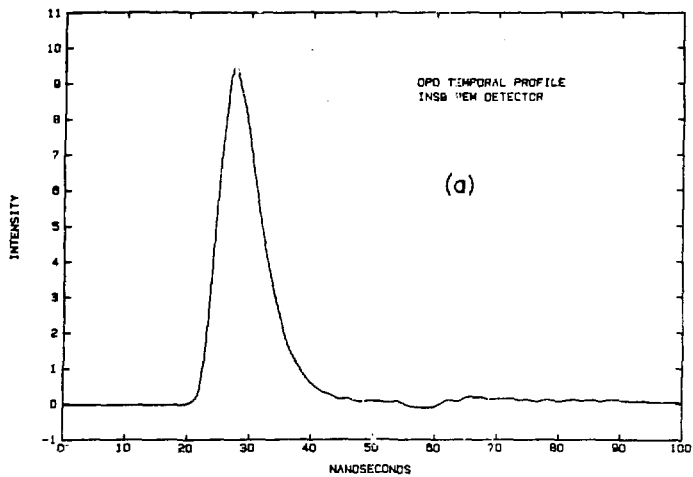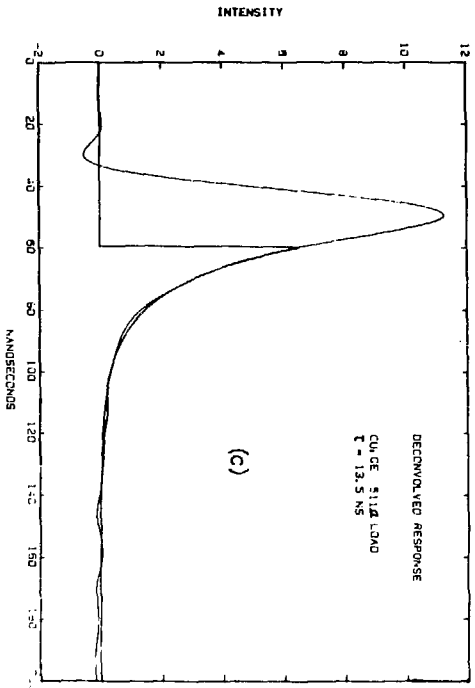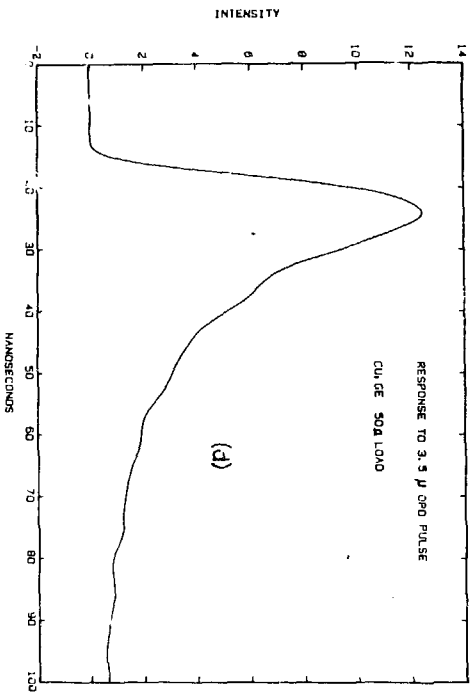
OPD TEMPORAL PROFILE
INSB PEM DETECTOR

(a)

INTENSITY

NANOSECONDS

RESPONSE TO 3.5 μ OPD PULSE

CU₊CE 511Ω LOAD

(b)

INTENSITY

NANOSECONDS

INTENSITY

RESPONSE TO 3.5 μ OPO PULSE

CU, GE 50Ω LOAD

(d)

NANOSECONDS

INTENSITY

DECONVOLVED RESPONSE

CU, GE 50Ω LOAD
τ = 13.5 NS

(c)

NANOSECONDS

Fig. 5:   General experimental schematic shown for front
          surface excitation. An interference filter
          (@ 77 K) is located inside the detector dewar
          to spectrally resolve the fluorescence.

FLUORESCENCE RECORDER

Ge:Cu 4°K

LENS

X100

TRANSIENT RECORDER

SIGNAL AVERAGER

CASSETTE

M

HELIUM REFRIGERATOR 9–40 K

COMPUTER TERMINAL

LENS

M

ω_i

FILTER

ω_s, ω_i

ANGLE TUNED LiNbO$_3$ PARAMETRIC OSCILLATOR

ω_p

Nd:YAG LASER
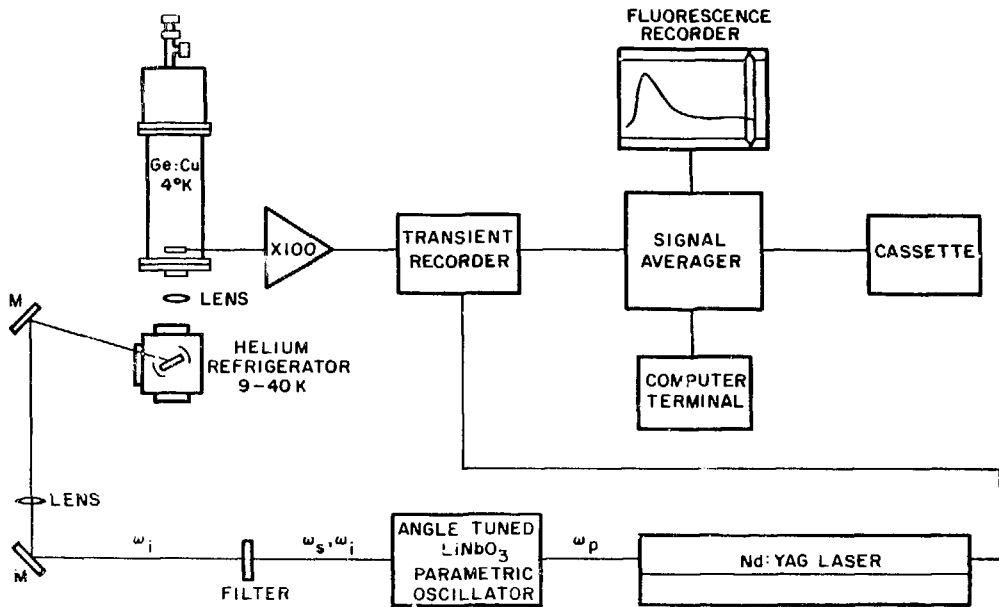
XBL 817-10759

CHAPTER III

Vibrational Relaxation of CH_3F in
Ar, Kr, Xe Matrices

I. INTRODUCTION

Recent studies are leading to a qualitative under-
standing of the factors governing the mechanism of vibra-
tional relaxation of diatomics isolated in monatomic hosts.
Isolated diatomic molecules may dissipate vibrational
energy either directly to the host lattice, by simulta-
neous emission of many bulk phonons, or indirectly, via
a local mode with subsequent relaxation to lattice modes.
The dominant channel of non-radiative relaxation appears to
be the one of lowest order, i.e. that requiring the smallest
quantum number change. Hence, low moment of inertia hy-
drides, e.g. HCl (1), NH (2), appear to relax via localized
rotational modes, whereas heavy diatomics O_2 (3), C_2^- (4),
probably relax via local phonon modes.

Relatively little is known about the mechanisms of
vibrational relaxation of matrix isolated polyatomics,
where the additional channels of intramolecular V-V transfer
are present. Most studies to date have been conducted
on electronically excited species by observation of vibra-
tionally unrelaxed emission. Inefficient mode-to-mode vi-
brational energy transfer is observed in the ClCF radical/Ar
system (5), in which the bend and high frequency stretch
decay independently by a multiphonon process. On the other
hand, extremely efficient intramolecular V-V processes

dominate the vibrational relaxation within the electronic-
ally excited states of matrix isolated CNN (6) and NCO (7),
such that deactivation of the high frequency stretch pro-
ceeds via energy transfer to the bending mode. The drastic-
ally different behavior can be explained by allowing efficient
cient energy transfer between levels known to be in Fermi
resonance, as are the bending overtones and stretching
fundamentals of CNN and NCO.

Even less is known about intramolecular V-V energy
transfer in the ground electronic state. The only reported
study is that of Abouaf-Marguin et.al. (8) where efficient
intramolecular V-V transfer (<1.6 μsec) from the ν_3
(CF stretch) to the ν_6 (deformation) was observed in
$^{12}CD_3F$ and $^{13}CD_3F$. This is attributed to the weak Coriolis
coupling between the two states and the modest exothermicity
of the process. The corresponding process in CH_3F is endo-
thermic and therefore not observed.

Existing data are still too sparse to be able to
generalize. Outstanding questions in polyatomic relaxation
are 1) the relative importance of inter vs. intramolecular
forces during the various stages in the relaxation process,
2) the role of symmetry in intramolecular vibrational relax-
ation, 3) the comparison to relaxation rates in other media,
i.e. liquid and gas phase.

CH_3F is a particularly useful molecule to study with
regard to these questions. The first question is addressed
by systematic study of V-V and V-R,P rates as a function of

host lattice. Secondly, initial population of symmetric(A_1)
and antisymmetric(E) CH stretches and deformation overtones
($2\nu_2, 2\nu_5$) can be accomplished with a tunable infra-
red source in the 3.5 μ region. Many lower lying levels
are infrared active, thus a mapping of the deactivation
path is possible by the observation of vibrational fluore-
scence. Finally, the deactivation of the lowest lying
fundamental, ν_3, has been studied in liquid solution
as well as in the matrix.

II. EXPERIMENTAL

A. Matrix preparation

Matrices were prepared by deposition of high pressure pulses (50-150 torr, 12 cm^3, 4 per min) of a premixed gaseous sample onto a CsI target mounted in an Air Products Inc. Model CSA 202 closed cycle helium refrigerator. The spray-on orifice consisted of 1/4 in. OD stainless steel tubing terminated 3/4 in. from the target. The deposition temperatures for Ar, Kr, and Xe hosts were 9, 20 and 25 K respectively. The temperature of the target could be raised from a minimum temperature of ca. 9 K to 300 K by increasing the effective heat load through resistive heating of a nichrome wire wrapped around the copper block in which the target holder was screwed. The temperature was monitored by a KP vs. Au 0.07 at% Fe thermocouple sandwiched between the CsI target and its holder. Temperature stability ranged from ±0.3 K at the lowest temperature to ±0.1 K at 40 K.

The gases used were CH$_3$F (Matheson, >99.0%), Ar (Matheson Ultra-high Purity >99.995%), Kr (Airco, >99.995%), and Xe (Airco, >99.995%). Kr and Xe were subjected to two freeze-pump-thaw cycles before use. CH$_3$F was purified by fractional distillation from 138 K to 77 K. Pressures were measured using a mercury triple McLeod gauge and mercury manometer to better than 2%. Matrix concentrations were assumed to be identical to those of the gaseous mixture. Absorption spectra of each matrix were taken with a Nicolet 7199 FTIR in order to determine quantitatively the optical

densities for absorbing and emitting transitions.

B. Fluorescence Experiments

The excitation source used in these experiments was a Nd:YAG pumped optical parametric oscillator. The typical pump pulse, produced by a Raytheon SS404 Nd:YAG oscillator amplifier system was 120-150 mJ at 1.06 μ, 15 ns (FWHM), 0.1 cm^{-1} bandwidth, 1 mrad divergence. Typical output characteristics of the $LiNbO_3$ parametric oscillator near 3 μ were 1.5 mJ idler energy, 2.0 cm^{-1} FWHM idler linewidth (w/o etalon), 0.2 cm^{-1} FWHM (w/etalon), 8 ns (FWHM), 10 mrad divergence.

A photoconductive Cu:Ge detector was used to monitor infrared fluorescence in these experiments. Changing the external load resistor during the course of the experiment allowed the two complementary configurations: fast response, low sensitivity and slow response, high sensitivity, to be attained without time consuming realignment. The high frequency time constant of each configuration was measured as the response to 3.5 μ OPO radiation (FWHM = 8 ns). The values obtained were 15 ns and 150 ns for the fast and slow configurations, respectively. The low frequency cut off, measured by chopping a heat lamp and observing the deviation from a square wave, was 2 ms. Cooled interference filters (77 K) were located inside the detector dewar in order to eliminate the maximum amount of 300 K background radiation. Broadband fluorescence at 9.6 μ was isolated with a set of two filters having a combined average transmission of 70%,

center frequency at 980 cm^{-1}, 10% points at 1132 cm^{-1} and 850 cm^{-1}. Overtone fluorescence at 4.8 µ was isolated using a set of three filters with a combined average transmission of 59%, center frequency at 2120 cm^{-1}, 10% points of 2030 cm^{-1} and 2220 cm^{-1} (48% transmitting at 2064 cm^{-1} CH_3F/Ar ($2\nu_3 \leftarrow 0$)). Observation of 6.8 µ fluorescence through a combination of filters and LiF flats yielded ca. 20% transmission at the ($2\nu_{2,5} \leftarrow \nu_{2,5}$) and ($\nu_{2,5} \leftarrow 0$) transition frequencies.

A schematic of the experimental set up is shown in Fig. 1. The infrared beam was collimated with a single 2 m quartz lens to a spot size of ca. 1 cm at the sample. A 5 cm f/1 NaCl lens focussed the fluorescence onto the 3x10 mm detector element. Both front (Fig. 1) and rear surface excitation geometries were used in experiments. During rear surface excitation, the infrared beam is directed straight through the sample at the detector. The fluorescenc signal was averaged at 10 Hz on a Tektronix 7912AD transient digitizer interfaced to a LSI-11/03 microcomputer. The resultant signals were analyzed by computer as either single or double exponential decays. Uncertainties in single exponential fits were ± 5% leading to an overall scatter in data of ±10%. Distortion of the signal due to the finite bandwidth of the amplifiers is at most 5%.

III. RESULTS AND ANALYSIS

A. Spectroscopy

The spectroscopy of CH_3F in Ar matrices (10) and of the v_3 region of CH_3F in Kr (11) has been previously reported. Dimeric bands were identified by diffusion and concentration experiments, in agreement with previous studies (10). The centers of all observable monomeric bands as a function of host are shown in Table I. A representative spectrum is shown in Fig. 2. The linewidths of the various bands are dependent on the symmetry of the normal mode, as can be seen in the figure and Table II, where integrated absorbances and linewidths are shown for each of the bands. The problems in assigning absolute absorption intensities to matrix isolated species are twofold. First, the magnitude of the transitio dipole moment of aggregates relative to monomer is generally unknown, thus absolute concentration measurements are not accurate for matrices in which polymer formation is substantial. Next, more dilute matrices suffer from problems in measuring thickness using the interference method, as surfaces parallel to an infrared wavelength are difficult to obtain for thick samples. Moreover, the density of the matrix is dependent upon the deposition temperature (17), leading to a possible systematic error in concentration measurements. The absolute intensity values shown in Table II are subject to these errors. Since the monomer and dimer contributions to overall band intensity overlap in some cases and not in others, matrices of high M/A are

required to obtain accurate relative intensities. The
relative intensities for a dilute matrix, M/A=4940, nor-
malized to the $B_{obs}(\nu_3)$ of Barrow and McKean, are
therefore also shown. The relative intensities of the
"monomer" absorption bands are subject only to errors in
baseline determination and the presence of <2% dimer. The
data appear nominally consistent with that of the gas phase,
but a more reliable set of gas phase cross sections is
needed in order to determine whether or not transition
dipole moments change between gas and matrix.

The contours of the parallel and perpendicular bands
are roughly those expected for a cooled gas phase molecule.
The parallel bands ($\Delta J=0$, $\Delta K=\pm 1$) exhibit a strong
Q-branch with weak shoulders to the red and blue. A rota-
tional envelope for a perpendicular transition of CH_3F
($\Delta K=\pm 1, \Delta J=0, \pm 1$) in the gas phase at 9 K is ca. $5cm^{-1}$
FWHM, very similar to the observed 5.2 cm^{-1} of the $\nu_4(E)$
vibration in Ar. Therefore it is suggested that the broad
linewidth of the bands of E symmetry is due to unresolved
rotational structure. The m-sub level degeneracy is lifted
by the crystalline field of the lattice and the vibrational
degeneracy by Coriolis coupling. These two factors, combined
with line broadening by host-guest interaction serve to
obscure the rotational structure predicted for a cooled gas
phase molecule. Similar observations have been made in and
interpretation applied to the ammonia chlorine complex (12).

B. Intramolecular V-V Transfer

In Fig. 3, the energy level diagram of CH_3F is shown. The four accessible bands in the 3.5 μ region: ν_4, ν_1, $2\nu_2$, $2\nu_5$ are of varying symmetry, (Table I). However, excitation of any of these levels leads to identical relaxation behavior. Fluorescence is observed only from the ν_3 manifold, both as fundamental and first overtone emission. Using the 150 ns configuration, no emission was observed from the ν_2, ν_5 or ν_6 manifolds after averaging 640 shots. The same number of shots produced S/N of 30 for $2\nu_3$ emission for which the Einstein A coefficient is 0.25 times that of the $\nu_{2,5} \rightarrow 0$ transition and 3.4 times that of ν_6. This null result implies that either relaxation does not occur through these modes or that the product of relaxation time and fraction of energy relaxing through $\nu_{2,5}$ is less than 2.5 ns, and through ν_6 less than 17 ns.

The rate of energy transfer to the ν_3 manifold is monitored by the risetime of the 9.6 μ fluorescence. This is in all cases, Ar, Kr, and Xe hosts at 9 K, similar to the time constant of the detection apparatus, 15 ns, as is shown in Fig. 4. Thus for all matrices $\tau_{V-V} < 5$ ns.

C. Deactivation of the ν_3 manifold

The decay of emission from the ν_3 manifold was monitored with the slow high sensitivity detector configuration. Overtone fluorescence ($2\nu_3 \rightarrow 0$, 4.8 μ) in all samples decayed as a single exponential, as shown in Fig. 5a. However, fundamental (9.6 μ) fluorescence decayed as a

double exponential, as seen in Fig. 5b. In the analysis,
it is assumed that the two components of the decay are due
to the transitions $2\nu_3 \rightarrow \nu_3$ and $\nu_3 \rightarrow 0$. Thus,
the rate of the fast component of the signal is fixed by
the $2\nu_3$ lifetime measured from the overtone fluorescence
signal.

Excitation on the front surface of the matrix yielded
rates identical to those obtained for excitation on the
rear surface. The ratio of the amplitude of the fast to
that of the slow component of the broadband decay, A_f/A_s,
decreased upon switching from back to front surface excita-
tion. This would be expected since optical attenuation
of $\nu_3 \rightarrow 0$ emission during passage through the matrix
would occur to a greater extent in the rear surface excita-
tion geometry, where the matrix itself serves as a filter
of $1 \rightarrow 0$ emission.

D. Host dependence of the deactivation rates

In Fig. 6 the dependence of the ν_3 and $2\nu_3$
lifetimes on host lattice is shown. The rates, plotted
as a function of the gas-matrix vibrational frequency shift,
increase almost two orders of magnitude when going from Xe
to Ar. This shows that the forces causing relaxation are
correlated to those at the potential minimum.

E. Temperature dependence of relaxation rates

In Fig. 7 the temperature dependence of the $2\nu_3$ de-
activation rate is shown for the various matrices. The

absence of a dramatic dependence on temperature suggests that the relaxation does not proceed via a multiphonon mechanism (18). In $\Gamma.g.$ 8 the temperature dependence of the v_3 relaxation rate is shown. The trends observed for $2v_3$ are also observed for v_3.
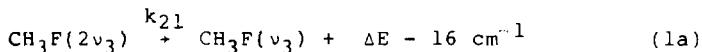
F. Concentration dependence of relaxation rates

In Fig. 9 the concentration dependence of the lifetimes of $2v_3$ and v_3 is shown for CH_3F in Ar. The v_3 lifetime is seen to increase by a factor of 2 when M/A increases from 1000 to 9750, whereas the $2v_3$ lifetime remains constant within experimental error.
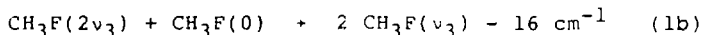
IV. DISCUSSION

The important features of CH_3F isolated molecule vibrational relaxation are as follows: 1) Relaxation from any of the levels, ν_4, ν_1, $2\nu_2$ or $2\nu_5$, proceeds through rapid energy transfer to the ν_3 manifold. 2) There is a small increase of ν_3 relaxation rate as a function of temperature. 3) There is a dramatic effect of host lattice on the relaxation rates of ν_3 and $2\nu_3$. 4) CD_3F relaxes an order of magnitude more slowly than CH_3F.

The observed fluorescence decays show that $2\nu_3$ decays by

$$CH_3F(2\nu_3) \overset{k_{21}}{\rightarrow} CH_3F(\nu_3) + \Delta E - 16 \text{ cm}^{-1} \qquad (1a)$$

$$\text{and/or}$$

$$CH_3F(2\nu_3) + CH_3F(0) \rightarrow 2 CH_3F(\nu_3) - 16 \text{ cm}^{-1} \qquad (1b)$$

The relaxation is completed by

$$CH_3F(\nu_3) \overset{k_{10}}{\rightarrow} CH_3F(0) + \Delta E \qquad (2)$$
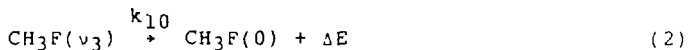
where $\Delta E = \nu_3/c = 1040 \text{ cm}^{-1}$ in Ar.

A. Mechanism of isolated molecule relaxation

After initial population of one of the 3.5 μ modes, energy may be transferred to any of a number of lower lying levels, as seen in Fig. 3. Endothermic processes are extremely improbable relative to exothermic ones; rates of one phonon endothermic processes being proportional to

$\Pi(\omega) = [\exp(-\hbar\omega/kT)/(1-\exp(-\hbar\omega/kT))]$ compared to $1+\Pi(\omega)$ for exothermic one phonon processes. A transition to $3\nu_3$ is in all cases endothermic; the endothermicity ranges from ca. 50 cm^{-1} for ν_4 excitation to ca. 200 cm^{-1} for 2ν excitation. Thus the observed transfer into the ν_3 manifold must occur via the $2\nu_3$ level. The fluorescence signal at 4.8 μ is due solely to the decay of the 2 ; level and is described by

$$S_2 = gA_{20}N_O \exp(-k_{21}t). \tag{3}$$

The broadband fluorescence observed at 9.6 μ is the sum of $(2\nu_3 \to \nu_3)$ and $(\nu_3 \to 0)$ emission. The broadband signal is then

$$S_{b} = gN_O \{ [A_{21} - \delta\xi A_{10}k_{21}/(k_{21}-k_{10})]\exp(-k_{21}t)$$
$$+ \delta\xi A_{10}k_{21}/(k_{21}-k_{10})\exp(-k_{10}t) \} \tag{4}$$

where $\quad$ = geometrical factor,

$\quad$ = optical density factor (varying from 0 to 1 as the sample goes from opaque to transparent)

$\quad$ = V-V equilibration parameter (varying from 1 to 2 as the percentage of molecules decaying by Process (1a) goes from 100% to 0%)

A_{20}, A_{10}, A_{21} = Einstein A coefficients for $2 \to 0$, $1 \to 0$ and $2 \to 1$ transitions, respectively.

$\cdots k_{21} - k_{10} \cdots$ duct $\delta\xi$ which can be evaluated from measured rate and amplitude ratios

$$\delta\xi = [2/(A_f/A_s-1)] \, x \, (1-k_{10}/k_{21}). \tag{5}$$

For the rear surface excitation geometry δ can be evaluated for the particular mode excited using a simple one dimensional model in which non-uniform excitation and emission according to Beer's Law is taken into account

$$\delta = \frac{\int_0^1 N_0 \, \exp(-\gamma_{ex}(1-x)) \, x \, \exp(-\gamma_{em}x' \, dx}{\int_0^1 N_0 \, \exp(-\gamma_{ex}x) \, dx} \tag{6}$$

where γ_{ex}, γ_{em} are defined by Beer's Law, $I/I_0 = \exp(-\gamma l)$. Observed values for a broadband signal resulting from rear surface excitation of the ν_4 mode of CH_3F in Ar are $k_{10}=3.2\times10^{-5} \, s^{-1}$, $k_{21}=1.30\times10^{-6} \, s^{-1}$ and $A_f/A_s = 6.5 \pm 1.5$. These numbers yield a value for $\delta\xi=0.27 \pm 0.1$. From the absorption spectrum, the value of δ is determined from the emitting ν_3 band of this particular matrix to be 0.26. This implies that $\xi=1 \pm 0.4$ and that (1a) is dominant, i.e. that endothermic intermolecular V-V processes are not very probable. The lack of a dramatic concentration dependence of $\tau(2\nu_3)$ further supports a relaxation mechanism in which intermolecular V-V processes are unimportant in the deactivation of $2\nu_3$. In addition, if (1b) were dominant one would expect a similar temperature dependence for k_{21} in all hosts since the endothermicity of

the V-V prccess is essentially equal for Ar, Kr and Xe ($\Delta E \sim 16$ cm^{-1}). However, this is not observed, the variation of rate with temperature being much greater in Xe than in Ar. Furthermore, the predicted temperature dependence of an endothermic 16 cm^{-1} process, $\Gamma \propto \Pi(\omega)$, is much much greater than that observed for any host. The values reported in Table III are isolated molecule relaxation rates for v_3 and v_3.

The v_3 lifet.mes are in good agreement with those of Abouaf-Marquin anu Gauthier-Roy (8) and with the less direct measurements of A$_i$ karian and Weitz (9). In the latter study strong pumping of v_3 v=0 $\rightarrow$ 1 led to population of higher levels within the $_3$ manifold via exothermic intermolecular V-V processe . Overtone emission near 5 μ was observed from molecules situated such that V-V transfer is faster than κ_{10}. 1 such a V $\rightarrow$ V coupled system CH$_3$F($2v_3$) should, and did, re.ax at a rate equal to $2k_{10}$ since its concentration is proportional to the square of the CH$_3$F(v_3) concentration (9). ince $2v_3$ is populated before v_3 in the present study, the reported relaxation rates probe a vastly different popu ation distribution within the $_3$ manifold, i.e. one in which CH$_3$F($2v_3$) is isolated with respect to resona t V $\rightarrow$ V transfer to CH$_3$F($_3$).

B. Temperature dependence

A mechanism in which rotation is the dominant accepting mode, with the excess energy being absorbed by bulk modes, has been proposed to explain the deactivation of the v_3 level(8). In this model, the vibrational energy is converted to the maximum amount of rotational energy consistent with exothermicity requirements. To minimize the quantum number change for CH_3F, rotation about the symmetry axis is assumed. For CH_3F this corresponds to a final rotational quantum number of J=14. Perturbations of this level by the matrix are expected to be small as an analysis of the v_3 parallel band has shown that the barrier to rotation about the symmetry axis is quite small in all hosts (8,21). The temperature dependence of the relaxation rate can then be primarily attributed to the emission rate of one or two phonons at the mismatch frequency. The calculated temperature dependence of a process which requires the emission of one bulk phonon of frequency ω is (1)

$$\Gamma \propto [\bar{n}(\omega) + 1].$$ (7)

The calculated dependence of rate on temperature, normalized to 9 K, is shown in Fig. 7 for various phonon frequencies. The temperature variation in rates can be fit quite well with processes requiring the emission of one bulk phonon. The phonon frequency required to fit the temperature dependence systematically decreases in the series Ar, Kr, Xe as does the magnitude of the $2v_3 \rightarrow v_3$ transition frequency

The trend is also present in the ν_3 relaxation rates. It is not possible to correlate the absolute magnitude of the phonon frequency which best fits the observed temperature dependence with the energy mismatch between the final and initial states as the spectroscopy of high J states in matrices is unknown.

C. Host effect

The relaxation rates of both ν_3 and $2\nu_3$ show a dramatic dependence on host lattice, the rate in Ar being a factor of 30 greater than those in Xe. The trend of increasing rate with decreasing host size is consistent with a model in which short range repulsive forces are responsible for inducing relaxation, similar to the gas phase description, where a binary collision model is used to explain the relaxation. For an extrapolation between phases to be meaningful, the relaxation probability per collision should be constant for identical collision partners. The relaxation probabilities of $CH_3F(\nu_3)$ in liquid Ar at 77 K and that in the gas phase (300 K) can be compared using a cell model for the collision frequency in the liquid phase,

$$Z = (8kT/\pi m)^{1/2} \times [2^{1/6}/\rho^{1/3} - \sigma^{1/2}]$$

where $m = CH_3F$ mass, ρ = liquid number density, σ = collision cross section. The values obtained for the relaxation probability are $P_{CH_3F-Ar}^{liq}(77K) = 2.6 \times 10^{-7}$ and $P_{CH_3F-Ar}^{gas}(300K) =$

5.16×10^{-6}. When kT is less than the two-body well depth, attractive forces influence the relaxation. For CH_3F/Ar, the well depth estimated from transport data is ca. 200 K. Thus a comparison between liquid and solid data would be more meaningful than one between high temperature gas (300 K) and liquid (77 K).

In the solid phase, the additional problem of defining a "collision" is present. Roughly the collision frequency can be estimated by the zero point motion of the guest. The frequency of this mode is estimated to be 80 cm^{-1} by fitting a harmonic oscillator potential to the two-body Lennard Jones potential near the minimum. A collision frequency of 4.8×10^{12} s^{-1} is obtained after multiplying by a factor of four to account for 2 turning points and 2 translational modes effective in relaxation. The relaxation probability is then calculated to be 6×10^{-8} at 9 K for CH_3F-Ar, about four times smaller than the liquid phase value obtained for an assumed collision frequency of 3×10^{12} s^{-1}. That the relaxation probability has increased by roughly a factor of four in going from 9 K to 77 K is encouraging in that the rates in the matrix show no great dependence on temperature. Indeed, the temperature dependence due to the emission of a 30 cm^{-1} phonon results in an increase in relaxation probability of a factor of two between 9 and 77 K when a constant collision frequency is assumed.

SUMMARY AND CONCLUSIONS

In this work, the mechanism of relaxation from the CH stretching fundamentals and bend overtones in matrix isolated CH_3F has been determined as a function of host and temperature. Despite differences in symmetry and intramolecular coupling, all levels near 3.5 μ depopulate via the same mechanism. On the experimental time scale of 5 ns, there is no measurable effect of host or temperature on the initial step of deactivation, rapid intramolecular $V \rightarrow V$ transfer to the $2\nu_3$, CF stretch overtone.

However, the rates of subsequent steps of deactivation of the ν_3 manifold, $CH_3F(2\nu_3) \rightarrow CH_3F(\nu_3)$ and $CH_3F(\nu_3) \rightarrow CH_3F(0)$, exhibit a dramatic variation with host and a weak dependence on temperature. In all cases, the deactivation rates measured are non-radiative, the radiative lifetime of ν_3, 67 ms, being roughly 500 times longer than the longest lifetime measured.

The trend of decrease in relaxation rates with increase in host mass is qualitatively explained by a model in which hard collisions with the repulsive wall of a lattice atom are responsible for the relaxation.

REFERENCES

1. J. M. Wiesenfeld and C. B. Moore, J. Chem. Phys. 70, 930 (1979).

2. V. E. Bondybey and L. E. Brus, J. Chem. Phys. 63, 794 (1975).

3. R. Rosetti and L. E. Brus, J. Chem. Phys. 71, 3963 (1979).

4. L. E. Brus and V. E. Bondybey, J. Chem. Phys. 63, 3123 (1975).

5. V. E. Bondybey and J. H. English, J. Chem. Phys. 66, 4237 (1977).

6. V. E. Bondybey and J. H. English, J. Chem. Phys. 67, 664 (1977).

7. V. E. Bondybey and J. H. English, J. Chem. Phys. 67, 2868 (1977).

8. L. Abouaf-Marguin and B. Gauthier Roy, Chem. Phys. (in press).

9. V. A. Apkarian and E. Weitz, Chem _nys. Lett. 76, 68 (1980)

10. A. J. Barnes et al, J. Chem. Soc. Faraday Trans. II, 738 (1972).

11. L. Abouaf-Marguin et al, Chem. Phys. 23, 443 (1977).

12. G. Ribbegård, Chem. Phys. Lett. 25, 333 (1974).

13. E. Weitz and G. W. Flynn, J. Chem Phys. 58, 2781 (1973).

14. S. Saëki et.al., Spectrochimica Acta 32A, 403 (1976).

15. G.D. Barnett, Thesis, University of Washington (1957)

16. G. M. Barrow and D. C. McKean, Proc. Roy. Soc. (London) A213, 27 (1952).

17. W. Schulze and D. M. Kolb, J. Chem. Soc. Faraday Trans. 2 70, 1098 (1974).

18. J. Jortner, Molecular Physics 32, 399 (1976).

19. G. Herzberg, Infrared and Raman Spectra, Van Nostrand Reinhold Co., New York (1945).

20. W. C. Smith and I. M. Mills, J. Mol. Spec. $\underline{11}$, 11 (1963).

21. Apkarian and Weitz, private communication.

Table I. Absorption band centers of CH_3F in various matrices[a,b] at 9 K.

Assignment	gas[c]	Ar	Kr	Xe
$\nu_3(A_1)$	1048.2	1040.0	1035.4	1030.1
$\nu_6(E)$	1195.5	1183	1180	1177
$\nu_2(A_1)$	1475.3	1463	1459	1455
$\nu_5(E)$	1471.1			
$2\nu_3(A_1)$	2081[d]	2064.5	2055.5	2044.0
$2\nu_5, \nu_2+\nu_5(E)$		2914 $\pm$ 1	2909 $\pm$ 1	2900 $\pm$ 1
$2\nu_5(A_1)$	2861.6	2863.7	2855.9	2846.5
$2\nu_2(A_1)$	2964.5	2968.8	2959.8	2948.7
$\nu_1(A_1)$				
$\nu_4(E)$	2982.2	3017.8	3009.0	2996.5

a. (A_1), (E) denote gas phase symmetries

b. Frequencies of transitions of A_1 symmetry are accurate to $\pm$ 0.1 cm^{-1} of E symmetry to $\pm$ 0.5 cm^{-1}

c. Ref. 19

d. Ref. 20

Table II. Integrated absorption coefficients of bands of CH_3F in (cm/mmol)

Band	$\Delta\nu_{1/2}(cm^{-1})$	A_{total}[a]	A_{corr}[b]	A_{norm}	A_{norm}^{mon} [c]	A_{gas}
$\nu(A_1)$	0.5	8660 ± 400	9010	11900	11900	11900,[d] 10400,[e] 9550[f]
$\nu_6(E)$	~3.0	118 ± 10[g]	122	161	125[g]	177,[d] 145,[e] 276[f]
$\nu_2(A_1)$ $\nu_5(E)$	~1.9[h]	870 ± 100	904	1190	1540	1030,[d] 714,[e] 977[f]
$2\nu_3(A_1)$	0.9	153 ± 14	159	210	164	
$(\nu_2+\nu_5)$ $2\nu_5(E)$	4.0	164 ± 20[g]	170	224	174[g]	
$2\nu_2$	0.7	787 ± 40	818	1080	1290	
$2\nu_5$ (A_1)	1.1	1630 ± 75	1690	2230	2610	8320[d] 6320[e] 8490[f]
$\nu_4(E)$	5.2	2570 ± 460	2670	3520	4220	

a. Measured from CH_3F/Ar = 1/516, ℓ =3.56 x 10^{-3} cm, $\rho(T_{dep}$ = 10 K) = 2.4 x 10^{22} cm^3. Absorber concentration assumed same as gas phase mixture. Length calculated from interference fringes in FTIR spectrum, assuming n_{Ar} = 1.3.

b. Concentration correction made assuming transition dipole moment of monomer and dimer aree equal. Refractive index correction is made assuming n_{Ar} = 1.3; $B_{obs}(s)/B_{obs}(g) = (1/n)[(n^2+2)/3]^2 (\nu_s/\nu_g)$.

c. Relative intensities observed for CH_3F/Ar = 1/4940, A_d/A_m <0.02, after annealing.

d. Reference 16.

e. Reference 15.

f. Reference 14.

g. Calculated from relative intensity to $2\nu_3$ band observed in M/A = 1000 matrix.

h. $\Delta\nu$ could be due primarily to $\nu_2(A_1)$ mode, since ν_2 and ν_5 are overlapped and the relative intensities unknown.

Table III. Isolated molecule decay rates of $2\nu_3$ and
ν_3 in various hosts at 9 K.

	Ar	Kr	Xe
$k(2\nu_3)ms^{-1}$			
This work	1200 ± 120	330 ± 30	33 ± 3
$k(\nu_3)ms^{-1}$			
This work	320 ± 40	88 ± 10	13 ± 2
Ref. 8	330 ± 30	87 ± 8	17 ± 2

Fig. 1: General experimental schematic shown for front
         surface excitation. An interference filter
         (@ 77 K) is located inside the detector dewar
         to spectrally resolve the fluorescence.

FLUORESCENCE
RECORDER

Ge:Cu
4°K

LENS

XIOO

TRANSIENT
RECORDER

SIGNAL
AVERAGER

CASSETTE

M

HELIUM
REFRIGERATOR
9-40 K

COMPUTER
TERMINAL

LENS

ω_i

M

FILTER

ω_s, ω_i

ANGLE TUNED
LiNbO$_3$
PARAMETRIC
OSCILLATOR

ω_p

Nd:YAG LASER
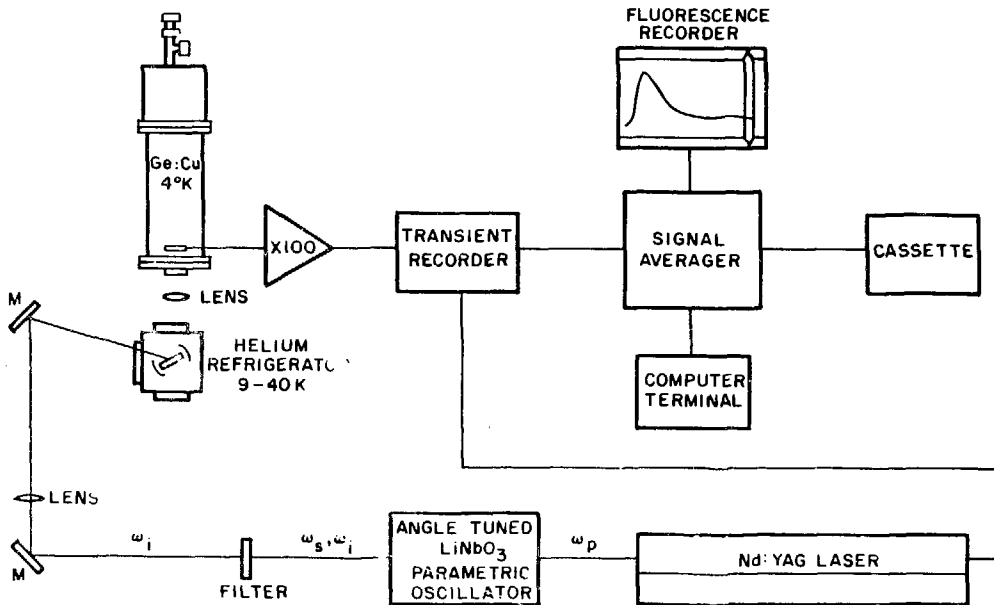
XBL 817-10759

Fig. 2: Absorption spectrum of CH_3F/Ar = 1/1000,
         9.9 mmol, 9 K deposition; CH_3F/Ar = 1/9750.
         D=dimer, P=polymer.

CH$_3$F/Ar   M/A = 1000
9 K
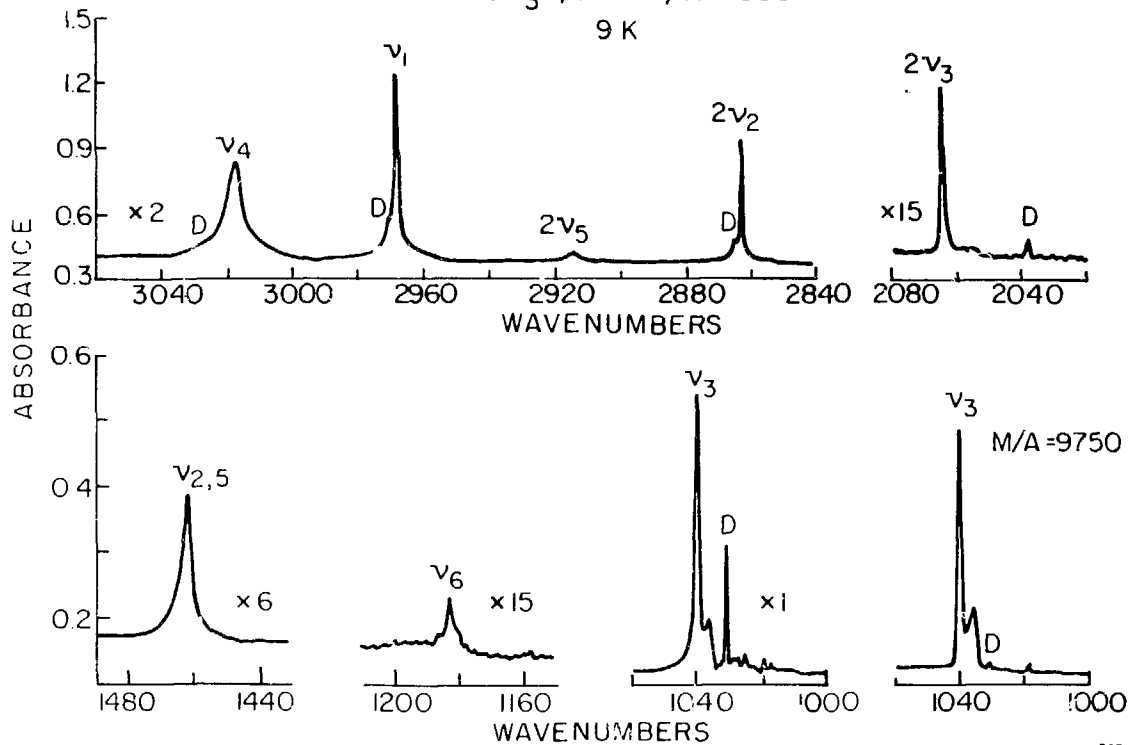
Fig. 3: Energy level diagram for matrix isolated CH_3F.
         Dashed levels are not observed spectroscopically.
         Solid arrows indicate laser excitation. Wiggly
         arrows denote levels detected in emission.
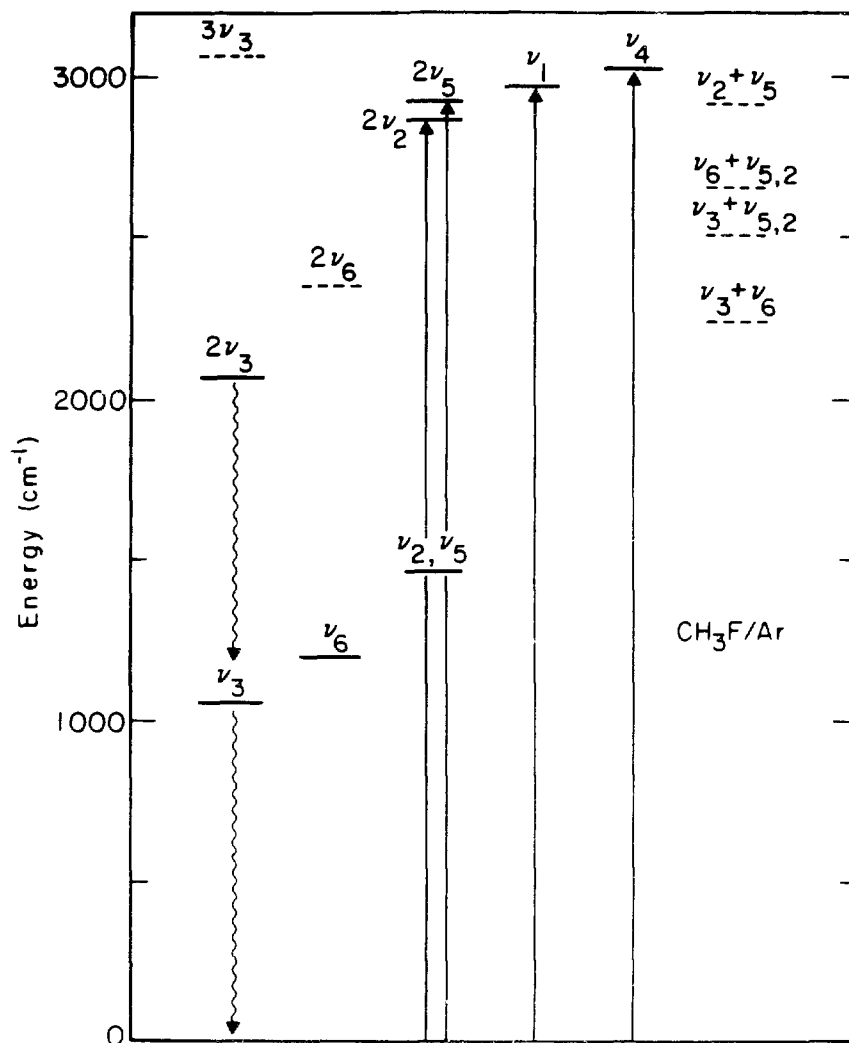
Fig. 4: Risetime of 9.6 μ fluorescence for excitation
of ν_4 CH_3F/Ar = 1/9750, 9 K; CH_3F/Kr = 1/9810,
9 K; CH_3F/Xe = 1/10800, 9 K.

FIGURE — Fluorescence Intensity vs Nanoseconds

$k = 4.8 \times 10^{7} \, s^{-1}$

$4.7 \times 10^{7} \, s^{-1}$

$4.8 \times 10^{7} \, s^{-1}$

Xe

Kr

Ar
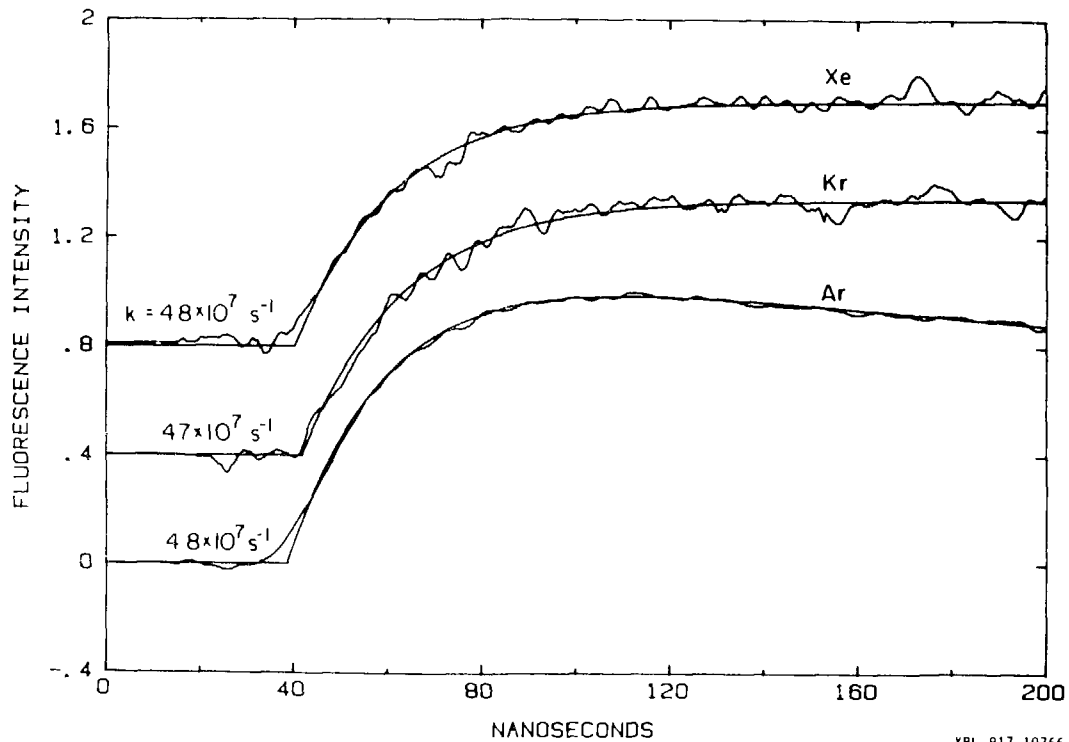
Fig. 5: Rear surface excitation of $2\nu_{2,5}$, ν_1
         $CH_3F/Kr = 1/9810$, 9 K.

         (a) $2\nu_3 \rightarrow 0$ fluorescence

         (b) Broadband 9.6 μ fluorescence

$CH_3F/Kr = 1/9810$

9 K

$k_{21} = 3.12 \times 10^5 \text{ s}^{-1}$

MICROSECONDS
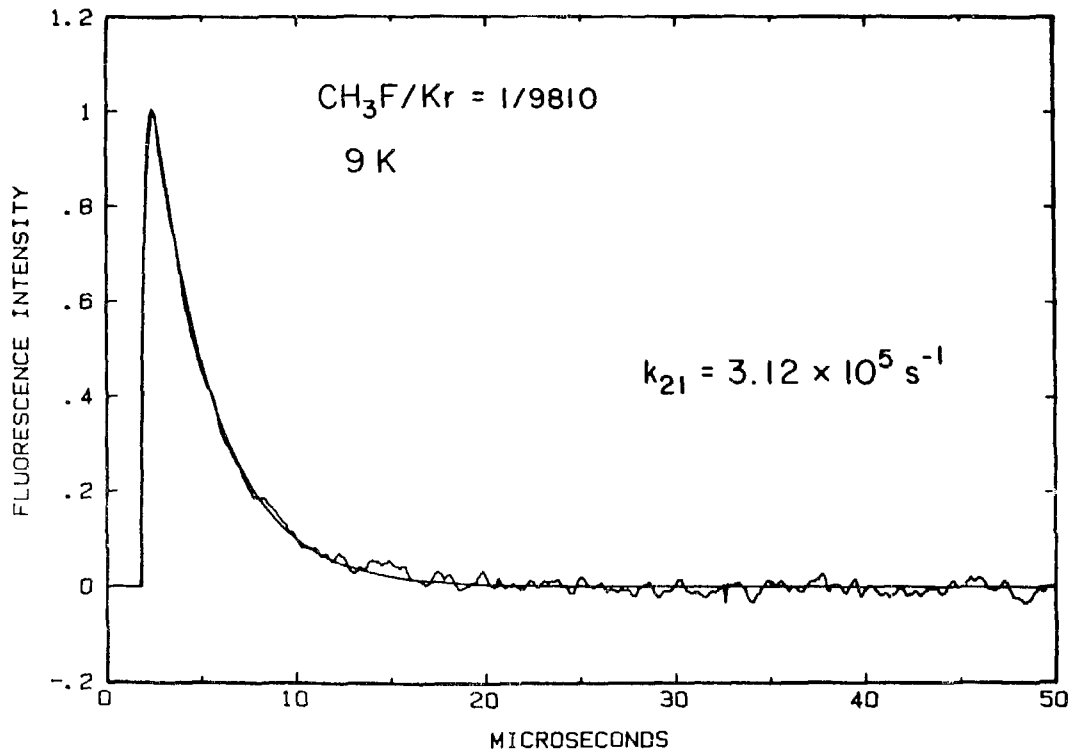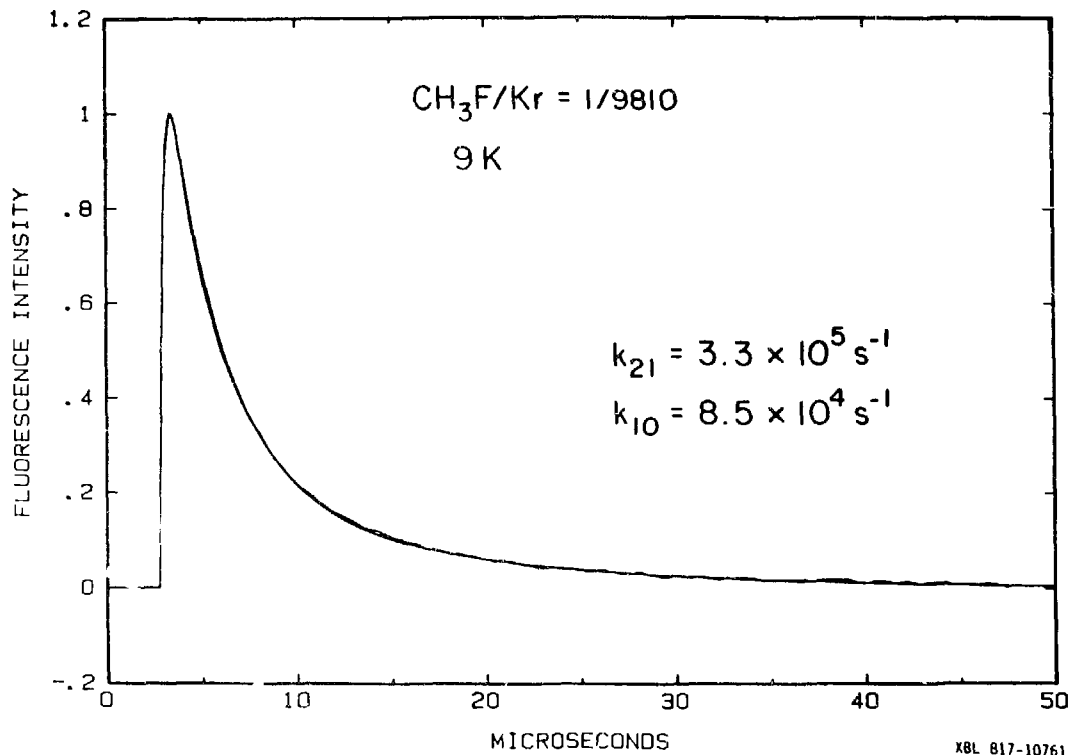
Fig. 6: Variation of $2\nu_3$ and ν_3 relaxation rates
         with gas to matrix shift. Abscissa is calculated
         from values given in Table I.

XBL 817-10764
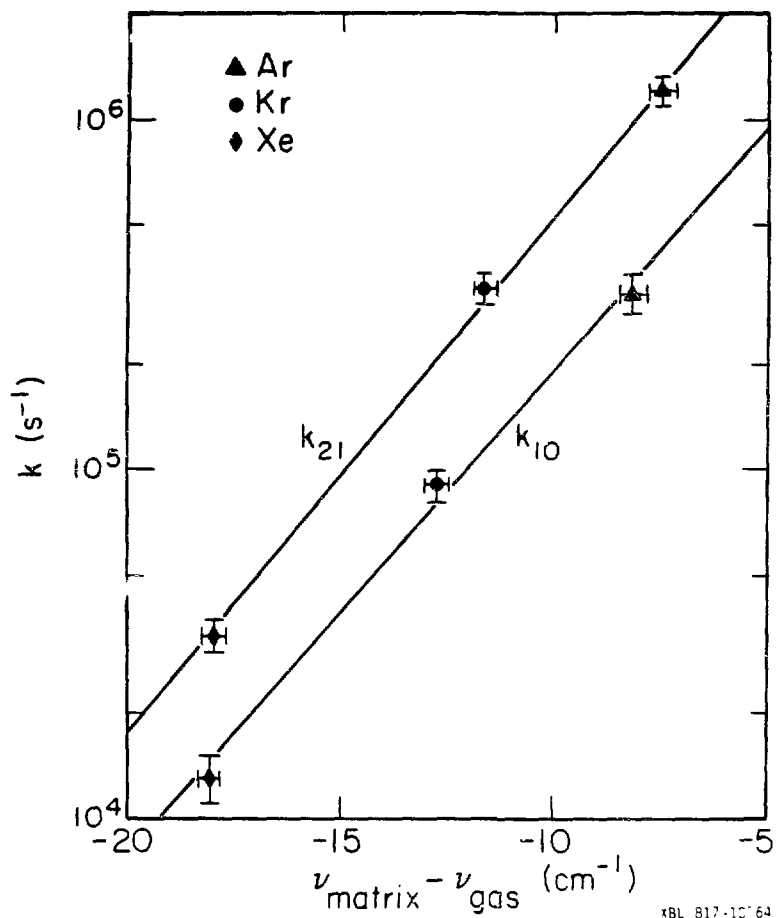
Fig. 7: Temperature dependence of $2\nu_3$ relaxation
rates. Solid lines are calculated temperature
dependences for processes involving the emission
of one phonon of frequency ν. Values of ν
are shown on graph.

XBL 817-10763
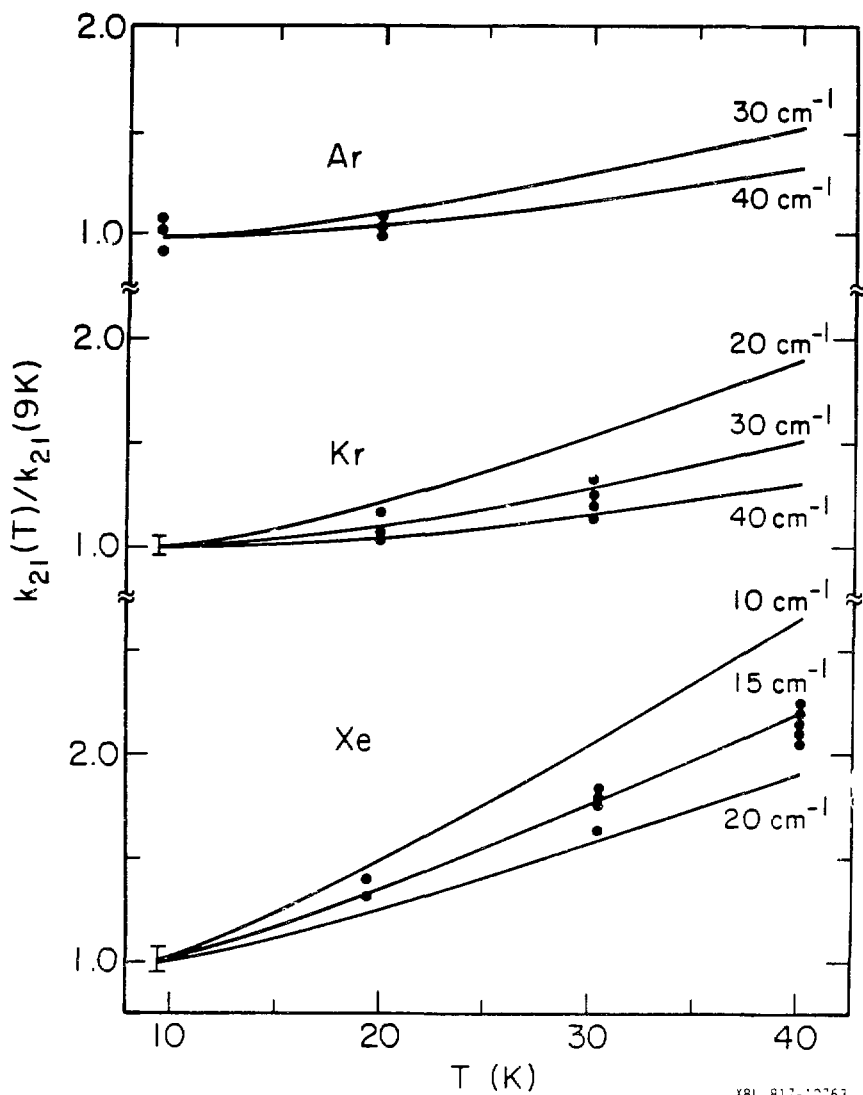
Fig. 8: Temperature dependences of ν_3 relax tion rates.
Solid lines are calculated tempera' re dependences
for processes involving the emissi 1 of one phonon
of frequency ν. Values of ν are sh wn on graph.

XBL 817-10760
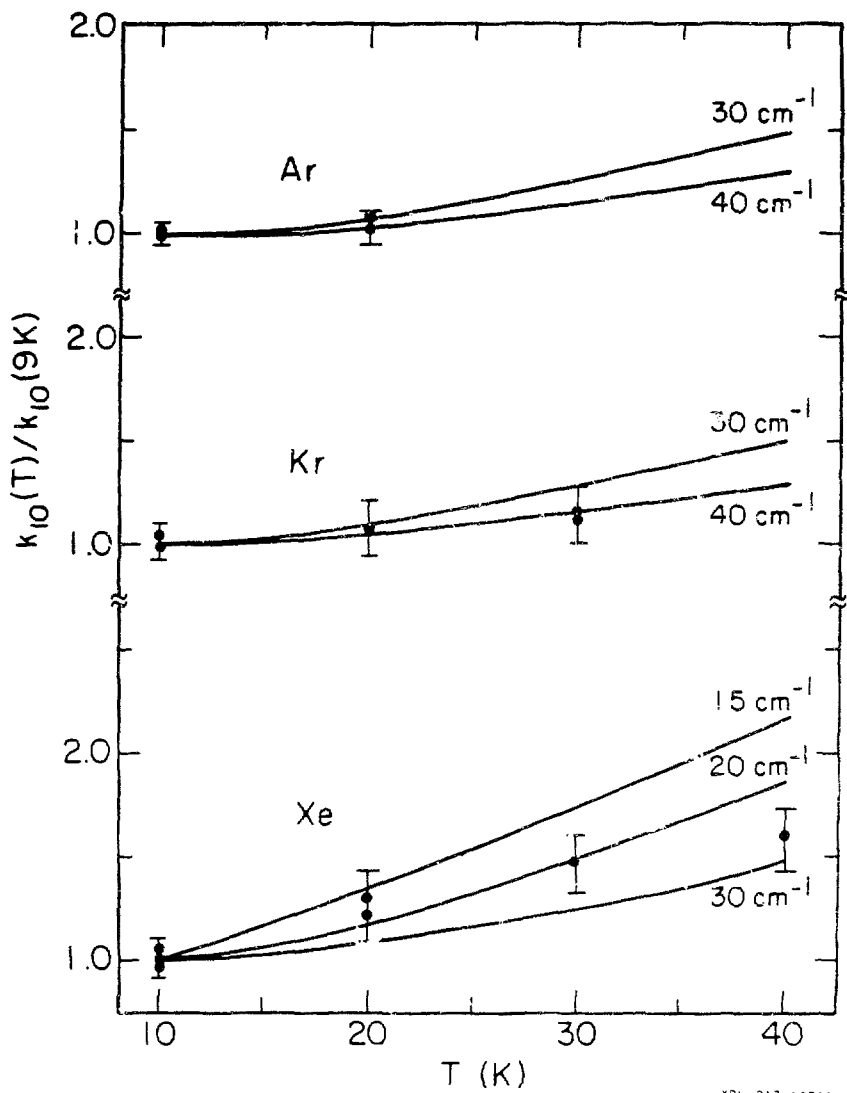
Fig. 9: Concentration dependence of $\tau(\nu_3) = \tau_1$ and
         $\tau(2\nu_3) = \tau_2$ for CH_3F in Ar at 9 K. Points
         are the average of between 4 and 23 decay curves
         with error bars given as 95% confidence limits.

XBL 817-10775
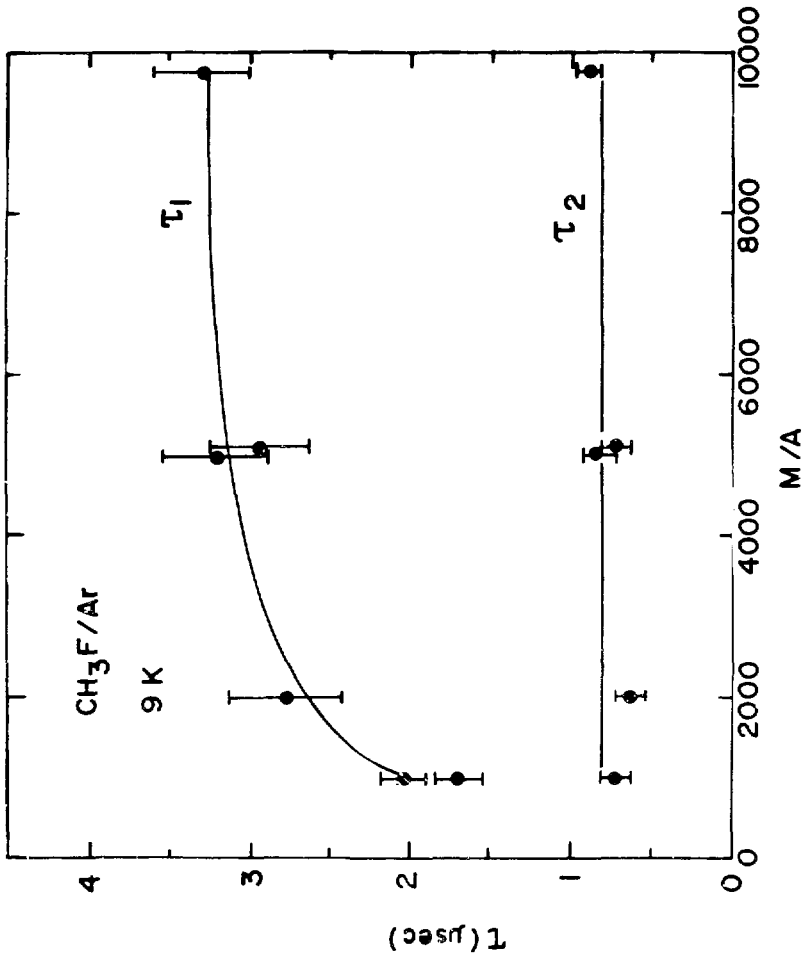
CHAPTER IV

Vibrational Relaxation of HCl v=1,2,3 in
Ar, Kr and Xe Matrices

I. INTRODUCTION

Recent studies have shown that vibrationally excited diatomics isolated in monatomic lattices dissipate their energy in a variety of ways: 1) by radiative decay, 2) by direct coupling to delocalized bulk phonons $(V \rightarrow P)$ or 3) by coupling to a mode localized at the lattice site of the guest, e.g. guest rotation or translation. It would be useful to be able to predict the relaxation rate and the dominant relaxation channel for a given guest-host system. A correlation between guest molecular parameters and observed rates gives the relative propensities of the two channels of non-radiative decay, Processes 2 and 3. That is, in cases studied so far, low moment of inertia hydrides relax via local rotation (1-3), whereas molecules with high vibrational frequencies and large moments of inertia tend to relax via local phonons (4). However, this correlation is of limited utility. The absolute rates of each process are not determined by such a correlation, thus even a prediction of the branching ratio of radiative to non-radiative decay is not possible.

It has been shown experimentally that the vibrational relaxation rate via localized modes, Process 3, of a specific species ranges over several orders of magnitude when the host is varied through the rare gas series (5,6).

Therefore, knowledge of the guest-host interaction potential
is mandatory for any serious calculation of relaxation
rates.   In general, such potentials are well characterized
only for stable molecular species in the ground electronic
state.   Previous studies of host dependence have either
been conducted on radical species, NH (5), or on polyatomic
molecules (6), for which intermolecular potentials are not
as well characterized. With the present study of HCl
isolated in Ar, Kr, Xe, we address a system in which the
two-body guest-host interaction has been thoroughly studied
in the gas phase through molecular beam scattering (7) and
through van der Waals dimer spectroscopy (8-13).   In
addition, the vibrational spectroscopy of matrix-isolated
HCl and DCl has been extensively studied (14,15) and the
forces responsible for the spectral perturbations are well
defined (15-17). Gas phase relaxation rates have also been
determined for rare gas collision partners (18).   For these
reasons, the HCl system is ideal for quantitative tests
of theories of vibrational relaxation via local mode par-
ticipation.

     These studies of the host, vibrational state and
temperature dependence of vibrational relaxation rates
in the matrix-isolated HCl/Ar,Kr,Xe systems are designed
to determine the mechanism by which the vibrational
excitation decays.   There are two possible local accepting
modes, guest translation and guest rotation.   A systema-
tic study of the dependence of the rate on host, v and

T should distinguish between the two limiting cases of
V → T (19,20) and V → R (21-23).

A more fundamentally interesting question is whether
or not the forces determined spectroscopically can be used
to model relaxation processes, i.e. whether relaxation
occurs when the guest and host are near equilibrium or
far from equilibrium. If relaxation occurs far from
equilibrium, the question arises as to whether or not
interaction with a single host atom is sufficient to
describe the relaxation process. Golden-Rule formulations
(19-26) and binary collision models (27,28) treat the near
equilibrium and far from equilibrium cases respectively.

In the present study, it is argued that V → T
transfer is not the dominant relaxation pathway, that
V → R is, and that the relaxation occurs far from equili-
brium.

II. EXPERIMENTAL

A. Matrix preparation

The matrix preparation procedure has been described previously (2,29). The gases used were: HCl (Matheson Electronic Grade, >99.99%), Ar (Matheson Ultrahigh Purity, >99.9995%), Kr (Airco, >99.995%) and Xe (Airco, >99.995%). Kr and Xe were subjected to two freeze-pump-thaw cycles before use. HCl was distilled at least once between 138 K and 77 K.

Infrared absorption spectra of the fundamental and first overtone regions were recorded on a Nicolet 7199 FTIR. For observation of the $4000-400$ cm^{-1} region, the s; ctrometer was equipped with a HgCdTe detector, KBr beamsplitter and Globar source. For the $6000-3200$ cm^{-1} region an InAs detector, KBr beamsplitter and tungsten halogen source were used. The wavelength accuracy, determined by observing atmospheric water lines is $\pm$ 0.06 cm^{-1} at 0.24 cm^{-1} resolution.

B. Fluorescence Experiments

Direct excitation of the $v=0 \rightarrow 2$ and $v=0 \rightarrow 3$ transitions required two separate laser systems. For first overtone excitation at 1.8 μ, the appropriately filtered output of a Nd:YAG-pumped optical parametric oscillator was used (29). Typical output characteristics at 1.8 μ were: 8 mJ, 2.0 cm^{-1} signal linewidth (w/o etalon), 0.2 c. 1 (w/etalon), 8 ns pulse duration, 10 mrad divergence. F

second overtone excitation at 1.2 μ, the Raman shifted
output of a Quanta-Ray Nd:YAG pumped dye laser was used.
With Rh640, adequate output for $v-0 \rightarrow 3$ excitation was ob-
tained from the second stokes line in H_2 at 400 psi.
Typical 1.2 μ output characteristics measured after a
Corning filter 7-56 (70% T) were: 2-3 mJ, 0.7 cm^{-1} band-
width FWHM, 7 ns pulse width. The 1.2 μ output was col-
limated with a single 1 m CaF_2 lens to a spot of ca.
1 cm^2 at the matrix site. For both first and second
overtone excitation, the rear surface excitation geometry,
in which the IR beam is directed through the matrix towards
the infrared detector, was used.

Fluorescence was focussed onto the 3×10^{-3} Hg:Ge de-
tector cooled to 4 K with a 5 cm f/1 CaF_2 lens. Cooled
interference filters (77 K) mounted inside the detector
dewar in addition to externally placed filters were
to discriminate against 300 K background radiation and
scattered light. Broadband emission was observed through
a combination of two filters with the following character-
tics: 2600 cm^{-1} center frequency, 3125 cm^{-1} - 2050 cm^{-1}
10% points, 70% average transmission. Due to the large
anharmonicities and low temperatures, HCl $v=3 \rightarrow 2$, $v=2 \rightarrow 1$,
and $v=1 \rightarrow 0$ fluorescence was easily resolved using a cooled
circular variable filter ($\Delta v = 33$ cm^{-1} FWHM peak
transmission) The high and low frequency response
of the detector and electronics were 75 ns re-
pectively.

Fluorescence traces were summed at 10 Hz on a Biomation 8100/Northern 575 signal averaging combination, and stored on magnetic tape for further processing by computer. Typically 256-4096 shots were averaged to give final decay curves with S/N greater than 25. Lifetimes for the $v=1,2,3$ levels were obtained by analyzing the spectrally resolved signals as single or double exponential decays. Distortion of the signal due to the finite bandwidth of the amplifiers was at most 7%. Uncertainites in fitted rate constants were ± 5% for single exponential decays, ± 10% for fits to the sum of a rising and falling exponential.

A fluorescence excitation spectrum of the $v=3$ region was obtained using a Tektronix 7912AD transient digitizer interfaced to an LSI 11/03 microcomputer to record the broadband fluorescence signal as a function of excitation frequency. The spectrum was obtained as follows: 1) A reference trace was acquired at a frequency which is not resonant with a molecular absorption. 2) The   ting was set to the starting frequency, after which the appropriate number of shots was averaged (typically 64). 3) The reference waveform was then subtracted from the one just acquired. 4) The resulting difference waveform was integrated and the value of the integral stored before stepping 0.4 cm^{-1} to the next wavelength. Thus the spectrum was a series of integrated broadband fluorescence traces as a function of excitation frequency. The result was not normalized for the ± 10% laser power fluctuations.

III. SPECTROSCOPY

Previous experimental (2) and theoretical (16,17) investigations have shown that the vibration-rotation spectra of matrix isolated HCl in the fundamental and first overtone regions can be explained by a model in which the major perturbation is rotation-translation coupling (RTC). This perturbation arises from the fact that the guest is constrained to rotate about its center of interaction, which is displaced from its center of mass. Thus the rotation of the guest is coupled to the oscillation of its center of mass. The center of mass translational motion, i.e. a localized lattice phonon, is also directly coupled to the IR active guest vibration to give the $Q_R(00)$ transition ($\Delta v=1$, $\Delta J=0$, $\Delta n=1$). The observed transition frequencies are listed in Table I. Representative spectra of the fundamental, first overtone and second overtone regions are shown in Figs. 1, 2 and 3 respectively. As can be seen by the figures, there is no appreciable change in the spectral contours with increasing vibrational quantum number, indicating that no new broadening mechanisms become important at this level of excitation.

Using the values listed in Table I, the frequencies of the purely vibrational transitions, ($\Delta v=1$, $\Delta J=0$, $\Delta n=0$) are calculated and listed in Table II. The anharmonicity, $\omega_e x_e$, calculated from the difference between the $v=0 \rightarrow 1$ and $v=1 \rightarrow 2$ transitions, increases with increasing host size and polarizability. However, the spectra of matrix isolated

HCl can not be described using a simple combination of a constant gas-matrix shift and the gas phase relationship

$$G(v) = \omega_e(v+1/2) - \omega_e x_e(v+1/2)^2 + \omega_e y_e(v+1/2)^3. \qquad (1)$$

In contrast good fits up to v=8 are obtained for the CO/Ar,Ne system using the relationship

$$\omega_{calc} = G(v+1) - G(v) - \Delta\omega_{vib} \qquad (2)$$

where $\Delta\omega_{vib}$ is the matrix vibrational shift calculated from the fundamental transition. The observed values and those obtained from equations (1) and (2) using gas phase values for ω_e, $\omega_e x_e$ and $\omega_e y_e$ are given in Table II The difference between the calculated and observed frequencies is shown as a function of vibrational quantum number for each of the hosts in Fig. 4. The differences do not increase monotonically in all matrices. Qualitatively the effects can be understood as follows. The trend with increasing quantum number is for shifts to increase until the bond is lengthened enough for the cage to become tight. Repulsive forces then cause the shift to decrease with increasing v.

Temperature dependent spectra are shown in Fig. 5 and 6 for the first and second overtone regions respectively. Fundamental spectra are not shown, but appear qualitatively similar. Shifts of fundamental and first overtone transition frequencies with increasing temperature are similar to the resolution at which the spectra were taken, $0.24 \ cm^{-1}$

and 0.5 cm^{-1}, respectively. Temperature effects on the
$v=0 \rightarrow 3$ transition frequency, shown in Fig. 7, can be
attributed to thermal expansion. In large hosts, Xe, Kr
where the transition is red shifted relative to gas phase/
matrix shift predictions, the transition frequency is
blue shifted with increasing temperature, i.e. with in-
creasing cage size and decreasing attractive interaction.
In the smallest host, the $v=0 \rightarrow 3$ absorption frequency is
unshifted or slightly red-shifted with increasing tempera-
ture due to the acccompanying decrease in the hitherto
dominant repulsive forces. In short, increasing the
temperature, hence cage size, reduces the overall medium
effect, restoring the potential to its gas phase contour.

IV. RESULTS AND ANALYSIS

The guest molecule is initially excited to a single vibration-rotation level. Temporally and spectrally resolved fluorescence monitors the decay of the vibrational excitation. In the following analysis, rapid rotational equilibration is assumed. The validity of this assumption is discussed later. For samples of sufficiently low concentration ($M/A > 2000$), where guest-guest interactions are negligible, the level populations decay exponentially. For single quantum sequential decay following excitation of N molecules to $v=3$ the populations of $v=3$, $n_3(t)$, $v=2$, $n_2(t)$ and $v=1$, $n_1(t)$ evolve as

$$n_3(t) = N \exp(-k_{32}t) \tag{3}$$

$$n_2(t) = N [k_{32}/(k_{32}-k_{21})] \times [\exp(-k_{21}t) - \exp(-k_{32}t)] \tag{4}$$

$$n_1(t) = N [\alpha\exp(-k_{10}t) - \beta\exp(-k_{21}t) + \gamma\exp(-k_{32}t)] \tag{5}$$

where

$$\alpha = \frac{k_{32}k_{21}}{(k_{32}-k_{10})(k_{21}-k_{10})}$$

$$\beta = \frac{k_{32}k_{21}}{(k_{32}-k_{21})(k_{21}-k_{10})}$$

$$\gamma = \frac{k_{32}k_{21}}{(k_{32}-k_{21})(k_{32}-k_{10})}$$

and k_{32}, k_{21} and k_{10} are the rates of deactivation of $v=3$, 2 and 1 respectively. Upon excitation of the $v=2$ level, the equations (3) and (4) apply after making the following

substitutions: $n_{\cdot} \rightarrow n_2$, $n_2 \rightarrow n_1$, $k_{32} \rightarrow k_{21}$ and $k_{21} \rightarrow k_{10}$. Fig. 8 shows the emission spectrum for HCl/Xe at 9 K obtained by normalizing the integrated fluorescence for Einstein A coefficients and lifetimes for the $v \rightarrow v-1$ transitions shown. From the temporal and spectral behavior of the emission, one of two inferences can be made. Either relaxation of the vth level does not occur via high rotational levels of $v-1$, or, such rotational levels decay very rapidly. If rotational relaxation were slow compared to vibrational relaxation, the following two observations would have been made. First, the population of low J levels of $v-1$ would rise at a rate slower than the decay of v. Secondly, emission would have been observed from high J levels of the $v-1$ state. Neither observation was made. Emission from low J levels of $v=2$ rises at a rate identical, within the experimental error of $\pm$ 10%, to the decay of the initially populated $v=3$ level, as shown in Fig. 9. There is no evidence for high J-level emission in the emission spectrum, Fig. 8.

A. Concentration Dependence

At higher guest concentrations, guest-guest interactions become important. The effect of increasing concentration is shown in Fig. 10 for the HCl/Kr system. Previously, the concentration dependence of the lifetimes of $v=1$ and $v=2$ had been studied extensively for the HCl/Ar system (2). As would be expected, the two systems exhibit similar behavior. Rates of resonant $V \rightarrow V$ transfer of $v=1$

among monomers and non-resonant $V \rightarrow V$ transfer to rapidly relaxing dimers ($\tau_d < 0.3$ μs) are enhanced with increasing guest concentration. The decrease in transition dipole moment for the $v=0 \rightarrow 2$ and $0 \rightarrow 3$ transitions, renders $v=2$ and $v=3$ excitation relatively immobile. This rationalizes the observed dependence of the $v=1$ lifetime and independence of the $v=2,3$ lifetimes on guest concentration. The mechanism is discussed in detail in Ref. 2. The following data concerns only samples in the isolated molecule limit.

The effect of impurities on the relaxation rates is measurable only for the $v=1$ level. In a sample HCl/air/Xe = $1/9.3/4800$, k_{10} increased less than 30% over that of an HCl/Xe=1/4729 mixture. The $v=3$ and $v=2$ lifetimes showed no noticeable effect.

B. Dependence on excitation parameters

Lifetimes for isolated HCl appear insensitive to the intensity of the excitation pulse between $5mJ/cm^2$ and 0.5 mJ/cm^2. The energy of the excitation pulse was varied over one order of magnitude through the use of neutral density filters. Energy density was varied by roughly a factor of thirty through the use of a CaF_2 4 cm lens. The measured $v=2$ lifetimes were constant to $\pm$ 7%.

Lifetimes for isolated HCl also do not vary systematically as the excitation frequency is scanned across the profile of a particular vibration-rotation transition Table III. Overall variation across the $v=0 \rightarrow 3$ $^{15}R(0)$

transition was $\pm$ 7%. In addition, excitation of the P(1), R(0) or R(1) transitions yields the same lifetimes Table IV. These results imply that rotational equilibrium is attained on time scales shorter than vibrational relaxation or that $k_{v,v-1}$ is not a function of J.

C. Host dependence

The dramatic variation of the deactivation rates of $v=1,2$ and 3 is with host lattice shown in Fig. 11 and Table V. The rates are seen to increase in the series Ar, Kr, Xe for each vibrational level. The deactivation rates increase with increasing spectral shift, hence with in-creasing host-guest attraction. This suggests that either the forces acting upon the guest at its equilibrium position induce relaxation or that these forces are correlated with those responsible for deactivation.

In addition, there is an increasing deviation from the harmonic approximation for the relaxation rate. $k_{v \to v-1} = v\ k_{10}$, in the series Ar, Kr, Xe. This trend is reflected by the absorption spectra. That is, the guest host system which deviates most from a harmonic oscillator model in transition frequency predictions, namely HCl/Xe,

so shows the most non-linear vibrational relaxation r es.

D. Temperature dependence

The effects of increasing temperature on the v=1, v=2 and v=3 relaxation rates are shown in Figs. 12,13 and 14, respectively. For v=1 and 2 there was no temperature at which rates began to decrease. Between 9 and 20 K the rates, in general, increase more rapidly with increasing vibrational excitation. The variation of the v=3 relaxation rates with temperature is curious in that the rates do not appear to increase monotonically. In Kr and Xe hosts, the deactivation rates of the v=3 level either show or hint at the existence of a temperature at which the rate begins to decrease with increasing T. In Ar, the v=3 → 2 emission does not decay as a single exponential at 9 K. Analysis of the observed signal at 9 K as a double exponential decay yields $A_s/A_f=3.2 \pm 0.6$ where $k_f = 1.2\times10^4$ s^{-1} and $k_s = 2.4\times10^3$ s^{-1}. Upon warming to 20 K, the amplitude ratio is decreased to 0 ± 0.3. The observation can be rationalized by assuming vastly different relaxation rates for the relevant rotational levels, J=0 and 1, in a system where rotational relaxation is slow compared to vibrational relaxation. More realistically, the fast and slow decays can be attributed to ∟ ntributions of relaxation from HCl(v=3) trapped in different sites.

V. DISCUSSION

The essential features of isolated molecule vibra-
tional relaxation of HCl in rare gas matrices are: 1) In
all hosts; Ar, Kr, Xe; the relaxation of v=1, 2 and 3 o 'urs
non-radiatively. 2) DCl, v=2, relaxes ~ 32 times more
slowly than HCl, v=2, in Ar (2). 3) For a given vibratio al
state, v, the relaxation rate $k_{v,v-1}$ increases in the
order k(Ar)<k(Kr)<k(Xe), as does the spectroscopic shift.
4) The dependence of the relaxation rate on v is superlinea
in all matrices; the deviation from linearity increasing in
the order Ar<Kr<Xe. 5) The relaxation rates become more
strongly dependent on temperature with increasing vibra-
tional excitation, as do the spectroscopic shifts.

Before proceeding with a comparison of the relevant
relaxation mechanisms, a description of the actual physical
situation is useful. This is presented in Section VA.
This description is followed in VB. by a brief discussion
of the relevant theories of relaxation, the simplifying
assumptions made in each and the consequences of these
assumptions. In Sections VC., VD., VE. and VF., the
isotope, host, v, and T trends are discussed, respectively.
Finally, in VG., a mechanism qualitatively consistent with
the experimental results is presented.

VA. Physical description

The three rare gases studied, Ar, Kr, Xe, are known
to crystallize in an fcc structure (30). An oversimplified
static picture of the situation is one in which the guest
molecule, HCl, occupies a substitutional site in an un-
distorted fcc lattice, as is shown in Fig. 15. The guest-
host interaction as well as guest-host distance vary with
host. Useful host properties are listed in Table VI.
In Fig. 16, the relative sizes of the lattice cage for
each of the hosts is shown. For clarity only one nearest
neighbor host atom is pictured.

In addition, the separation of the guest's center
of mass and its center of interaction, defined as the
point about which the average angular dependence of the
intermolecular interaction is minimal, is depicted in
Fig. 16. The cm to ci distance, a, is almost a molecular
constant, being 0.098, 0.093, 0.095 and 0.090 Å for HCl in
Ne, Ar, Kr, and Xe hosts, respectively. The consequence
of the non-coincidence of the cm and ci is to couple
guest rotation about its ci to cm guest translation.
The magnitude of this rotation-translation coupling, RTC,
is proportional to the ci to cm distance. This distance,
and hence RTC, is decreased roughly 30%, to 0.07 Å (16),
upon deuteration. In a static model the ci is the realistic
occupant of the lattice point, as shown in Fig. 16.

In actuality, neither the guest or host lattice is
stationary. The guest undergoes rotation and translation,

the latter at a frequency given by that of the local phonon. The local phonon frequencies for HCl in Ar, Kr, and Xe are, respectively, 73, 61 and 45 cm^{-1} (2.2 x 10^{12} s^{-1}, 1.8 x 10^{12} s^{-1} and 1.4 x 10^{12} s^{-1}). Furthermore, the host atoms oscillate about their equilibrium positions at frequencies similar to those of local phonons. The Debye frequencies for Ar, Kr, and Xe are, respectively, 64, 50 and 44 cm^{-1}.

It is also simplistic to assume that the lattice structure immediately surrounding the HCl molecule remains undistorted. The cage probably collapses somewhat to form an ellipsoidal cavity around the highly asymmetric guest (31).

Theoretical treatments tend to simplify the physical situation in order to obtain a tractable problem, as will be seen in the following section.

VB. Existing theories of relaxation

The essential features of relaxation processes for the HCl/rare gas system enumerated above are inconsistent with a process in which vibrational energy is transferred directly to bulk phonon modes. Theories for this process (32-37), in the limit of weak coupling to the lattice, predict that DCl should relax more rapidly than HCl since fewer bulk phonons, 34 vs. 44 in Ar, are required to match the vibrational energy gap for DCl than for HCl. The opposite trend is observed. In addition, the relaxation rates are pre-

dicted to increase in the order k(Xe)<k(Kr)<k(Ar), due to
the corresponding increase in bulk phonon frequencies and
resultant decrease in the order of the multiphonon process.
The opposite trend is observed. Furthermore, the variation
of rates with v is not predicted to be large, since the
major cause of enhanced relaxation rates is a decrease in
the order of the multiphonon process. The opposite trend
is observed, especially in Xe where $k_{32}/k_{21}/k_{10}$ =
260/33/1.0. Finally, the dependence of the rates on tem-
perature is predicted to be steep for multiphonon decay.
The observed relaxation rates depend only weakly on tem-
perature. Although it is possible to fit an individual
trend to the multiphonon model, by varying guest-host
interaction parameters, it is impossible to reconcile all
kinetic and spectroscopic observations, simultaneously (2).
Therefore, it is concluded that vibrational excitation of
HCl is not directly converted to excitation of bulk phonon
modes.

The relaxation must therefore proceed through some
localized motion of the guest, i.e. rotation or trans-
lation. Relaxation is an extremely improbable event.
The local translational oscillation of the guest occurs
at a frequency υ_L = 3 x 10^{12} s^{-1}, whereas the relaxa-
tion rates, $k_{v,v-1}$, vary between 10^3 - 10^6 s^{-1}. The guest,
therefore, samples a wide range of the cage potential
before relaxation occurs. As a result, a major problem
in theoretical treatments is the determination of an

instantaneous configuration at which relaxation occurs.
It is logical to distinguish betweeen those treatments
in which relaxation occurs when the guest is positioned
at the lattice point, (Golden Rule formulations) from
those in which relaxation occurs when the guest is dis-
placed from the lattice point (binary collision formu-
lations). A summary, first of the Golden Rule, then of
the binary collision formulations, follows.

1. Golden Rule formulations

In these treatments, the obvious choice for a coordi-
nate system is one in which the origin is located at a
lattice point. Depending on the individual description,
either the molecular cm or c_i is located at the lattice
point. The lattice structure, and guest-host interaction
potentials also vary with the individual treatments. The
essential features of each treatment are listed in Table
VII. The theories can be divided into three classes:
1) Primarily V → T transfer (19,20); 2) V → R (21-23);
3) V → R,T (24-26). The restrictions which result from
the approximations made are discussed for each of the
classes.

V → T theories, in which the predominant accepting
mode is designed to be translational motion of the guest,
have restrictions on the change in rotational quantum
number, $\Delta J = \pm 1,2$. These follow from two assumptions;
first that the c_i is located at the lattice point, and

second, that the potential has spherical symmetry about the lattice point. After truncating the expansion of the potential in q, the vibrational displacement coordinate, in either first or second order, the restrictions in ΔJ are obtained. The mismatch in energy between the initial and final $|v\rangle|J\rangle$ states is compensated for in terms of an effective width of the final rotational state. These theories describe the limiting case when $V \rightarrow T$ is the predominant path of decay.

$V \rightarrow R$ theories, in which the predominant accepting mode is designed to be rotational motion of the guest, also have restrictions on the change in rotational quantum number. These arise from two assumptions; first, that the molecular cm resides at the lattice point; and second, that the potential about the lattice point has n-fold symmetry. This leads to restrictions on the change in rotational quantum number, $\Delta J = 0$, $\pm n$, $\pm 2n$ etc. The energy mismatch between final and initial states is artifically removed by converting the sum over final roπtional states to an integral, thus creating a continuum of rotational states. These theories describe the limiting case when $V \rightarrow R$ is the predominant path of decay.

The $V \rightarrow R,T$ theory makes no restrictions on the change in rotational quantum number since static distortions are introduced in the lattice structure and a dumb-bell form for the potential is assumed. The energy mismatch between final and initial vibration-rotation levels is absorbed by

emission of a bulk or local phonon. As this theory has
no built-in bias toward either the rotational or trans-
lational channel, it is the most realistic, as well as the
most difficult computationally.

2. Binary collision treatments

There are two treatments which use this formalism, in
which the rate constant is given as the product of a colli-
sion frequency and a relaxation probability per collision.
The basic features of both models are detailed in Table VIII.
One model (28) involved guest interaction with a single
host atom, analogous to gas phase relaxation. The other
model includes the potential created by a planar hexagonal
array of host atoms. In both cases, the symmetry of the
configuration at which relaxation occurs is low since the
guest is assumed to be far from the lattice point. There-
fore, no unrealistic selection rules result from these
two treatments.

With this short synopsis of existing relaxation
theories, we now proceed to discuss the results.

VC. Isotope effects

The isotope effect has been measured previously in
these labs for HCl/DCl $v=2$ in Ar (2). The result,
$k_{21}(HCl)/k_{21}(DCl) \approx 32$, can be reproduced semi-quantita-
tively by all theories in which a local accepting mode
is postulated when the reasonable assumption that guest-
host interactions change negligibly upon deuteration is made.

V → T theories reproduce the observed isotope effect
because the coupling of the vibrational displacement to
the rotation and translation of the molecule is greater
in HCl than in DCl. This is a direct consequence of the
greater cm to ci distance in HCl than DCl. Physically,
the cm to ci distance can be thought of as the length of a
lever arm which induces rotation. Thus in the assumed
spherically symmetric cavity, its magnitude is proportional
to the V → R coupling, for J=0 → J=1 transitions, as well as
coupling between rotation and the phonon bath (20).

   V → R theories also reproduce the observed isotope
effect. The trends in these treatments can be understood
in terms of the magnitude of the ΔJ changes and correspond-
ing potential anisotropies, required in order to match
the vibrational energy gap. The rotational states most
nearly coincident with the v=2 → 1 transition are J_f=15
and 18 for HCl and DCl respectively. Thus, higher order
terms in a Legendre polynomial expansion of the potential
are required to induce the near resonant V → R transition
for DCl than for HCl. With the assumed undistorted lattice
structures, nearest neighbor host atoms are not arrang-
ed with enough asymmetry to produce a ΔJ=15 or 18 transi-
tion. As a consequence, higher order ΔJ transitions are
induced by contributions from shells outside that of the
nearest neighbors. These contributions drop off rapidly
as a result of the increasing distance of the relevant
shells.

The V → R,T theory of Gerber and Berkowitz predicts
that the dominant relaxation channel is vibration to
rotation energy transfer. The isotope effect is there-
fore reproduced rather well, for the simple reason that
higher order anisotropies are required to produce DCl re-
laxation that HCl relaxation.

Similarly, binary collision models find (27) or as-
sume (28) V → R relaxation to be the dominant relaxation
channel. Again, the greater rotational quantum number
change for DCl leads to a decreased relaxation probability.

VD. Host effects

The essential feature of the dependence of the relax-
ation rates on host is that, for all v, $k(Ar) < k(Kr) < k(Xe)$.
The essential spectroscopic feature is that $\Delta v_{Ar} < \Delta v_{Kr}$
$< \Delta v_{Xe}$.

V → T theories have a difficult time reconciling these
observations. The number of local phonons required to match
the vibrational energy gap increases in the order $n_f(Ar) <$
$n_f(Kr) < n_f(Xe)$ in the three models commonly used to des-
cribe local translational motion of a particle trapped in
a spherically symmetric cage. The model potentials commonly
used to describe the cage contour are, harmonic oscillator,
spherical box and Lennard-Jones-Devonshire cell, as shown
in Fig. 17. For the first two potentials, closed form
expresssions are known for the energy levels (19). However,
this is not the case for the LJD cell, which is described

by (38)

$$V(r/d)-V(0) = 4Z\epsilon \ [1.01(\sigma/d)^{12}L(y) - 1.205(\sigma/d)^6M(y)]$$

where $L(y) = (1+12y+25.2y^2+12y^3+y^4)(1-y)^{-10} - 1$
$M(y) = (1+y)(1-y)^{-4}-1$
$y = r^2/d^2$
d = nearest neighbor distance
r = displacement of the molecular ci from the center of the cell
$Z = 12$.

The LJD model is the most realistic of the three, therefore the translational energy levels for this potential cage were calculated. Potential parameters were determined ᵇy the empirical combining laws $\epsilon = (\epsilon_{HC1}\epsilon_M)^{1/2}$ and $\sigma = (\sigma_{HC1}+\sigma_M)/2$. The energy levels were then calculated by the WKB method using the QLEVEL program from the National Resource for Computation in Chemistry, Lawrence Berkeley Lab (39). The results are shown in Table IX and Fig. 18. The increasing order of the process $n_f = 24$, 32 and 43 in Ar, Kr and Xe hosts, respectively, suggests that relaxation rates should decrease in the order Ar,Kr,Xe. In fact the opposite is observed. This implies that V → T transfer is not the dominant process in vibrational relaxation for matrix isolated HCl.

V → R models require a greater anisotropy in larger hosts to reproduce observed relaxation rate trends. This requirement is unreasonable in the assumed undistorted lattice.

Since the V → R,T model predicts that rotation is the dominant accepting mode, a greater anisotropy, or equiva-

lently greater lattice distortion, is required in larger
hosts to reproduce the observed trends. This is not ob-
served in terms of a barrier to rotation at equilibrium,
as, spectroscopically, rotational structure of HCl is more
similar to gas phase rotational structure in larger hosts.

Binary collision V + R models require an increased
relaxation probability with host mass in order to counter-
act the decrease in collision frequencies which occur
with increase in host mass. For the model in which inter-
action with a single host atom is considered as in the
gas phase, this requirement can not be fulfilled, since
the magnitude of the relaxation probability is governed
primarily by the steepness of the repulsive wall. Thus,
binary collision theory considering only one host atom
appears to fail in the description of vibrational relaxa-
tion of HCl in inert gas matrices. When the other host
atoms are taken into account (27), a greater anisotropy
of the potential in terms of a barrier to rotation is
sufficient to produce the observed trends.

VE. Vibrational state effects

The essential feature of the dependence of the relaxa-
tion rates on vibrational excitation is that in all hosts
that the superlinearity increases in the order Ar,Kr,Xe.
The essential spectroscopic feature is that $\Delta \nu_{matrix}$
increases with v in the order Ar,Kr,Xe.

All theories use the harmonic oscillator approxima-
tion for the matrix elements of q. Thus, in first order

perturbation, all theories predict a linear dependence of $k_{v,v-1}$ on v if potential interactions between the host and guest in the v and $v-1$ states and energy mismatches remain constant. It is useful to determine the effect of using the more realistic Morse oscillator wavefunctions to calculate the matrix element of q.

$$|<v|q|v-1>|^2 = \frac{(2K_{BC}-2v+1)(2K_{BC}-2v-1)}{(2K_{BC}-v)(K_{BC}-v)^2} \; v \; x \; \frac{(\hbar K_{BC})}{4\mu_{BC}\omega_{BC}}$$

where $K_{BC} = \omega_{BC}/2(\omega x_e)_{BC}$ with ω_{BC} being the frequency of the BC bond and $(\omega x_e)_{BC}$ its anharmonicity (40). For a perturbation linear in the vibrational coordinate and treated by first order perturbation theory, $k_{v,v-1}$ will scale as the square of the matrix element, as shown above. Fitting the most anharmonic oscillator, i.e. HCl in Xe with the values $\omega = 2946 \text{ cm}^{-1}$, $\omega x_e = 53.6 \text{ cm}^{-1}$, the rates normalized to k_{10} are: $k_{32}/k_{21}/k_{10} = 3.1/2.0/1.0$. This is in marked disagreement with the observed 260/33/1.0 at 9 K. The superlinearity of the rates is therefore not simply a consequence of using the harmonic oscillator approximation, and must arise partially from the change in potential interaction upon vibrational excitation.

That guest-host interactions are a function of the vibrational state of the guest follows from the spectroscopic data, which show a change in $\Delta\nu_{matrix}$ in $v \to v-1$ transitions with v. Friedman and Kimel have modelled the vibrational frequency shift as the result of dispersive, inductive and repulsive forces acting upon a molecule with

its center of interaction fixed at a lattice point in a Lennard-Jones-Devonshire cell (16). By varying the two-body Lennard-Jones potential between the guest and a single host atom the cell potential, hence $\Delta \nu_{matrix}$, can be altered The parameters to be varied are ρ, the fractional increase in well position and δ, the fractional increase in well depth with v, as shown in Fig. 19. The observed matrix shifts can be reproduced with various combinations of ρ and δ, as shown in Fig. 20 for Ar, Kr and Xe matrices. From Fig. 20 it is clear that the magnitudes of ρ and δ required to fit the observed frequency shifts increase with increasing host mass. Thus, the guest-host interaction depends more strongly on v in the larger hosts.

VF. Temperature effects

The essential feature of the dependence of the relaxation rates is that rates, in general, depend more strongly on temperature with increasing vibrational exciation; but in all cases the dependence is weak. Similarly, the spectroscopic shift depends more strongly on temperature with increasing vibrational excitation. Theories derive the dependence of rate on temperature primarily from the modelling of the energy mismatch.

V → T theories are not explicit in defining a dependence of relaxation rate on temperature. Assuming the potential interactions to remain constant with temperature, the dependence of relaxation rates on temperature is given by that of the final rotational state linewidth on

temperature. Spectroscopically, the linewidth of the $^{35}R(0)$ transition increases monotonically with temperature, although the issue is confused by the fact that the spectroscopically measured width and that of $|\bar{\upsilon}_f\rangle$ are not equivalent (19).

V → R theories predict either no (21) or a slight dependence of the rate on temperature, being essentially independent for temperatures from 0 K to 20 $\hbar B/k_B$, where B is the rotational constant for the molecule in the lattice (22,23).

The Gerber and Berkowitz V → R,T theory derives a temperature dependence of $k_{v,v-1}$ primarily from the requirement of the emission of a bulk or local phonon at the mismatch frequency. The rate of a process requiring the emission of a single bulk phonon of frequency ω is proportional to $[\bar{n}(\omega)+1]$, and thus slowly, but monotonically increases with temperature.

Binary collision models derive a variation in rate with temperature from the thermal average of local translational motion. This again yields a slowly, monotonically increasing relaxation rate with temperature.

All theories predict no or slight dependence of rate with increasing temperature, but none predicts a decrease in rate with temperature, as observed at higher vibrational excitation in Xe and Kr. In order to account for this observation, a change with T in the guest-host interaction potential is required. There is spectroscopic evidence for

such a change (Fig. 7), in the temperature dependent line positions. The effect of increasing temperature is to decrease the guest-host interaction strength by increasing the HCl-M distance. This effect may, at some point be large enough to counteract the typical increase in rate with temperature. After this point, a further increase in temperature might result in a decrease in rate.

VG. Proposed mechanism of relaxation

First a recapitulation of the points of agreement and disagreement with the various theories is presented. All relevant theories reproduce the isotope effect rather well. The trend of increasing relaxation rates with increasing host mass is not easily reconciled with V → T theories due to the fact that a higher order process is required in larger hosts. The vibrational state effect and temperature effect on the relaxation rates can only be explained by variation in the guest-host interaction potential as a function of v and T.

The variation in the guest-host interaction potential as a function of v and T is reflected in the spectroscopic measurements. As discussed previously, the variation of the spectroscopic shift can be fit by changing either, or both, ρ and δ. The molecular polarizability increases with increasing vibrational excitation (16), thus the two-body HCl-M well depth will increase also. It is not too far fetched to assume that a van der Waals complex between the guest and a single host atom is formed as an

intermediate in the relaxation process, and that its form-
ation becomes more probable with increasing polarizability
of the guest. Indeed, such complexes are known to exist in
the gas phase with well depths of 135, 169 and 204 cm^{-1}
for HCl complexation with Ar, Kr and Xe, respectively (10).
The corresponding van der Waals minima occur at Cl-M dis-
tances of 4.006, 4.078 and 4.258 Å for Ar, Kr and Xe com-
complexes. An important feature of these van der Waals
complexes is that the anisotropy, as manifested by the
average < MClH and related barrier to rotation, increases
with increasing host size. Fig. 21 shows the inert gas to
ci distances and nearest neighbor distances (Table VI)
superimposed on a plot of the two-body Lennard-Jones
potentials for each of the rare gases. As can be seen by
well depth and cage size considerations, the attraction of
the guest toward a single host atom increases with in-
creasing host size.

At this point it is worthwhile to note that numerical
calculations by Child (41) show the ArHCl complex to
vibrationally predissociate via primarily the rotational
channel. In addition, of those diatomics for which vibra-
tional relaxation is thought to occur via rotation, only
$NH^*(A^3\pi)$ and HCl show the host effect k(Ar)<k(Kr)<k(Xe).
In the ground electronic state $NH(X^3\Sigma)$, the reverse host
effect is seen. One major difference between the two
electronic states is their polarizabilities, and hence
propensities for complex formation. From the fragmentary

evidence available, it appears that complex formation, with the attendant symmetry breaking properties, serves to enhance vibrational relaxation rates of matrix isolated species.

If a van der Waals complex is formed as an intermediate in the relaxation process, and its relaxation occurs via dissociation to form a highly rotationall· xcited HCl molecule, Fig. 22, then the effect of increasing temperature, i.e. cage expansion, must be to decrease the anisotropy of the potential experienced by the guest when it is in this configuration. Such a decrease in the angular dependence of the potential, will lead to reduced vibration-rotation coupling to high J states and thus to reduced rates. Of course, there are other factors influencing the observed temperature dependence, e.g. the probability of local or bulk phonon emission, all of which lead to a monotonic increase in rate with temperature. The observed rate variation with temperature may then by explained as the product of the two effects of temperature dependent guest-host interactions and phonon emission probabilities.

VI.   SUMMARY AND CONCLUSIONS

Through single photon excitation to a specific vibra-
tion-rotation level followed by temporally and spectrally
resolved infrared fluorescence, non-radiative lifetimes
for matrix isolated HCl v=1,2,3 have been determined as
a function of host and temperature. The major findings
are as follows: 1) For a given vibrational level, the
relaxation rate $k_{v,v-1}$ increases in the order k(Ar)<k(Kr)<
k(Xe). 2) The dependence of the relaxation rate on v
is superlinear in all matrices, the superlinearity increas-
ing in the order Ar<Kr<Xe. 3) The dependence of the rates
on temperature is enhanced at higher vibrational excita-
tion.

Combining the present results with those concerning
the deuteride (2), a mechanism wherein V → R is the domi-
nant relaxation process is proposed. That V → R occurs
far from equilbrium is inferred from the combination of
the host effect on the relaxation rates and spectra, which
show HCl to be more freely rotating in larger hosts. Com-
plex formation probably aids in the relaxation process
by effectively displacing the guest from the lattice point.
This increases the magnitude of the higher order terms in
the Legendre polynomial expansion of the potential about
the cm, hence coupling, required for large ΔJ transitions.
The effect of increasing temperature on relaxation rates
may then be understood as a combination of the decreasing
guest-host interaction and increasing phonon emission

probabilities.

Spectroscopic shifts as a function of v and tempera-
ture must be fit by models in which guest-host interactions
vary as a function of these two parameters. Matrix shifts
for v → v-1 transitions increase monotonically with v, as
might be expected since polarizabilities and thus guest-
host interactions also increase with v, until the bond is
lengthened such that repulsive forces dominate. The
effect of temperature on the v=0 → 3 transition frequency
may be thought of as due to cage expansion and the
resultant decrease in guest-host interaction.

Finally, it is seen that changing potential inter-
actions between guest and host as functions of v and T
are required to model both kinetic and spectroscopic data.
Reliable quantitative calculations of rates as a function
of v and temperature can not be made in ignorance of such
changes.

REFERENCES

1. V.E. Bondybey and L.E. Brus, J. Chem. Phys. 63, 794 (1975).

2. J.M. Wiesenfeld and C. Bradley Moore, J. Chem. Phys. 70, 930 (1979).

3. L.E. Brus and V.E. Bondybey, J. Chem. Phys. 63, 786 (1975).

4. R. Rosetti and L.E. Brus, J. Chem. Phys. 71, 3963 (1979).

5. V.E. Bondybey and J.H. English, J. Chem. Phys. 73, 87 (1980).

6. L. Abouaf-Marguin and B. Gauthier-Roy, in press Chemical Physics

7. J.M. Farrar and Y.T. Lee, Chem. Phys. Lett. 26, 428 (1974).

8. S.E. Novick, P. Davies, S.J. Harris, and W. Klemperer, J. Chem. Phys. 59, 2273 (1973).

9. S.E. Novick, K.C. Janda, S.L. Holmgren, M. Waldman, and W. Klemperer, J. Chem. Phys. 65, 1114 (1976).

10. K.V. Chance, K.H. Bowen, J.S. Winn, and W. Klemperer J. Chem. Phys. 70, 5157 (1979).

11. A.W. Mizioleck and G.C. Pimentel J. Chem. Phys. 65, 4462 (1976).

12. E.W. Boom and J. van der Elsken, J. Chem. Phys. 73, 15 (1980).

13. T.J. Balle, E.J. Campbell, M.R. Keenan, and W.H. Flygare, J. Chem. Phys. 71, 2723 (1979).

14. H.E. Hallam in Vibrational Spectroscopy of Trapped Species, edited by H.E. Hallam (Wiley, New York, 1973) Chap. 3.

15. A.J. Barnes in Vibrational Spectroscopy of Trapped Species, edited by H.E. Hallam (Wiley, New York, 1973) Chap. 4.

16. H. Friedmann and S. Kimel, J. Chem. Phys. 43, 3925 (1965).

17. H. Friedmann and S. Kimel, J. Chem. Phys. 47, 3589 (1967).

18. R.V. Steele and C.B. Moore, J. Chem. Phys. 60, 2794 (1974).

19. H. Friedmann and S. Kimel, presented at Sixth International Conference Molecular Energy Transfer, 16-20 July 1979, Rodez, France (unpublished).

20. D.J. Diestler and H.D. Ladouceur, Chem. Phys. Lett. 70, 287 (1980).

21. D.J. Diestler, E.W. Knapp, H.D. Ladouceur, J. Chem. Phys. 68, 4056 (1978).

22. K.F. Freed and H. Metiu, Chem. Phys. Lett. 48, 262 (1977).

23. K.F. Freed, D.L. Yeager and H. Metiu, Chem. Phys. Lett. 49, 19 (1977).

24. M. Berkowitz and R.B. Gerber, Chem. Phys. Lett. 49, 260 (1977).

25. M. Berkowitz and R.B. Gerber, Phys. Rev. Lett. 39, 1000 (1977).

26. M. Berkowitz and R.B. Gerber, Chem. Phys. 37, 369 (1979).

27. H.K. Shin, in press (J. Chem. Phys.)

28. J.M. Wiesenfeld, Ph.D. thesis, University of California, Berkeley.

29. L. Young and C.B. Moore, in preparation.

30. C. Kittel, Introduction to Solid State Physics 4th ed., Wiley, New York (1971).

31. J. Manz, J. Am. Chem. Soc. 102:6, 1801 (1980).

32. A. Nitzan and J. Jortner, Mol. Phys. 25, 713 (1973).

33. A. Nitzan, S. Mukamel, and J. Jortner, J. Chem. Phys. 60, 3929 (1974).

34. A. Nitzan, S. Mukamel, and J. Jortner, J. Chem. Phys. 63, 200 (1975).

35. J. Jortner, Mol. Phys 32, 379 (1976).

36. D.J. Diestler, J. Chem. Phys. 60, 2692 (1974).

37. S.H. Lin, H.P. Lin, and D. Knittel, J. Chem Phys 64, 441 (1976).

38. I. Prigogine, The Molecular Theory of Solutions
    (North Holland Publishing Company, Amsterdam 1957).

39. R.J. LeRoy, Guelph-Waterloo Centre for Graduate Work
    in Chemistry, University of Waterloo, Waterloo,
    Ontario, Canada.

40. J.A. Beswick and J. Jortner in Photoselective Chemistry
    Part I, p.363-506, (John Wiley & Sons, Inc., 1981
    edited by J. Jortner, R.D. Levine, and S.A. Rice).

41. M.S. Child, Faraday Disc. Chem. Soc. 62, 307 (1977).

TABLE I. Absorption frequencies of HCl in Ar, Kr, Xe
at 9 K.[a]

Assignment		Ar	Kr	Xe
$v=0 \rightarrow v=1$				
$Q_R(00)$		2944	2916	2884
R(1)		2896	2885	2874
R(0)	$H^{35}Cl$	2887.9	2872.7	2858.0
	$H^{37}Cl$	2885.6	2879.6	2856.1
P(1)	$H^{35}Cl$	2853.6	2836.8	2819.6
	$H^{37}Cl$	2851.6	2834.8	2817.8
dimer		2818	2816	2816
$v=0 \rightarrow v=2$				
R(1)				5600.7
R(0)	$H^{35}Cl$	5657.7	5621.6	5588.1
	$H^{37}Cl$	5650.4	5617.8	
P(1)	$H^{35}Cl$	5621.4	5587.2	5551.4
$v=0 \rightarrow v=3$				
R(1)				8222.5
R(0)	$H^{35}Cl$	8320.2	8267.8	8212.3
	$H^{37}Cl$	8314.4	8261.9	8206.3
P(1)	$H^{35}Cl$	8287.7	8261.9	8206.3
	$H^{37}Cl$	8282.2	8227.0	8169.6

[a] Uncertainty in $v=0 \rightarrow v=1$ frequencies = $\pm$ 0.12 cm^{-1};
in $v=0 \rightarrow v=2$ frequencies = $\pm$ 0.25 cm^{-1};
in $v=0 \rightarrow v=3$ frequencies = $\pm$ 0.7 cm^{-1}

TABLE II. Comparison of observed and calculated frequencies
for the purely vibrational transitions $v=0 \to v=1$,
$v=1 \to v=2$, $v=2 \to v=3$ for $H^{35}Cl$.[a][b]

	Ar		Kr		Xe	
	calc	obs	calc	obs	calc	obs
$\omega_{0 \to 1}$	2871.3	2871.3	2855.1	2855.1	2838.8	2838.8
$\omega_{1 \to 2}$	2767.7	2767.4	2751.5	2749.6	2735.2	2731.6
$\omega_{2 \to 3}$	2664.4	2666.2	2648.2	2747.0	2631.9	2624.7

[a] $\omega_{v \to v+1} = G(v+1) - G(v)$

$G(v) = \omega_e(v+1/2) - \omega_e x_e (v+1/2)^2 + \omega_e y_e (v+1/2)^3$

$\qquad\qquad + v \Delta \nu_{matrix}$

$\omega_e = 2989.74 \text{ cm}^{-1}$
$\omega_e x_e = 52.05 \text{ cm}^{-1}$
$\omega_e y_e = 0.056 \text{ cm}^{-1}$

[b] $\Delta \nu_{matrix}$ determined from fundamental absorption frequencies

$\Delta \nu = -14.5 \text{ cm}^{-1}$
$\Delta \nu = -30.8 \text{ cm}^{-1}$
$\Delta \nu = -47.0 \text{ cm}^{-1}$

TABLE III. Dependence of v=3 lifetime on excitation
          frequency.[a]

Excitation Wavelength (cm^{-1})	k_{32} (s^{-1})
8215.9	$(4.9 \pm 0.4) \times 10^{5}$
8215.1	4.5 ± 0.3
8214.3	4.8 ± 0.2
8213.5	4.7 ± 0.2
8212.7	5.1 ± 0.2

a. HCl/Xe = 1/4720 at 20 K, 72 mmol.

TABLE IV. Dependence of v=3 lifetime on rotational state excited.[a]

Transition	Frequency(cm^{-1})	T(K)	$k(s^{-1})$
$^{35}R(0)$	8215.0	20	$4.3 \pm 0.2 \times 10^5$
$^{35}P(1)$	8176.7	20	4.5 ± 0.2
"Q(0)"	8145	20	6.1 ± 0.6
$^{35}R(0)$	8215.6	30	4.2 ± 0.2
$^{35}P(1)$	8177.8	30	4.3 ± 0.2

a. HCl/Xe = 1/4720, 72 mmol.

TABLE VA.   Relaxation rates for isolated HCl/Ar (ms^{-1}).

M/A	T 9	15	20
$v = 3 \to 2$			
4960	13/2.5[a]	6.2	12
1980	12/2.4		12.0
1000	12/2.2		11
$v = 2 \to 1$			
4960	3.6	4.1	4.1
1980	4.1		4.3
Wiesenfeld[b] and Moore	3.8		5.7
$v = 1 \to 0$			
4960	0.76	0.83	0.87
1980	0.89		
Wiesenfeld[b] and Moore	0.81		1.1

[a] Decay was analyzed as a double exponential. Fast and slow rates are given.

[b] Ref. 2.

TABLE VB. Relaxation rates for isolated HCl/Kr (ms^{-1}).

M/A	9	14	20	22	27
v = 3 → 2					
5240		57			
5220		55		78	85
2200	32				
2320	27		69		
4520	33				
v = 2 → 1					
930	11 ± 1.2		16		
1140	11 ± 1.1		16		
1/7.1/2500	13 ± 1.5		15		
2900	11 ± 1.3		12		
4900	12 ± 0.8				
5220		10		13	16
10400	12				
v = 1 → 0					
2320	1.2				
4900	1.1 ± 0.1		1.2		
5220		1.3		1.4	
10400	1.0 ± 0.1				

TABLE VC. Relaxation rates for isolated HCl/Xe (ms^{-1}).

M/A	T 9	14	20	22	30	40	42
$v = 3 \rightarrow 2$							
3020	290						
3200		340		480	460		430
4720	270		440		430	400	
1/9.3/4810	260		460		470	420	
$v = 2 \rightarrow 1$							
2200	39						
3020	33						
3200		43		58	59		
4720	45		62		58		67
1/9.3/4810	33		60		60		62
$v = 1 \rightarrow 0$							
3020	1.2						
3200		1.2		1.8	2.4	3.0	
4720	0.94		1.0		1.8	3.0	
1/9.3/4810	1.0		2.1		2.6	3.0	

TABLE VI. Some physical properties of rare gas solids.[a,b]

		Ne	Ar	Kr	Xe
Crystal structure		fcc	fcc	fcc	fcc
Lattice constant (Å)		4.46	5.31	5.64	6.13
Nearest neighbor dist. (Å)		3.16	3.76	3.99	4.34
Number density ($10^{22}/cm^3$)		4.52	2.67	2.23	1.73
Mass density (g/cm^3)		1.51	1.77	3.09	3.78
Melting temp. (K)		24.6	83.3	115.8	161.4
Debye temp. (K)		75	92	72	64
Debye frequency (cm^{-1})		52	64	50	44
ϵ/K (K)[c]		36.3	119	159	228
σ (Å)[c]		3.16	3.87	4.04	4.46
Heat capacity (cal/mole/K)	10K	1.25	0.90	1.46	1.94
	20K	4.37	2.82	3.67	4.00
	30K		4.39	5.01	5.19
	70K		6.96	6.57	6.32
Thermal conductivity (mW/cm/K)	2K	30			
	3K	46			
	4.2K	42		4.8	
	8K		60		
	10K	8	37	17	
	20K	3	14	12	
	77K		3.1	3.6	
Refractive index, λ =	.500μ[d]		1.28	1.34	1.47
	.546μ[e]	1.23	1.26	1.28	
	.645μ[d]			1.34	1.43
	.694μ[d]		1.27		
	10.0μ[f]		1.41		

Footnotes to Table VI.

[a] Data with unspecified temperature is for 4.2 K. Only heat capacity and thermal conductivity vary by more than a few percent between 0 and 20 K.

[b] Sources for unreferenced data:
  H. E. Hallam, _Vibrational Spectroscopy of Trapped Species_, Wiley, New York (1971).

  C. Kittel, _Introduction to Solid State Physics_, 4th ed., Wiley, New York (1971).

  D. E. Gray, ed., _American Institute of Physics Handbook_, 3rd ed., McGraw-Hill, New York (1972).

[c] Parameters for Lennard-Jones (6-12) potential.

[d] J. Marcoux, Can. J. Phys., $\underline{48}$, 1949 (1970).

[e] J. Kruger and W. Ambs, J. Opt. Soc. Am., $\underline{49}$, 1195 (1959).

[f] G. J. Jiang, W. B. Person, and K. G. Brown, J. Chem. Phys., $\underline{62}$, 1201 (1975).

TABLE VII. Summary of Golden Rule formulations of vibrational relaxation in matrices.[a]

	FR[b]	DL[c]	DKL[d]	FM[e]	GB[f]
Primary accepting mode	T	T	R	R	R,T
Lattice structure	cell	undefined	square planar	simple cubic	distorted fcc, bcp
Occupant of lattice point	ci	ci	cm	cm	cm
Potential	spherical box	dumb-bell	$\sum_{i=1}^{4} V_o \exp(\alpha\cos4\phi)$	$\sum_{i=1}^{\infty} V_o \exp(\alpha\cos4\phi)$	dumb-bell
Number of interacting host atoms	not applicable	undefined	4	∞	12
Angular dependence	$P_o(\phi)$	$P_0(\phi)$	$P_4(\phi)$	$P_4, P_8 \ldots$	
Order of expansion in (q)	$O(q^2)$	$O(q)$	$O(q)$	$O(q)$	$O(q)$
Restrictions on ΔJ	±1, ±2	±1	0, ±4, ±8...	0, ±4, ±8...	none
Initial State	HO, RR	HO, RR	HO, planar HR	HO, planar RR	HO, RR
Final State	HO, RR LP	HO, RR	HO, planar RR	HO, planar RR	HO, RR LP, BP
ΔE Compensation	width of $|J_f\rangle$	width of $|J_f\rangle$	∫rotational states	∫rotational states	∫LP,BP

Footnotes to TABLE VII.

a Abbreviations used:

       ci = center of interaction of HCl
       cm = center of mass of HCl
       q = vibrational displacement = $(r-r_{eq})_{HCl}$
       HO = harmonic oscillator
       RR = free rigid rotor
       HR = hindered rotor
       LP = local phonon
       BP = bulk phonon

b Ref. 19

c Ref. 20

d Ref. 21

e Ref. 22,23

f Ref. 24, 25, 26

g spherical box potential = $V(r) = 0$, $r < r_f$; $V(r) = \infty$, $r > r_f$.

h dumb-bell potential = $A_1 \exp(-\alpha_1 |R_A - R_1|) + A_2 \exp(-\alpha_2 |R_B - R_1|)$.

TABLE VIII.   Summary of binary collision formulations.[a]

	Shin[b]	Wiesenfeld[c]
Predominant accepting mode	R	R
Lattice mode	planar hexagonal	not applicable
Potential	$\sum\limits_{i=1}^{6} A\exp-[(1-d)/R]$	$A\exp(-\alpha R)$
Restriction in ΔJ	none	none
Initial state	HO, HR	HO, RR
Final state	HO, RR	HO, RR
ΔE Compensation	local translation	local translation
Collision frequency	$\simeq$ local phonon frequency	$\simeq$ local phonon frequency

[a]   Abbreviations same as Table VII.

[b]   Ref. 27

[c]   Ref. 28

TABLE IX.   Translational energy levels for HCl in Ar,Kr,Xe
Lennard-Jones Devonshire cells (in cm^{-1}).[a]

n	Ar	Kr	Xe
0	46	33	21
1	140	100	64
2	236	169	109
3	335	239	155
4	430	311	209
5	539	385	252
6	644	461	303
7	751	537	355
8	861	616	408
9	972	695	462
10	1086	777	518
11	1201	859	575
12	1319	943	633
13	1438	1029	691
14	1559	1115	752
15	1682	1203	813
16	1807	1293	875
17	1933	1383	938
18	2061	1475	1002
19	2191	1568	1068
20	2323	1662	1133
21	2457	1758	1201
22	2592	1854	1269
23	2728	1952	1338
24	2867	2051	1408
25	3007	2151	1479
26	3185	2253	1559
27		2355	1624
28		2454	1697
29		2564	1771
30		2670	1847
31		2776	1923
32		2884	2000
33		2993	2078
34		3104	2157
35			2236
36			2317
37			2390
38			2480
39			2563
40			2646
41			2730
42			2816
43			2902
44			2988

a ε_{HCl} =250 cm-1, σ_{HCl} =3.31 A.

Fig. 1. Absorption spectrum of fundamental region of
         HCl/Kr = 1/4520, mmol, 9 K. Resolution =
         0.5 cm^{-1}. The weak "Q" branch may be due to
         complex formation.

HCL/KR = 17,5.29
0.5 CM-1
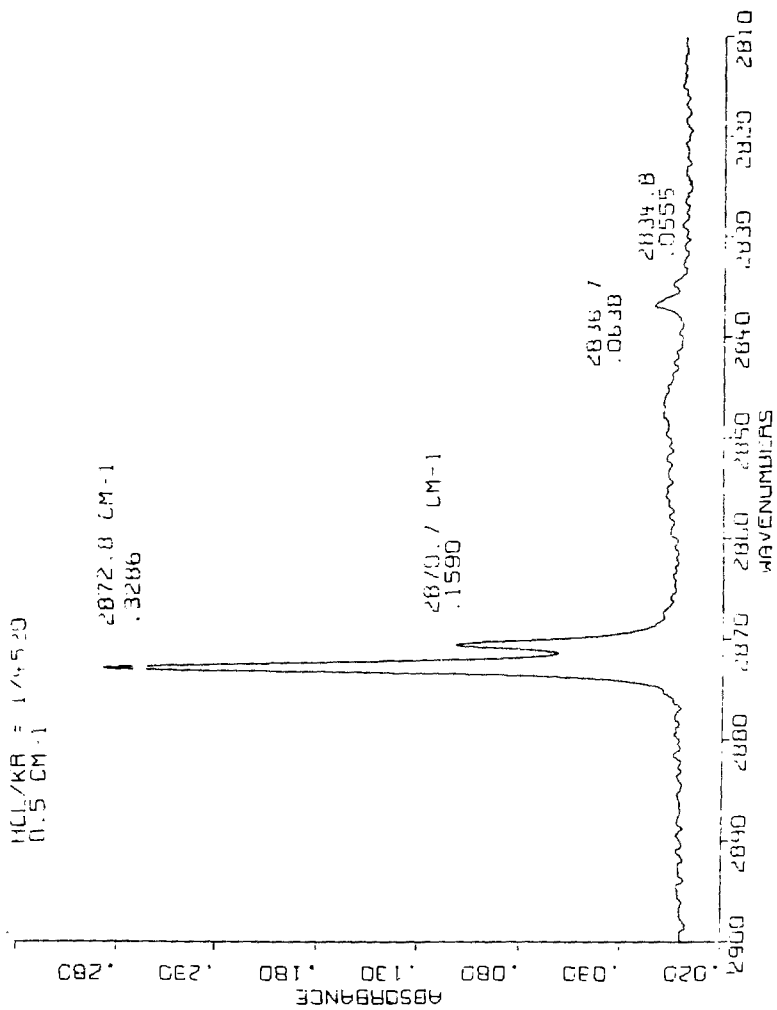
2872.8 CM-1
.3286

2870.7 CM-1
.1590

2836.7
.0638

2834.8
.0555

Fig. 2. Absorption spectrum of first overtone region of
HCl/Kr = 1/290, 11.5 mmol, 9 K. Resolution =
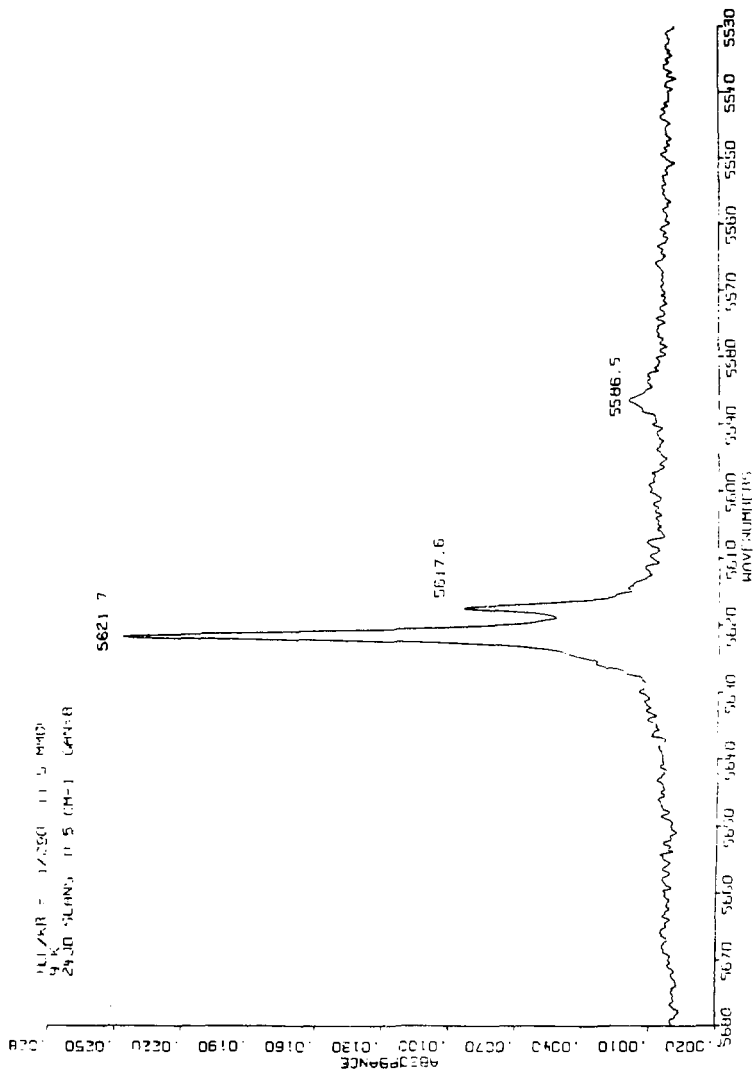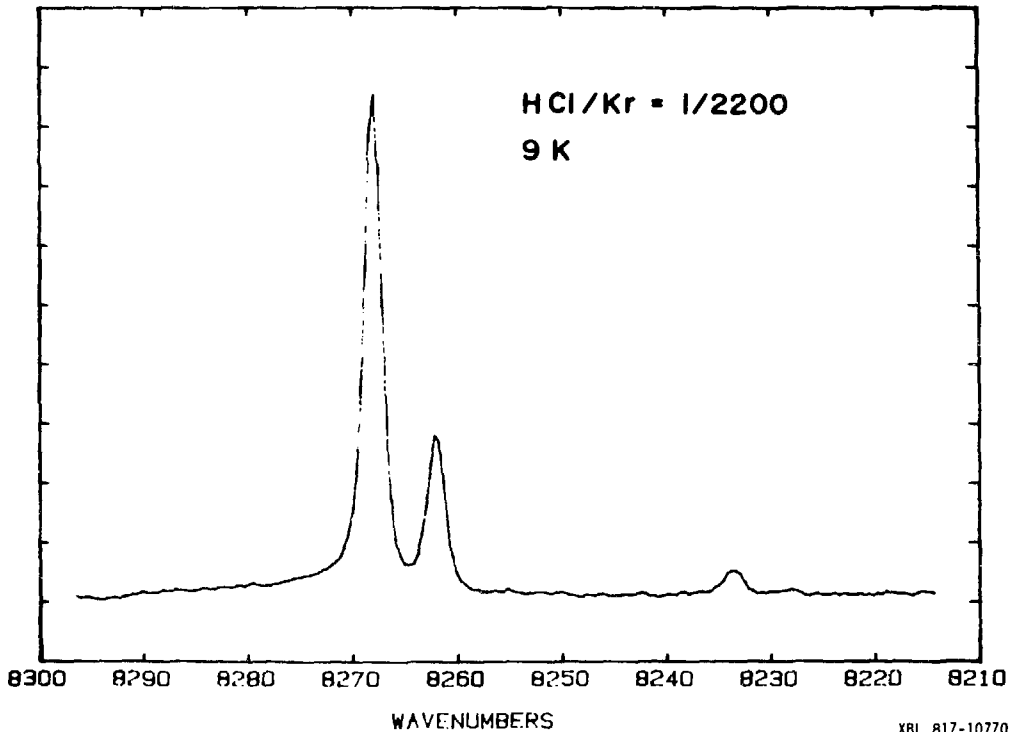0.5 cm^{-1}. The weak "Q" branch may be due to
complex formation.

Fig. 3. Fluorescence excitation spectrum of second
overtone region of HCl/Kr = 1/2200, 44 mmol, 9 K.
Resolution = 1.0 cm^{-1}.

EMISSION INTENSITY

HCl/Kr = 1/2200

9 K

WAVENUMBERS

XBL 817-10770

129

Fig. 4. Matrix shift as a function of vibrational quantum
number, v. Values of the ordinate are obtained
from the observed and calculated transition fre-
quencies given in Table II.

KBL 81? 10777
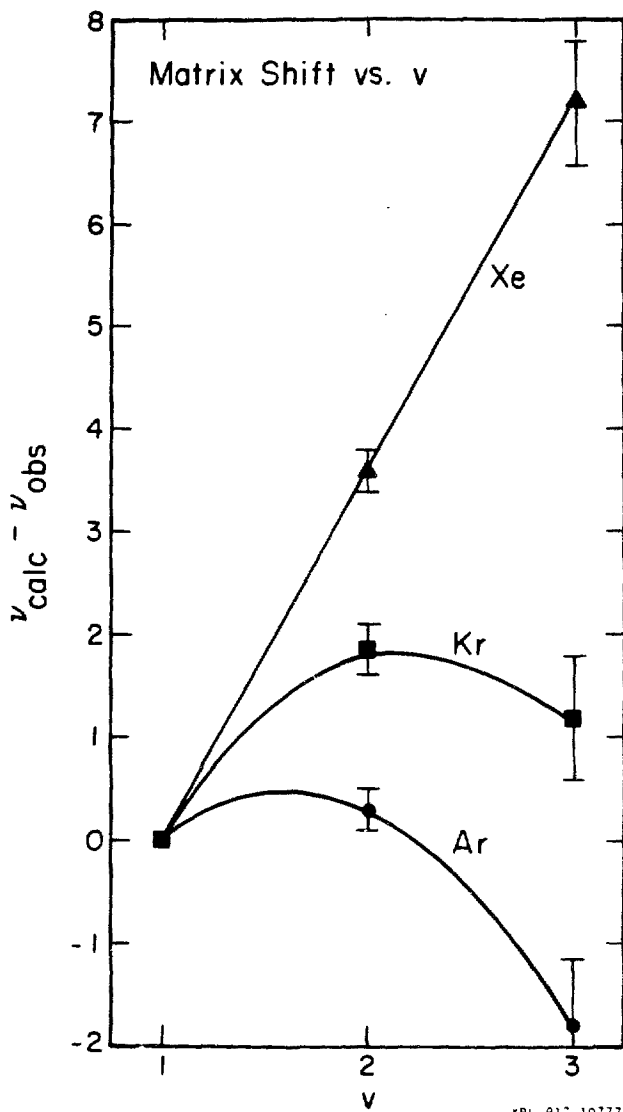
Fig. 5. (a) v=0 → 2 absorption spectrum of HCl/Kr = 1/290,
11.5 mmol, at 9, 20 and 30 K.

(b) v=0 → 2 absorption spectrum of HCl/Xe = 1/190,
9.0 mmol, at 9 and 20 K.

HCL/KR V=0.2

9 K

20 K

31 K

HCL/XE   V=0.2

9 K

21 K

ABSORBANCE

.0220 .0190 .0160 .0130 .0100 .0070 .0040 .0010 -.0020 -.0050

5650   5630   5610   5590   5570   5550   5530   5510
WAVENUMBERS
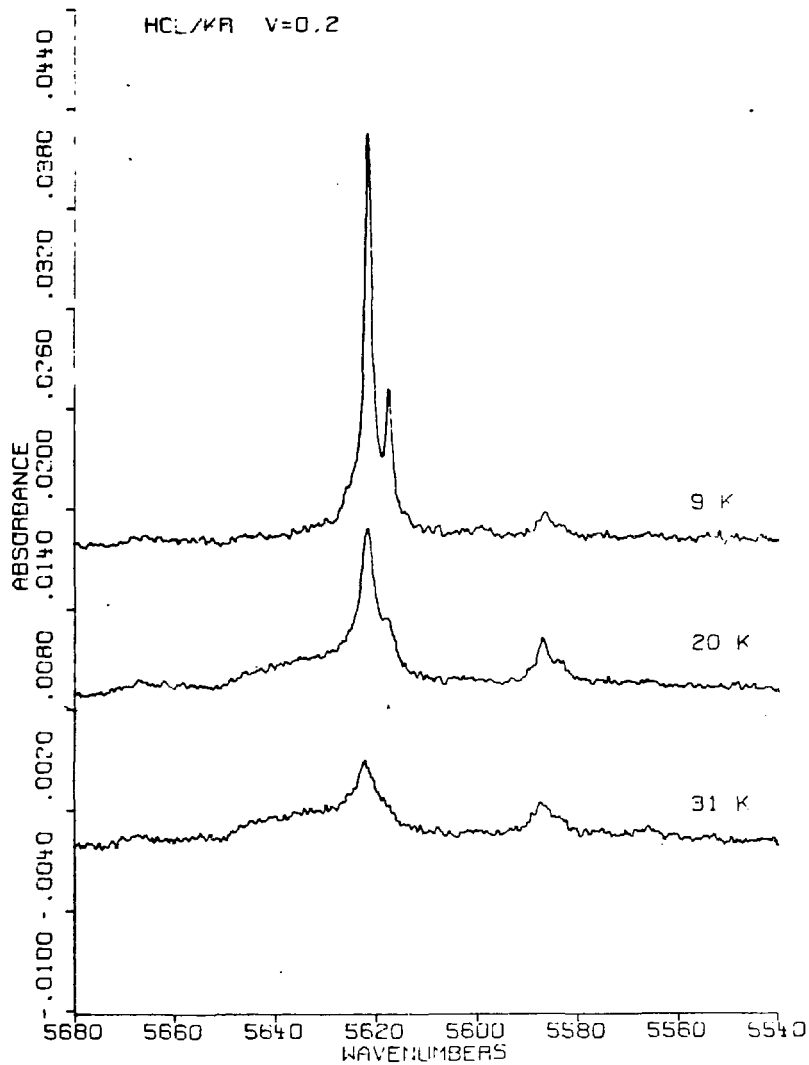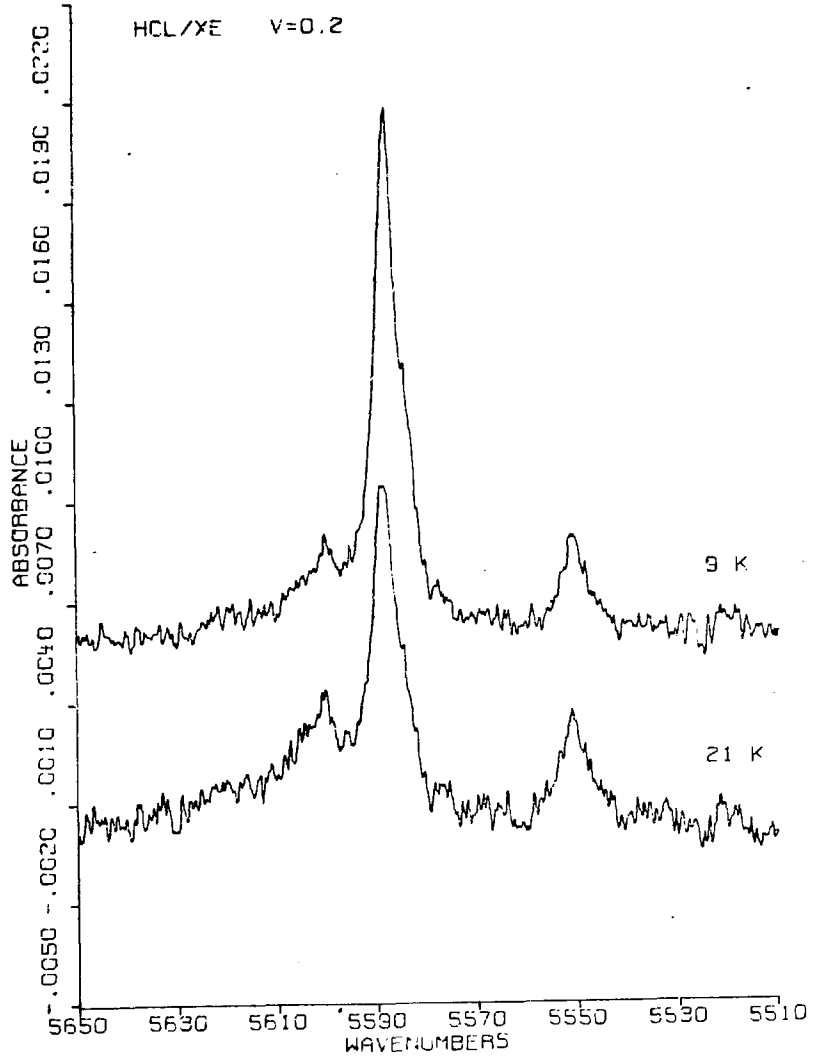
Fig. 6. (a) v=0 → 3 fluorescence excitation spectrum of
         HCl/Kr = 1/2200 44 mmol at 9, 20 and 30 K.

       (b) v=0 → 3 fluorescence excitation spectrum of
           HCl/Xe = 1/4720, 72 mmol, at 9, 20 and 40 K.
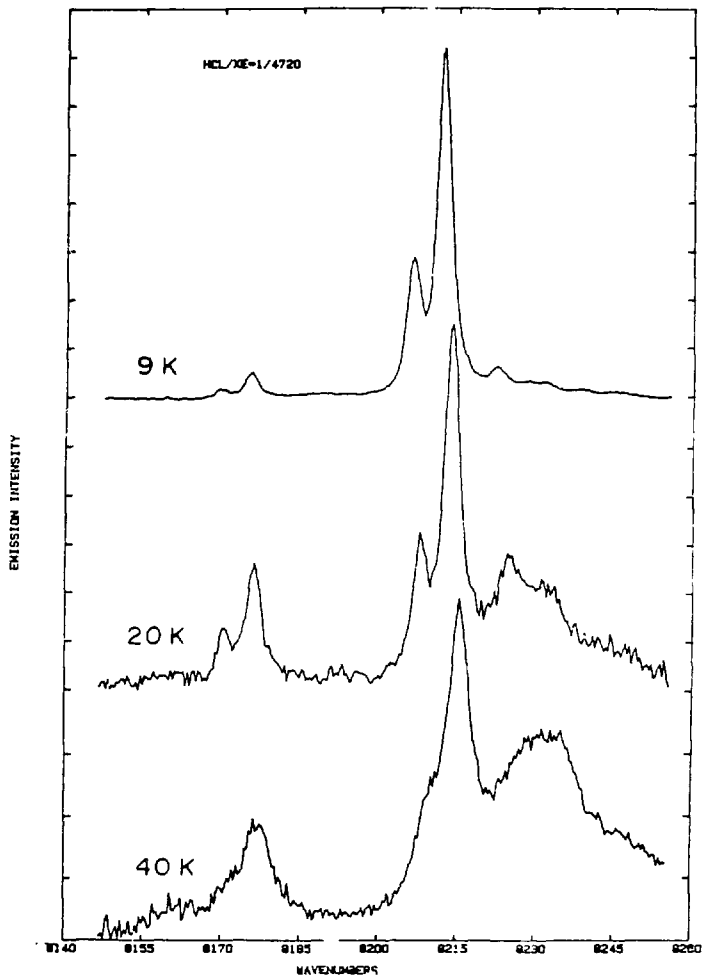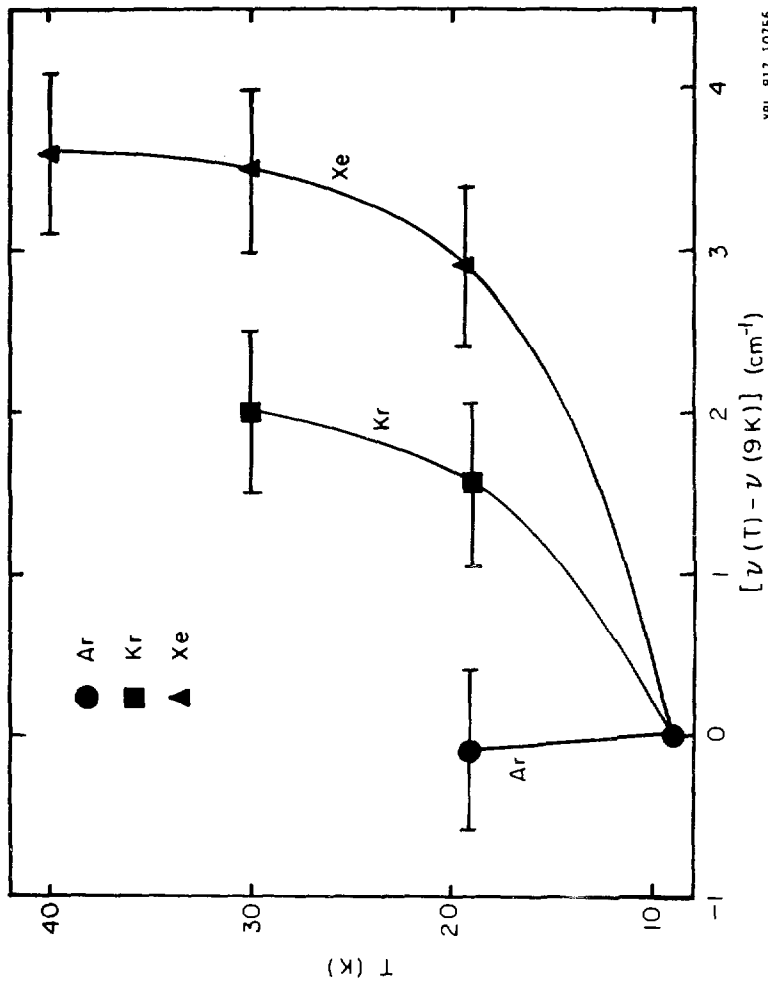   Wavelength scale reversed.

XBL 817-10757

HCL/XE=1/4720

9 K

20 K

40 K

EMISSION INTENSITY

WAVENUMBERS
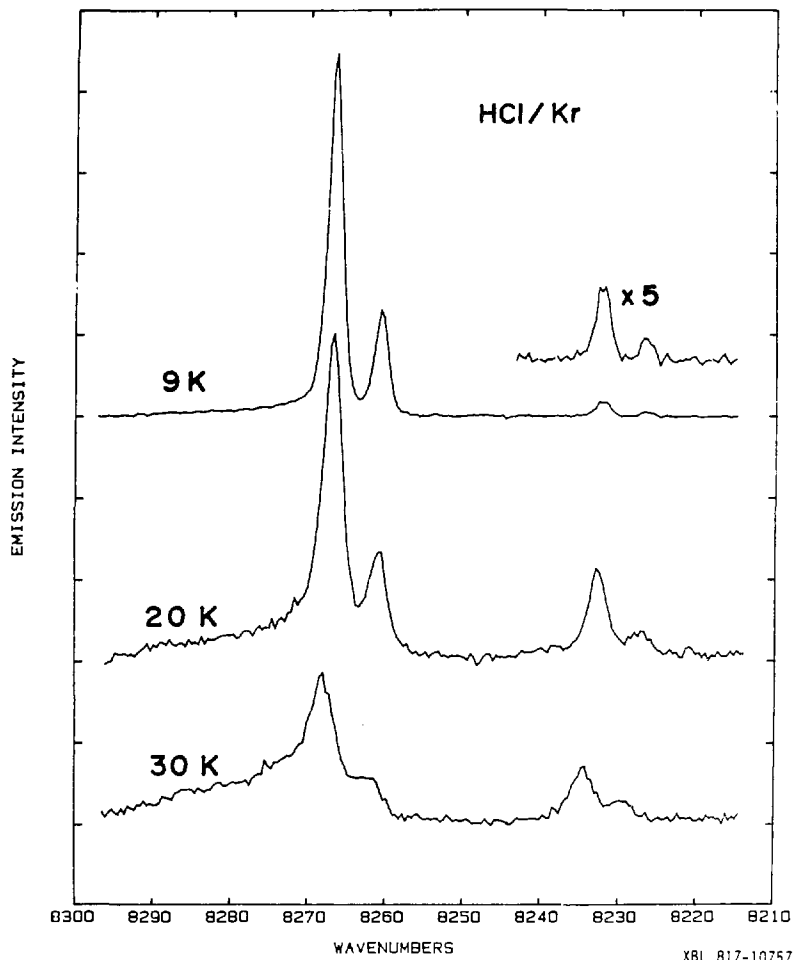
Fig. 7. v=0 → 3 transition frequency as a function of
         temperature. Determined by fluorescence excita-
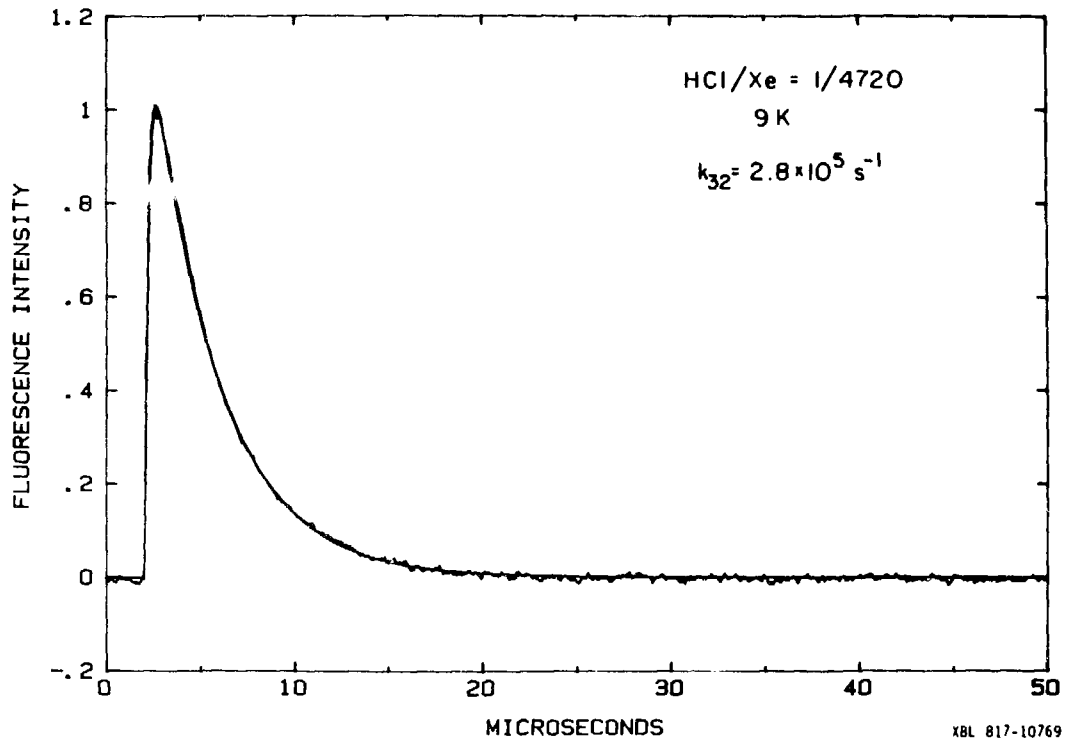   tion spectroscopy.

XBL 817-10756

Fig. 8. Emission spectrum for HCl/Xe = 1/4720 at 9 K.
Points are integrated fluorescence traces nor-
malized by Einstein A coefficients and decay
times; $I_{corr} = I_{obs}/A\tau$. Histograms indicate
emission from a Boltzmann distribution of rota-
tional levels.
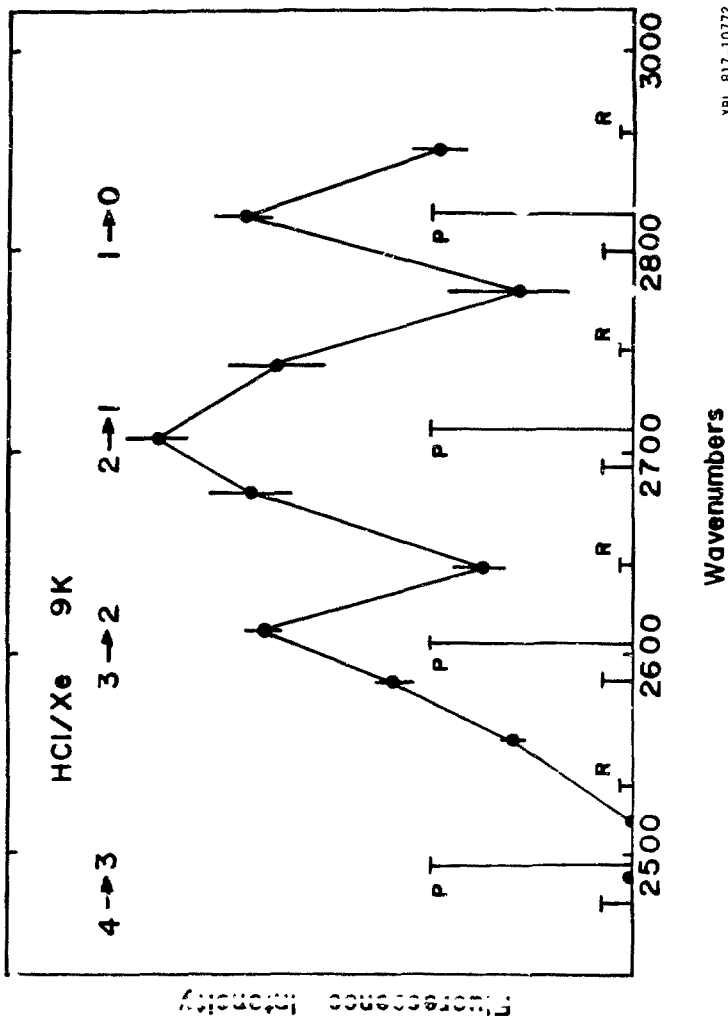
XBL 817-10772

Fig. 9. (a) v=3 → 2 fluorescence after v=0 → 3 excitation.

(b) v=2 → 1 fl orescence after v=0 → 3 excitation.

HCl/Xe = 1/4720

9 K

$k_{32} = 2.8 \times 10^5 \text{ s}^{-1}$

XBL 817-10769

143

FLUORESCENCE INTENSITY

MICROSECONDS

HCl/Xe = 1/4720
9 K

$k_{32} = 3.1 \times 10^5 \ s^{-1}$
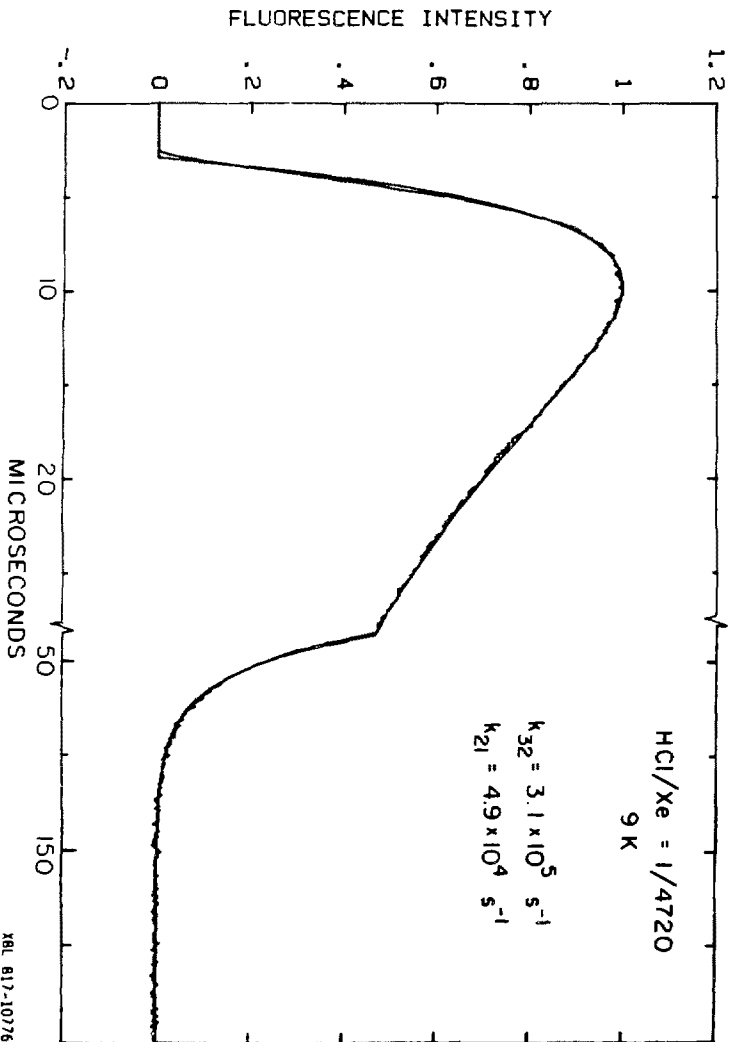$k_{21} = 4.9 \times 10^4 \ s^{-1}$

XBL 817-10776

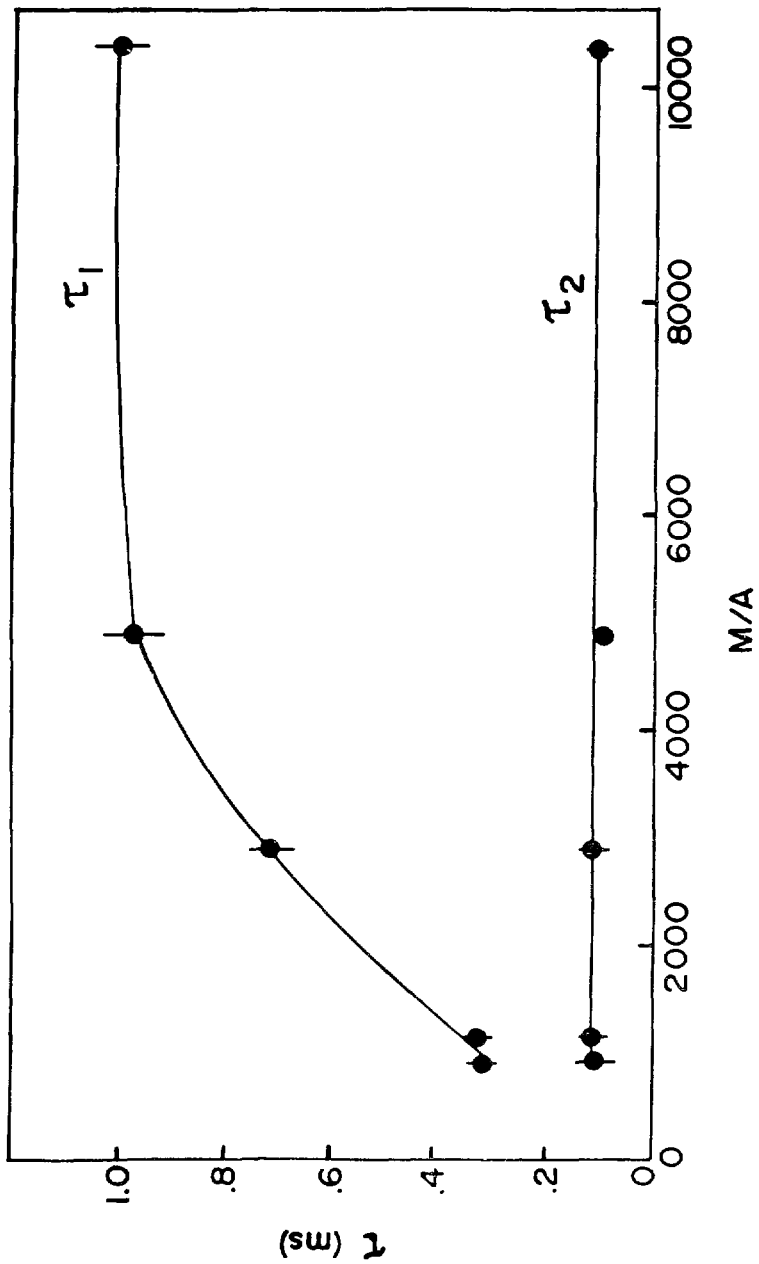Fig. 10.   Concentration dependence of v=1 and v=2 lifetimes
           for HCl/Kr system.

Fig. 11.   Relaxation rates of $v=1$, 2 and 3 at 20 K as a
function of gas-matrix shift. Values of the
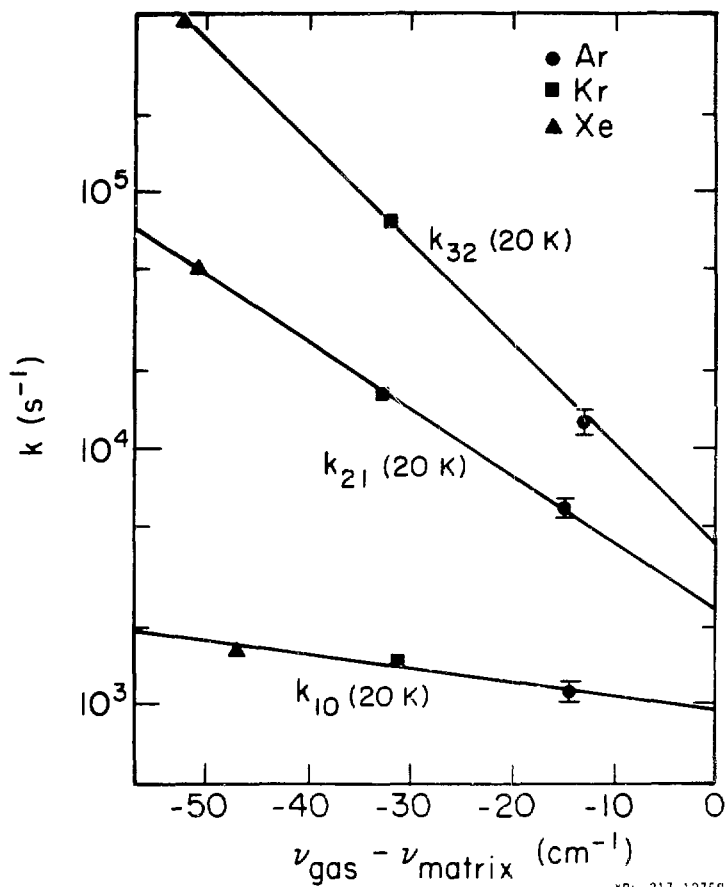abscissa are calculated from $\nu_{gas}(v)-\nu_{matrix}(v)$.

XBL 317-10758

Fig. 12. Temperature dependence of v=1 relaxation rate in
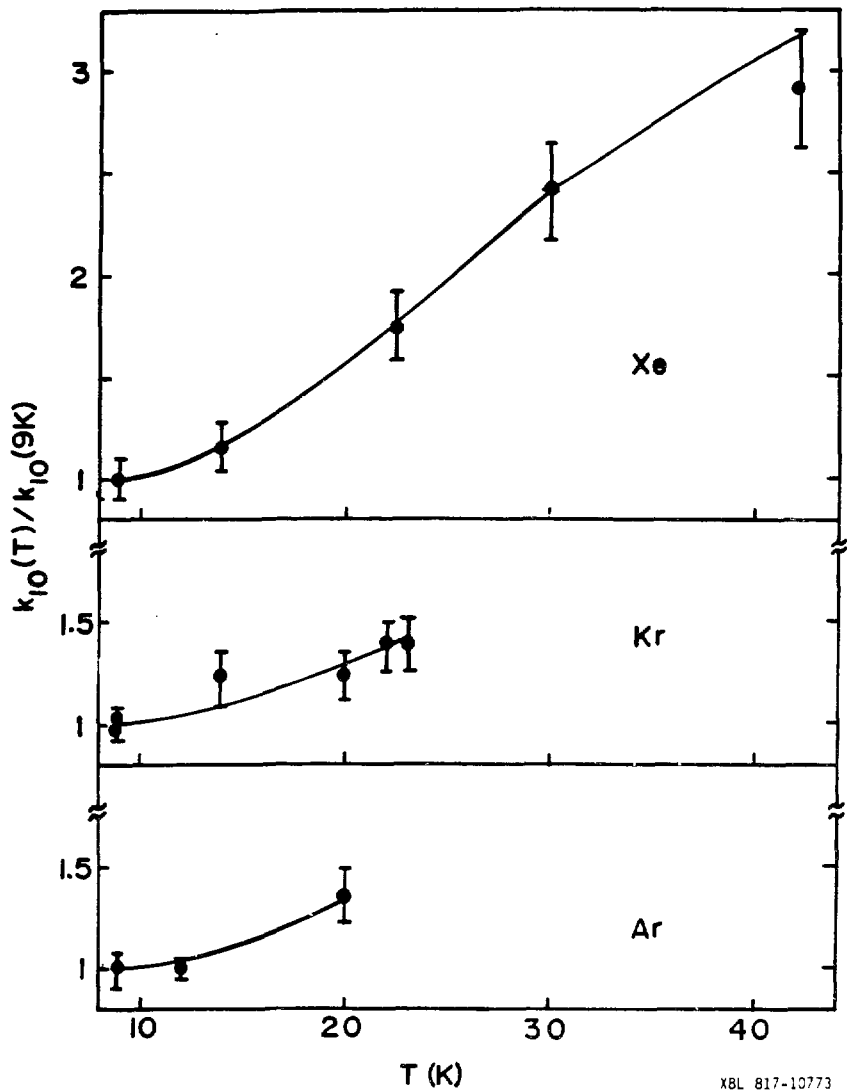Ar, Kr and Xe matrices.

XBL 817-10773

Fig. 13.   Temperature dependence of v=2 relaxation rate in
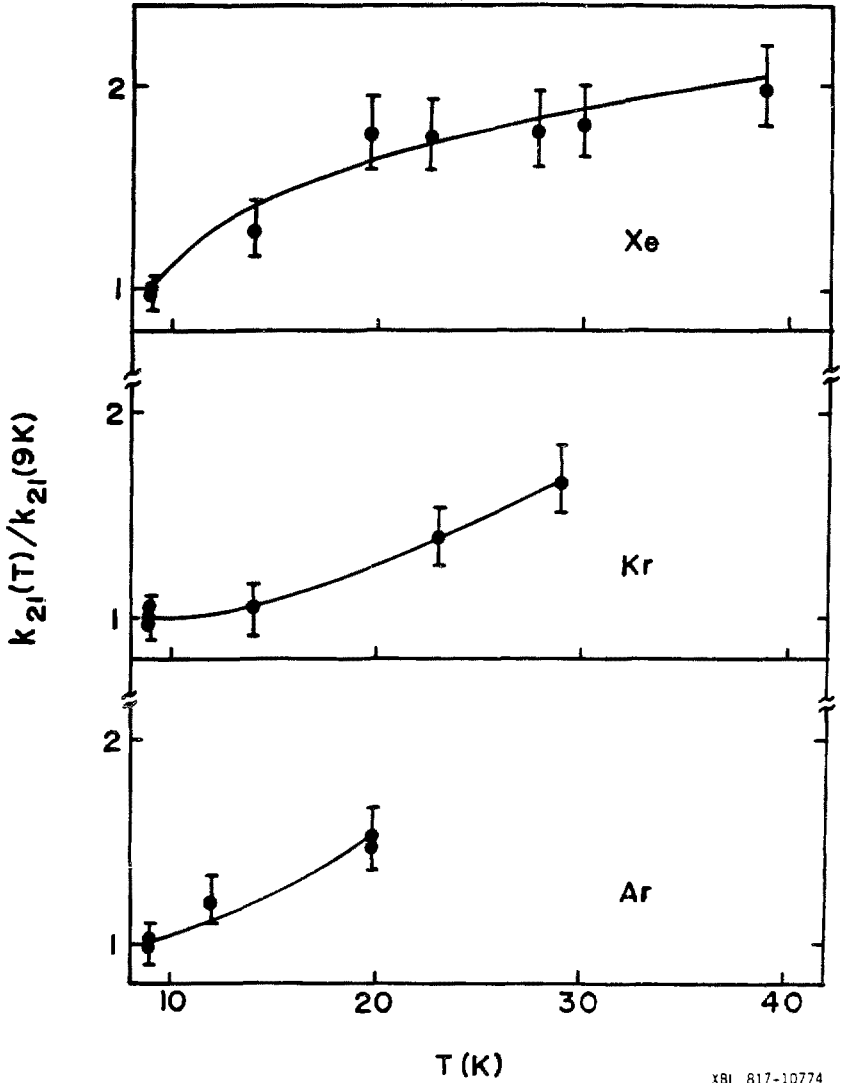Ar, Kr and Xe matrices.

XBL 817-10774

Fig. 14. Temperature dependence of v=3 relaxation rate in
Kr, and Xe matrices.
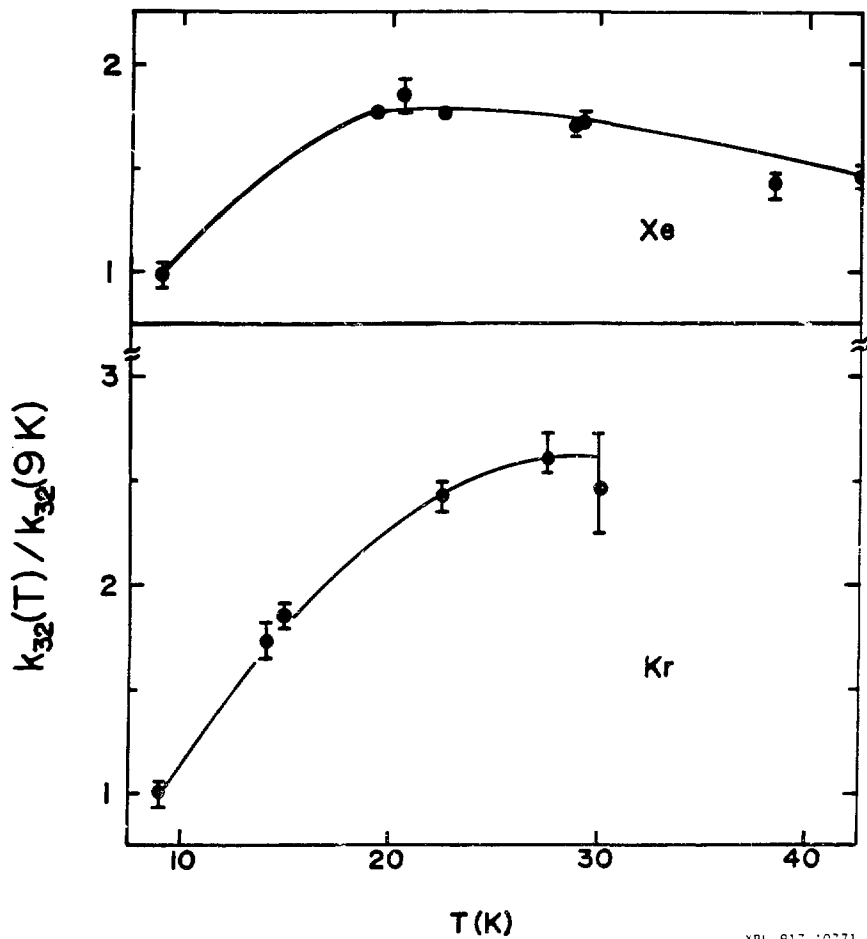
Fig. 15. Geometry of HCl trapped in a substitutional
          site of an fcc lattice. The c_i of the HCl is
          located at the lattice point in the center
          plane.   The four Ar atoms in the plane are
          symmetrically arranged about the c_i. Nearest
          neighbor atoms in adjacent planes are arranged
          in a square array rotated 45° with respect to
          the center plane. The HCl molecular axis is
          perpendicular to the center plane.

.
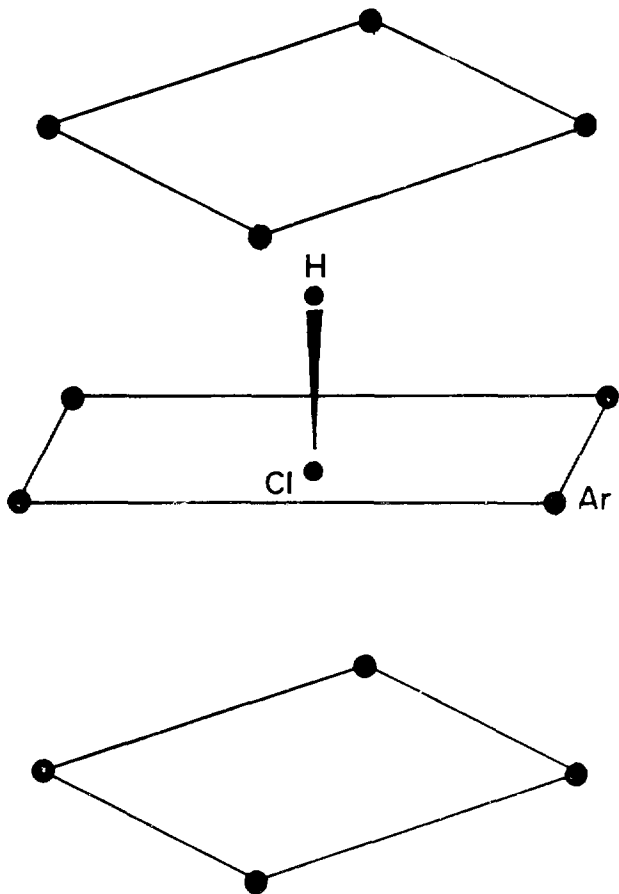
Fig. 16.   The relative size of host cages is shown.
            Atomic radii of inert gas is used to determine
            cage size. The ci of the HCl is located at
            the lattice point. The cm is located on the
            molecular axis at the inside edge of the
            point representing the Cl atom. γ is the
            angle between the molecular axis and the ith
            host atom.
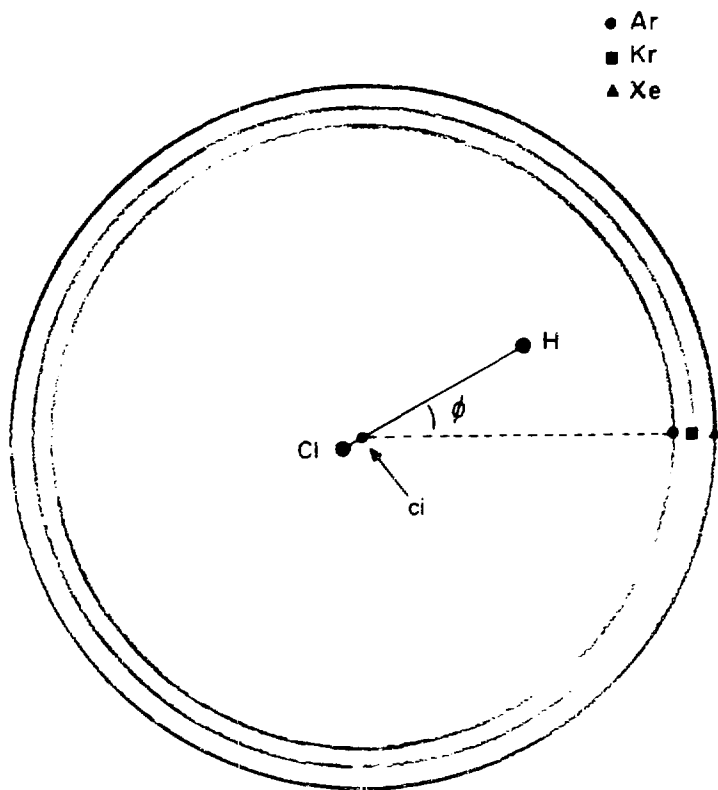
Fig. 17. Lennard-Jones-Devonshire, harmonic oscillator
          and spherical box potentials for Ar, Kr and Xe.
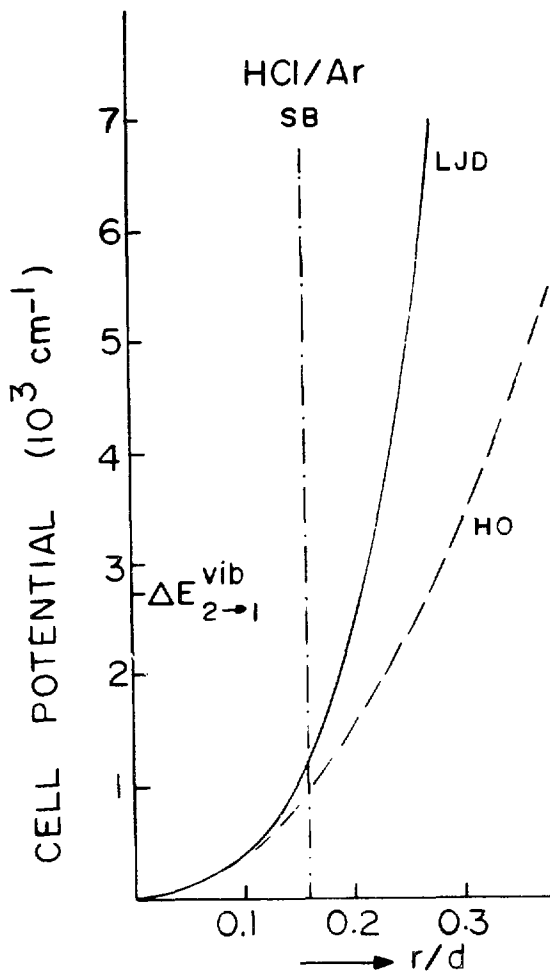
Fig. 18.   Translational energy levels for HCl in
           Lennard-Jones-Devonshire cell of Ar, Kr and
           Xe. Values are listed in Table IX.
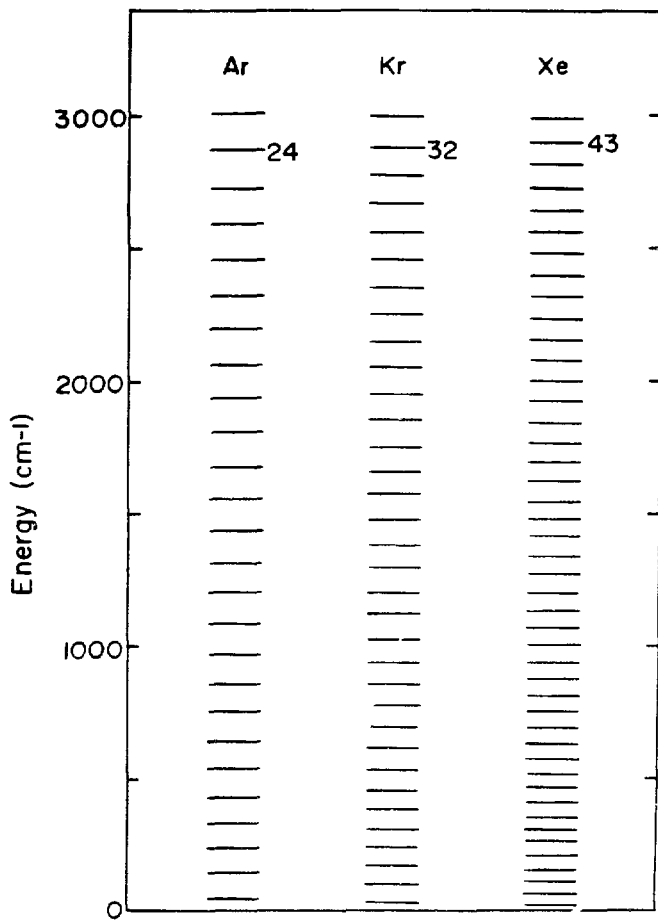
Fig. 19.   Variation of two-body Lennard-Jones HCl-M
           interaction with vibrational excitation. The
           variables δ and ρ are defined as
           $\delta = (E-E0)/E0$ and $\rho = (S-S0)/S0$.

VARIATION OF L-J POTENTIAL WITH
VIBRATIONAL STATE
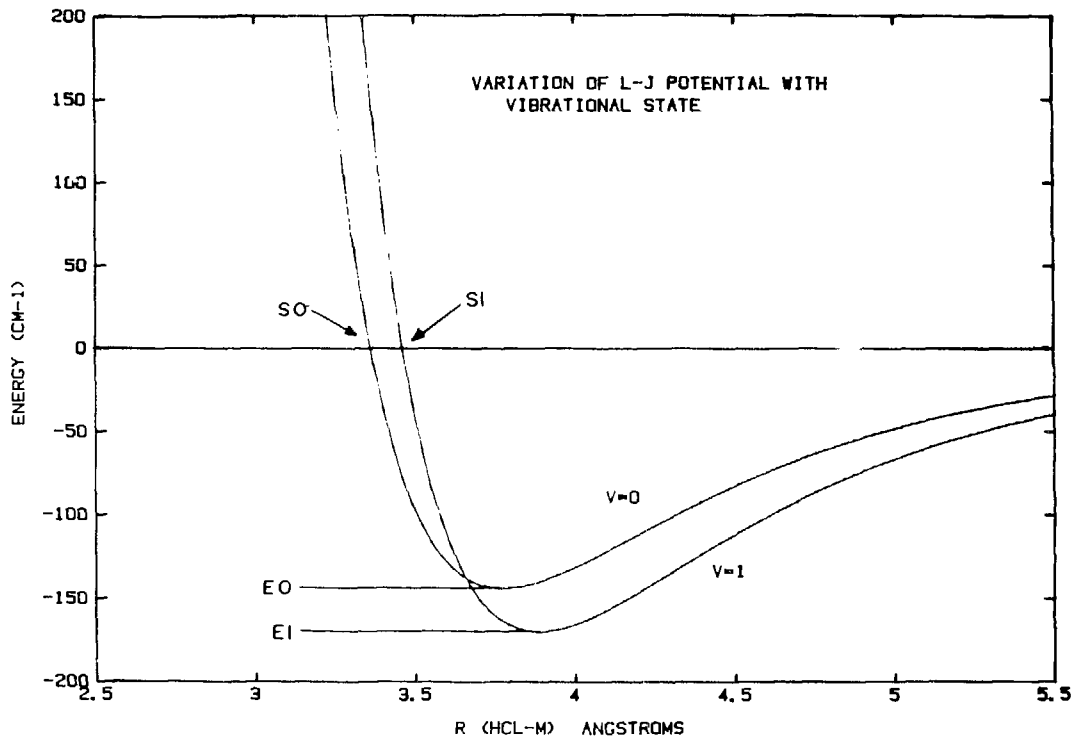
Fig. 20.   Ordinate = observed 0 → v gas to matrix shift.
            Range of the parameters $\delta = (E-E0)/E0$ and
            $\rho = (S-S0)/S0$ which are sufficient to fit
            the spectroscopic shift observed for v=1,
            2 and 3. Spectroscopic shift for a particular
            v state can be fit by any combination of δ
            and ρ which intersect the appropriate line.

VIBRATIONAL FREQUENCY SHIFT AS FCN OF
FRACTIONAL CHANGE IN INTERMOLECULAR WELL DEPTH

HCL-AR
EØ = 144 CM-1
SØ = 3.36 ANGSTROMS
L = 3.76 ANGSTROMS

.001 = (S ·SO)/SO

.01

.05

V=1
V=2
V=3

V-VO (CM-1)

(E-EO)/EO

Plot of V_D (CM-1) versus $(E-E0)/E0$ for HCL/KR, with $E0=169.4$ CM-1, $S0=3.48$ Å, $L=3.99$ Å. Curves labeled $.001 = (S-S0)/S0$, $.005$, $.01$, $.02$. Vertical lines marked $V=1$, $V=2$, $V=3$.

HCL/XE

E0 = 199.8 CM-1
S0 = 3.64 A
L = 4.34 A
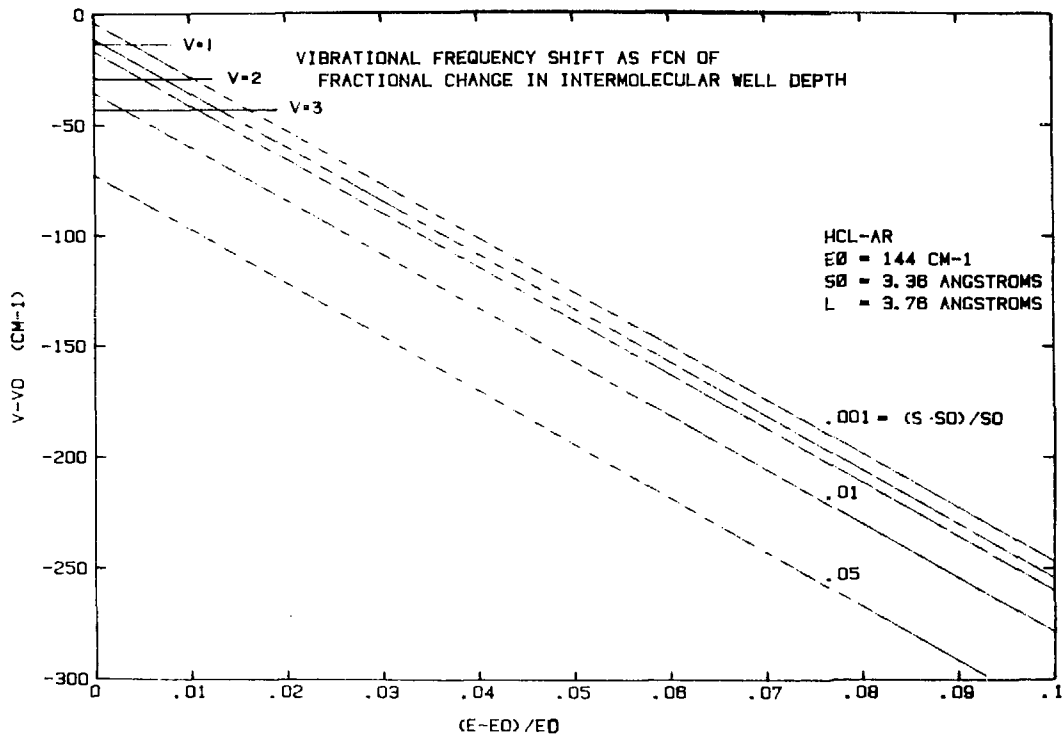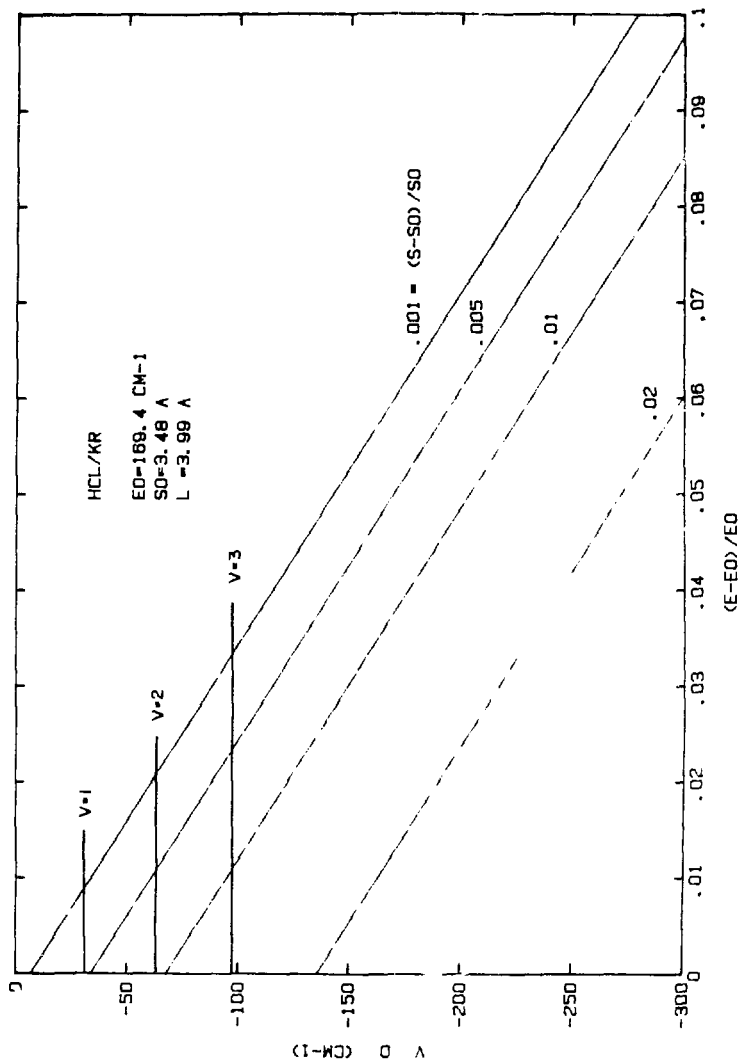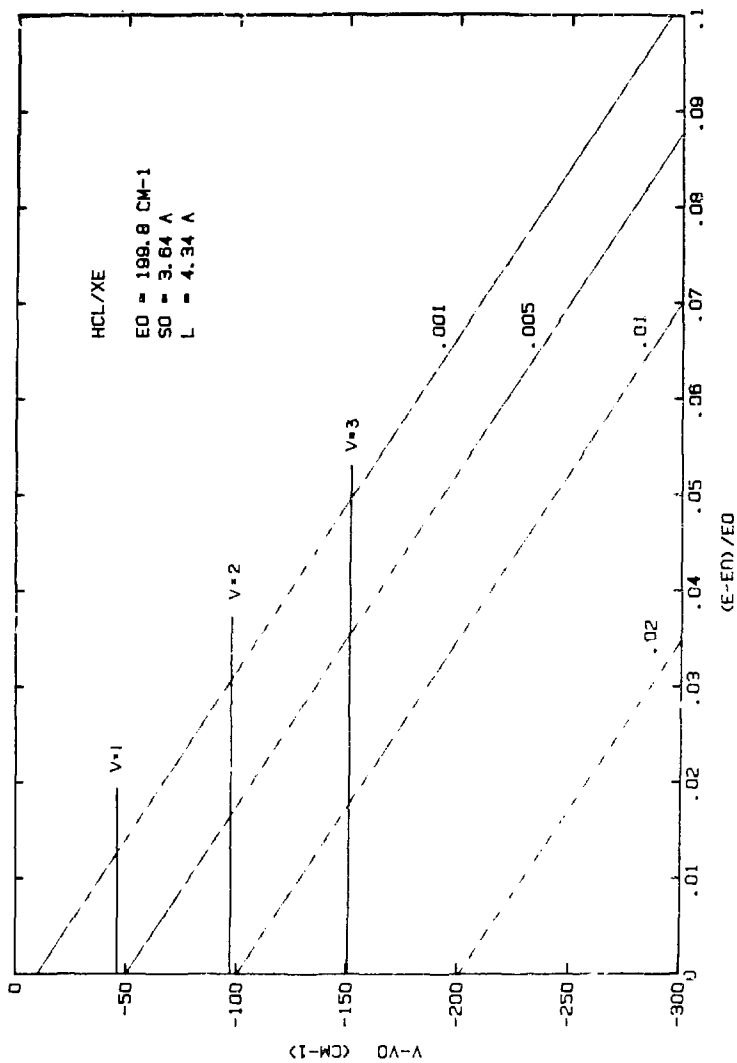
Fig. 21. Lennard-Jones two-body HCl-M potentials.
          Triangles indicate the distance between the
          molecular ci and host atom in a van der Waals
          complex. Circles indicate the nearest neigh-
          bor distance.

LENNARD-JONES POTENTIAL FOR HCL-M

▲ cl-M DISTANCE in vdW COMPLEX

● NEAREST NEIGHBOR DISTANCE

ENERGY (CM-1)

R(HCL-M) ANGSTROMS

171

Fig. 22. General schematic of proposed mechanism. I=
van der Waals complex of HCl-M. Vibrational,
rotational, translational energy levels for
HCl/Ar. Rotational energy levels are calculated
using the gas phase B value, 10.5 cm^{-1}. Trans-
lational energy levels calculated for a particle
in a spherically symmetric potential with walls
described by a Lennard-Jones-Devonshire cell
model.
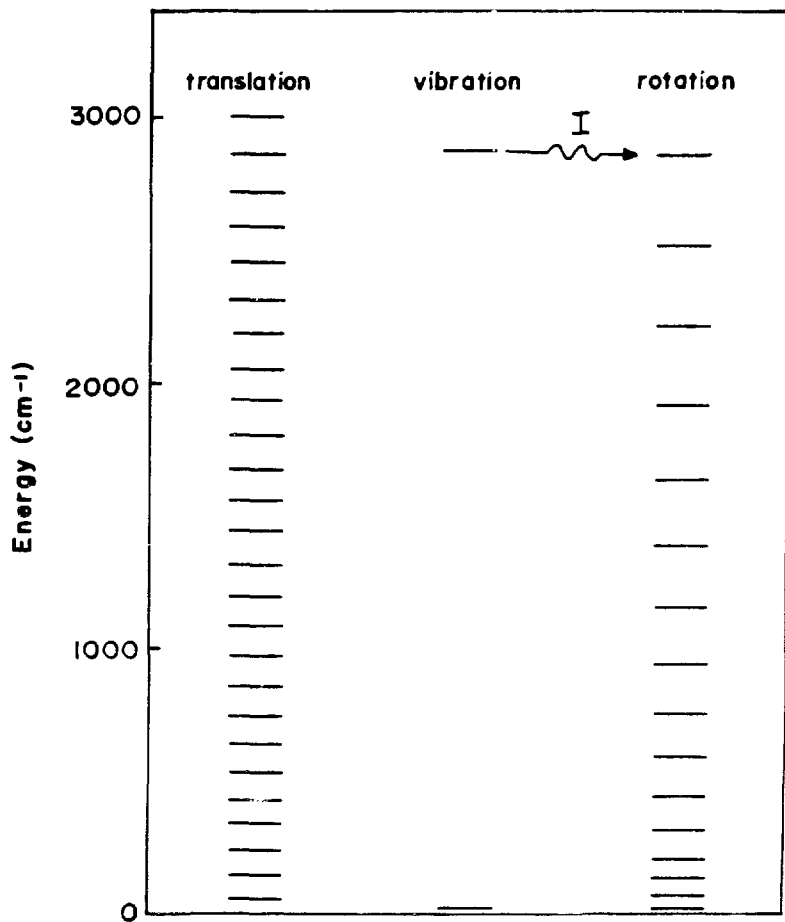
APPENDIX I. DATA COLLECTION PROGRAMS

```
 TYPE DX1:GRAYSC.BAS
10 REM  PROGRAM TO PERFORM EXCITATION SPECTRA ON Q-R DYE LASER
20 LOAD DX0:'OPI.SPS'
30 SIFTO 80,-1
35 LA=0+32
40 TA=0+64
45 SA=0+96
50 PRINT 'STARTING WAVELENGTH';
55 INPUT SX
60 PRINT 'ENDING WAVELENGTH';
65 INPUT EX
66 PRINT 'GRATING ORDER';
67 INPUT GO
68 G=.012/GO
70 PRINT 'INPUT # OF STEPS/INCREMENT(';G;'NM/STEP), MAX=255'
71 PRINT 'INPUT NEGATIVE NUMBER TO SCAN TO SHORTER WAVELENGTH'
75 INPUT CX
78 DELETE FI
79 M=ITP(ABS((SX-EX)/CX/G))
80 PRINT M;'INCREMENTS IN THIS SPECTRUM'
81 DIM FI(M-1)
85 PRINT '# OF TRACES TO BE AVERAGED AT EACH INCREMENT/64 ?'
90 INPUT N
91 X=SX
95 IF CX<0 THEN 115
100 IR=ABS(CX)+256
105 GOTO 120
115 IR=ABS(CX)
120 C1=0
121 C2=0
125 IF IR 64 THEN 155
130 IR=IR-64
140 C1=C1+1
150 GOTO 125
155 IF IR 8 THEN 175
160 IR=IR-8
165 C2=C2+1
170 GOTO 155
175 R$=STR(C1)&STR(C2)&STR(IR)
180 PRINT 'SET FDL GRATING AT STARTING WAVELENGTH'
185 PRINT 'DIGITIZING CRT DEFECTS 2048 TIMES'
190 PUT 'DIG DEF,2048' INTO @0,LA,SA
200 PUT 'READ DEF' INTO @0,LA,SA
210 GOSUB 2000
220 DELETE DF
230 INTEGER DF(SIZ(QO)-1)
240 DF=QO
245 PUT 'MOD TV' INTO @0,LA,SA
250 PRINT 'SET UP 7912 TO ACQUIRE ZERO REF'
260 PRINT 'PRESS ANY KEY WHEN READY'
270 SIFCOM @0,LA,SA,'GTL'
275 DELETE WR
280 WAVEFORM WR IS R(511),SF,HP$,VP$
285 WAIT
290 GOSUB 1000
295 WR=WA
300 GOSUB 1500
310 PRINT 'REFERENCE TRACE, OK?';
315 INPUT ANS
320 IF ASC(ANS)>89 THEN 250
330 PRINT 'SETUP 7912 TO ACQUIRE DATA'
340 PRINT 'PRESS ANY KEY WHEN READY'
350 GOTO 2700
500 K=K+1
510 X=X+CX
515 IF K=SIZ(FI) THEN 710
520 PUTLOC '167772',R$
```
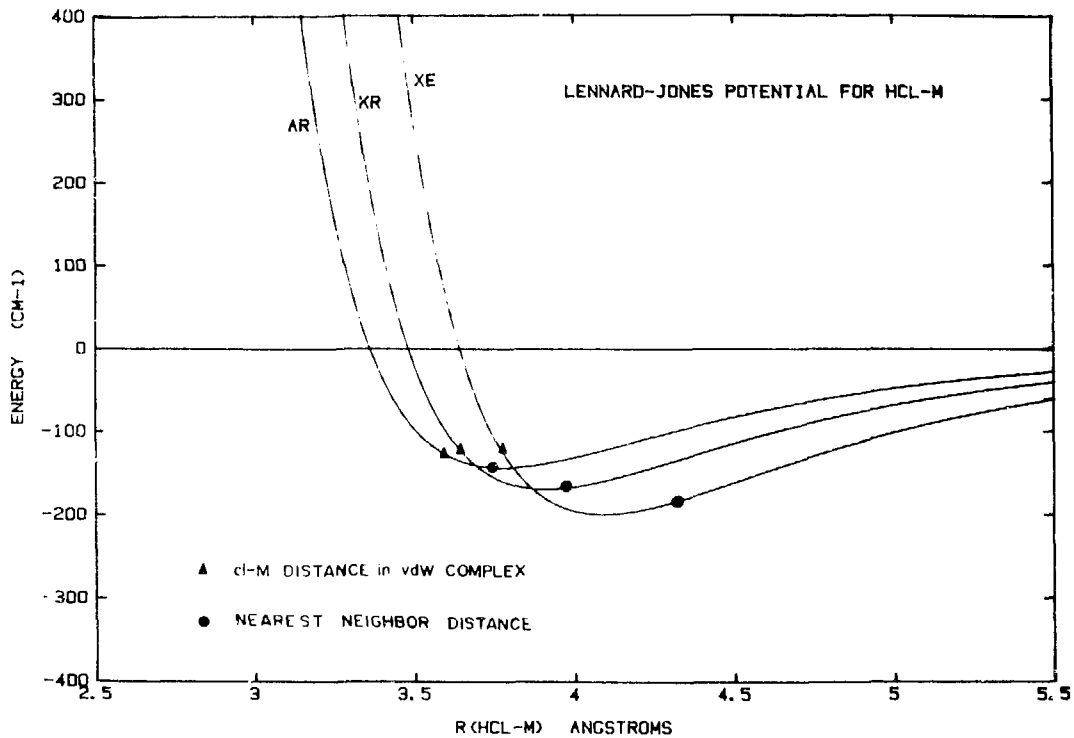
```
520 PUTLOC '167772',R$
530 GOTO 330
600 PRINT 'SET PDL AT STARTING WAVELENGTH, PRESS KEY TO START'
601 DELETE W$
602 WAIT
603 PRINT M$'INCREMENTS OF '$CX$G$'NM'
604 PRINT 'INTENSITY','INCRMT','WAVELENGTH'
605 K=0
606 XC=BX
610 GOSUB 1000
620 WA=WA-WR
625 LOAD DX1:'INT.SPS'
630 INT WA,WA
635 RELEASE 'INT.SPS'
640 FI(K)=A(511)
650 PRINT FI(K),K,XC
660 XC=XC+CX$G
670 K=K+1
680 IF K>SIZ(FI -1 THEN 710
690 PUTLOC '167772',R$
700 GOTO 610
710 PRINT 'SCAN COMPLETE, PRESS KEY FOR EXC. SPECTRUM'
720 WAIT
730 PAGE
740 WAIT 1000
750 GRAPH FI
755 SMOVE 100,750
760 PRINT 'STORE EXC. SPECTRUM?'
770 INPUT AN$
780 IF ASC(AN$)<>89 THEN 850
790 PRINT 'PUT DATA DISKETTE IN DX1:, INPUT FILE NAME'
800 INPUT F$
810 OPEN #1 AS DX1:F$ FOR WRITE
820 WRITE #1,FI,SX,EX
830 CLOSE #1
840 PRINT 'EXC. SPECTRUM STORED AS DX1:'iF$
850 END
1000 REM SUBROUTING TO AVERAGE N$64 TRACES
1005 DELETE WA
1010 WAVEFORM WA IS A(511),SF,HP$,VP$
1020 WA=0
1030 FOR I=1 TO N
1040 PUT 'DIG SA,64' INTO @0,LA,SA
1050 PUT 'READ SA' INTO @0,LA,SA
1060 GOSUB 2000
1070 WA=WA+QQ
1080 NEXT I
1090 NO=N$64
1095 SIFCOM @0,LA,SA,'GTL'
1110 PUT 'MODE TV;HS1?' INTO @0,LA,SA
1115 GET A$ FROM @0,TA,SA
1120 SP=VAL(SEG(A$,5,LEN(A$)-1))/51.2
1125 PUT 'VS1?' INTO @0,LA,SA
1130 GET A$ FROM @0,TA,SA
1135 VA=VAL(SEG(A$,5,LEN(A$)-1))/64
1140 PUT 'HU1?' INTO @0,LA,SA
1145 GET A$ FROM @0,TA,SA
1150 HF$=SEG(A$,5,LEN(A$)-1)
1155 VP$='COUNTS'
1160 RETURN
1500 REM
1510 REM SUBROUTINE TO GRAPH WAVEFORM WA
1520 REM
1620 VIEWPORT 200,800,100,700
1630 SETGR VIEWPORT,NOPLOT
1640 PAGE
1650 WAIT 1000
1660 GRAPH WA
```

```
1665 DISPLAY 1,WA
1670 SMOVE 10,750
1680 PRINT VA;" VOLTS/COUNT"
1700 SMOVE 400,750
1710 PRINT NO;" SWEEPS COMPLETED"
1715 SMOVE 400,730
1720 RETURN
2000 REM
2010 REM   SUBROUTINE TO READ DATA ARRAY
2020 REM
2030 DELETE QQ
2040 IFDTM @0,"UNP"
2050 GET X FROM @0,TA,SA
2060 IF CHR(X)<>"X" THEN STOP
2070 IFDTM @0,"PAK",'HBF"
2080 GET CW FROM @0,TA,SA
2090 CW=(CW-1)/2-1
2100 INTEGER QQ(CW)
2110 GET QQ FROM @0,TA,SA
2120 IFDTM @0,"UNP"
2130 GET X FROM @0,TA,SA
2140 GET X FROM @0,TA,SA
2150 IF CHR(X)<>"I" THEN STOP
2160 RETURN
2400 WA=WS-WR
2410 GOSUB 1500
2420 PRINT "SIG-REF, PRESS ANY KEY ; DISPLAY INTEGRAL"
2430 WAIT
2435 LOAD DX1:"INT.SPS"
2440 INT WA,WA
2445 RELEASE "INT.SPS"
2450 GOSUB 1500
2460 PRINT "INTEGRAL ="#A(511)
2470 PRINT "PRESS ANY KEY FOR MENU"
2475 WAIT
2500 REM SUBROUTINE OPTION
2501 PAGE
2502 WAIT 1000
2510 PRINT "OPTION"
2520 PRINT "   1     SUBTRACT/INT/DISPLAY
2530 PRINT "   2     STORE RAW"
2540 PRINT "   3     CONTINUE
2550 PRINT "   4     AUTOSCAN/STORE INT
2560 PRINT "   5     ABORT
2570 INPUT OP
2610 IF OP=1 THEN 2400
2620 IF OP=2 THEN 3000
2630 IF OP=3 THEN 500
2640 IF OP=4 THEN 600
2650 IF OP=5 THEN 760
2700 SIFCOM @0,LA,SA,"GTL"
2710 WAVEFORM WS IS S(511),SP,HP$,VP$
2720 WAIT
2730 GOSUB 1000
2750 GOSUB 1500
2755 WS=WA
2760 PRINT "SIGNAL TRACE, PRESS ANY KEY FOR MENU"
2765 WAIT
2770 GOTO 2500
3000 PAGE
3010 WAIT 1000
3015 PRINT "PUT DATA DISKETTE INTO DISK DRIVE 1"
3020 PRINT "INPUT NAME OF DATA FILE IN XXXXXX.XXX FORMAT"
3030 INPUT B$
3040 OPEN #1 AS DX1:B$ FOR WRITE
3050 WRITE #1,WS,HP$,NS,VS
3060 CLOSE #1
3070 PRINT "DATA FILE ",B$," HAS BEEN STORED ON  1.
3080 GOTO 2500
```

```
     TYPE DX1:CTXFE2.FOR
C       THIS PROGRAM TRANSFERS DATA FROM 4923 CASSETTE TO
C        DISKETTE.  CASSETTE DATA IN FORMAT OF DIG R/O FROM
C        NORTHERN 575 FOR 1024 CHANNELS.
        LOGICAL#1 STRING(8000)
        REAL#4 EXPDAT(1024)
        INTEGER U,AV
    13 CONTINUE
        TYPE 5
      5 FORMAT (//INPUT 1 FOR 575 DATA'/'       2 FOR 575A DATA'/)
        READ (5,#) NS
        TYPE 1
      1 FORMAT (/' INSERT CASSETTE INTO TEK 4923, REWIND TO DESIRED
       1 FILE'/)
        PAUSE 'PRESS RTN,ENTER DATA STREAM,PRESS ALTMODE'
        CALL BUFRCV(STRING,NUMCHR)
        WRITE(5,100)
    100 FORMAT(// FOLLOWING STREAM IS STORED IN STRING')
        WRITE (5,105) STRING
    105 FORMAT (1X,62A1,1X)
        TYPE 2
      2 FORMAT (1H1,' DECODING STRING')
        GOTO (14,15),NS
     14 DECODE (7938,110,STRING) EXPDAT
    110 FORMAT (1X,128(5X,8(F6.0,1X),1X),1X)
        GOTO 16
     15 DECODE (7938,12  STRING) EXPDAT
    125 FORMAT (2X,128(5X,8(F6.0,1X),1X),1X)
     16 WRITE(5,115)EXPDAT
    115 FORMAT (8(F8.0))
        PAUSE 'PRESS RTN WHEN READY'
        TYPE 3
      3 FORMAT (1H ,' INPUT 1 TO SAVE DATA'/'       2 TO ABORT'/
       1'         3 TO RESTART'/)
        READ (5,#) L
        GOTO (11,12,13),L
     11 DEFINE FILE 2 (1,2054,U,AV)
        WRITE (5,120)
    120 FORMAT (/' INPUT NAME OF DATA FILE AS DX1:XXXYYY.YYY'/)
        CALL ASSIGN (2,NAME,-1,'NEW')
        WRITE (5,150)
    150 FORMAT (/' INPUT TBF,TBS,DELAY IN E7.2 FORMAT'/)
        READ (5,160)  TBF,TBS,DLY
    160 FORMAT (3E7.2)
        WRITE (2'1) (EXPDAT(K), K=1,1024),TBF,TBS,DLY
        CALL CLOSE(2)
        TYPE 4
      4 FORMAT (/' DATA HAS BEEN STORED'/' INPUT 2 FOR ABORT'/
       1'         3 TO RESTART'/)
        READ (5,#) L
        GOTO (11,12,13),L
     12 STOP
        END
```

```
TYPE DX1:CTLOAD.MAC
        .TITLE CASSETTE 4923 FAST ACQUISITION
;
;       BY JAMES LEE CHAO    12/19/79
;
;       HIGH SPEED ASCII TELETYPE LOADER FOR
;       1200 BAUD (+) APPLICATIONS.
;
;       ESCAPE (ALTMODE) SEQUENCES ARE USED AS DELIMITERS
;
;
        .MCALL .PRINT
        .GLOBL BUFRCV

        RCSR =  177560
        RBUF =  177562
        XBUF =  177566

BUFRCV: MOV     #7,XBUF                 ;RING BELL
        MTPS    #200                    ;DISABLE INTERRUPTS
        INC     R5                      ;ADDRESS BUFFER POINTER
        INC     R5
        MOV     (R5)+,R0                ;FETCH BUFFER POINTER
        MOV     R0,R1                   ;STORE BUFFER POINTER
        CLR     RCSR                    ;DISABLE TTY INTERRUPT
1$:     TSTB    RCSR                    ;DATA VALID?
        BPL     1$                      ;BRANCH 1$ IF NOT
        MOVB    RBUF,(R0)               ;YES, STORE IN BUFF
        CMPB    #175,(R0)+              ;ESCAPE KEY?
        BNE     1$                      ;BRANCH 1$ IF NOT
                                        ;YES, STOP
        MOV     #100,@#RCSR             ;REENABLE INTERRUPT
;
        SUB     R1,R0                   ;DETERMINE # CHARACTERS
        DEC     R0                      ;SUBTRACT 1 FROM R0
        MOV     R0,@(R5)                ;SEND BACK NUMCHR
        MTPS    #0                      ;ENABLE INTERRUPTS
        BR      2$
;
;       INTEGRITY TEST
        CMP     #8000.,R0               ;SEE IF OVERFLOW BUFFER REGION
        BGE     2$
        .PRINT  #MSG                    ;PRINT WARNING
2$:     MOV     #7,XBUF                 ;RING BELL
        RTS     PC
MSG:    .ASCIZ  /WARNING, BUFFER OVERFLOW DETECTED/
        .END
```

APPENDIX II. DATA ANALYSIS PROGRAM

```
TYPE DX1:FIT2DT.BAS
10 REM PROGRAM TO FIT THE FUNCTION
20 REM Y=A1*(EXP(-A2*X)-EXP(-A3*X))
30 REM TO A DUAL TIME BASE WAVEFORM OF 512 PTS
40 M=3
50 BF=3
60 C1=.985
70 C2=.906
80 DIM A(M),AU(M),AO(M),D1(M),D2(M),C(M,M),F(M)
90 WAVEFORM Y IS WY(511),SY,HY$,VY$
100 WAVEFORM Z IS WZ(511),SZ,HZ$,VZ$
110 PAGE\WAIT 700
120 PRINT\PRINT\PRINT "PLEASE ENTER FILE NAME OF WAVEFORM TO BE FIT ";
130 INPUT A$
140 S1=1
150 OPEN #1 AS DX1:A$ FOR READ\READ #1,Z\CLOSE #1
160 PAGE\WAIT 700\GRAPH Z \SMOVE 200,750\PRINT A$
170 SMOVE 400,750
180 PRINT "TO, VO ?"
190 GIN BO$,TO,VO
200 SMOVE 600,750
210 PRINT "T1, V1 ?"
220 GIN B1$,T1,V1
230 SMOVE 800,750
240 PRINT "T2, V2 ?"
250 GIN B2$,T2,V2
260 SMOVE 400,720
270 PRINT "T3, V3 ?"
280 GIN B3$,T3,V3
290 IF T1<TO THEN T1=TO
300 I0=ITP(TO/SZ)\IF I0<0 THEN I0=0
310 I1=ITP(T1/SZ)\IF I1<0 THEN I1=0
320 I2=ITP(T2/SZ)\IF I2>511 THEN I2=511
330 I3=ITP(T3/SZ)\IF I3>511 THEN I3=511
340 SMOVE 600,720
350 PRINT "TBS/TBF = ";\INPUT LY
360 SMOVE 600,690
370 PRINT "VO=";VO;\INPUT VO
380 FOR I=0 TO 511\WZ(I)=WZ(I)-VO\NEXT I
390 K=0
400 PAGE\WAIT 700
410 GOTO S1 OF 550,500,500
420 PRINT\PRINT
430 PRINT "DO YOU WANT TO TERMINATE THE FIT OF WAVEFORM NO. ";A$;" ";
440 INPUT S$
450 IF S$="Y" THEN GOTO 2230
460 PRINT\PRINT
470 PRINT "DO YOU WANT TO SET A NEW FIT RANGE ";
480 INPUT S$
490 IF S$="Y" THEN GOTO 160
500 PRINT\PRINT
510 PRINT "DO YOU WANT TO RUN THE PROGRAM USING THE CURRENT PARAMETERS A(I) ";
520 INPUT S$
530 IF S$="Y" THEN GOTO 830
540 GOTO 590
550 IF ABS(V2)<ABS(V3) THEN 590
560 A2=LOG(V2/V3)/(T3-T2)/LY
570 PRINT "FIRST APPROXIMATION FOR THE DECAY PART OF THE CURVE :"
580 PRINT\PRINT "A1 =";V2*EXP(A2*(T2-TO));"        A2 =";A2
590 PRINT\PRINT
600 PRINT "PLEASE ENTER THE INITIAL VALUES FOR THE PARAMETERS A(I)"
610 PRINT
620 A1=0\S1=2
630 FOR I=1 TO M
640 PRINT "A";I;" = ";A(I);"  ";
650 INPUT A(I)
660 A1=A1+A(I)*A(I)
```

```
660 A1=A1+A(I)*A(I)
670 AU(I =A(I)/BF\A0(I)=A(I)*BF
680 IF A(I)>0 THEN GOTO 700
690 A1=A0(I)\A0(I)=AU(I)\AU(I)=A1
700 D2(I)=A(I)
710 NEXT I
720 PRINT\PRINT
730 PRINT "ARE THESE PARAMETERS OK ";
740 INPUT S$
750 IF S$="N" THEN GOTO 590
760 A1=SQR(A1)
770 B2=SQR(M)
780 SF=1/B
790 PRINT\PRINT
800 PRINT "DO YOU WANT A GRAPH WITH THESE PARAMETERS ";
810 INPUT S$
820 IF S$="Y" THEN GOTO 2020
830 PRINT\PRINT
840 PRINT "PLEASE ENTER MAXIMUM NUMBER OF ITERATIONS:  KMAX = ";
850 INPUT KM
860 IF KM=0 THEN GOTO 460
870 PRINT\PRINT
880 PRINT "PLEASE ENTER CONVERGENCE LIMIT:   E = ";
890 INPUT E
900 GOTO S1 OF 910,910,920
910 K=0
920 PAGE\WAIT 700
930 K1=0
940 K=K+1\S1=3
950 K1=K1+1
960 IF K1<11 THEN GOTO 1000
970 K1=0
980 WAIT 10000
990 PAGE\WAIT 700
1000 PRINT " "
1010 PRINT "ITERATION NO. ";K,
1020 GOSUB 2370
1030 FOR I=1 TO M
1040 F(I)=-F(I)
1050 NEXT I
1060 REM GAUSS' ALGORITHM
1070 REM REARRANGEMENT OF LINEAR EQUATION SYSTEM
1080 FOR I=1 TO M-1
1090 D=ABS(C(I,I))
1100 L=I
1110 FOR J=I+1 TO M
1120 IF ABS(C(J,I))<=D THEN 1150
1130 D=ABS(C(J,I))
1140 L=J
1150 NEXT J
1160 IF L=I THEN 1260
1170 FOR J=I TO M
1180 D=C(I,J)
1190 C(I,J)=C(L,J)
1200 C(L,J)=D
1210 NEXT J
1220 D=F(I)
1230 F(I)=F(L)
1240 F(L)=D
1250 REM SUCCESSIVE ELIMINATION OF EQUATIONS
1260 FOR J=I+1 TO M
1270 D=C(J,I)/C(I,I)
1280 FOR L=I+1 TO M
1290 C(J,L)=C(J,L)-D*C(I,L)
1300 NEXT L
1310 F(J)=F(J)-D*F(I)
1320 NEXT J
```

```
1330 NEXT I
1340 REM RESOLVE EQUATION SYSTEM
1350 FOR I=M TO 1 STEP -1
1360 D=0
1370 IF I=M THEN 1410
1380 FOR J=I+1 TO M
1390 D=D+C(I,J)*D1(J)
1400 NEXT J
1410 D1(I)=(F(I)-D)/C(I,I)
1420 NEXT I
1430 REM CONVERGENCE CRITERION
1440 B1=0
1450 FOR I=1 TO M
1460 B1=B1+D1(I)*D1(I)/(A(I)*A(I))
1470 NEXT I
1480 B1=SQR(B1)
1490 IF B1>E THEN 1550
1500 FOR I=1 TO M
1510 A(I)=A(I)+D1(I)
1520 NEXT I
1530 GOTO 1920
1540 REM ANGLE CRITERION
1550 CA=0
1560 FOR I=1 TO M
1570 CA=CA+D1(I)*D2(I)/(A(I)*A(I))
1580 NEXT I
1590 CA=CA/(B1*B2)
1600 IF CA>C1 THEN SF=2*SF
1610 IF CA<C2 THEN SF=SF/2
1620 IF SF>1 THEN SF=1
1630 IF SF<1/1024 THEN SF=1/1024
1640 FOR I=1 TO M
1650 D1(I)=D1(I)*SF
1660 NEXT I
1670 B1=SF*B1
1680 A1=0
1690 FOR I=1 TO M
1700 A(I)=A(I)+D1(I)
1710 REM BOUNDARY CRITERION
1720 IF A(I)<AO(I) THEN GOTO 1760
1730 A(I)=AO(I)
1740 SF=SF/2
1750 PRINT CHR(7);"BOUNCE !",
1760 IF A(I)>AU(I) THEN GOTO 1800
1770 A(I)=AU(I)
1780 SF=SF/2
1790 PRINT CHR(7);"BOUNCE !",
1800 A1=A1+A(I)*A(I)
1810 D2(I)=D1(I)
1820 NEXT I
1830 IF SF<1/1024 THEN SF=1/1024
1840 A1=SQR(A1)
1850 B2=B1
1860 REM OUTPUT OF CURRENT ITERATION
1870 PRINT "SF  =";SF
1880 FOR I=1 TO M
1890 PRINT "A";I;" = ";A(I),
1900 NEXT I
1910 IF K<KM THEN 940
1920 PAGE\WAIT 700
1930 PRINT "AFTER";K;" ITERATIONS :"
1940 PRINT
1950 FOR I=1 TO M\PRINT "A";I;" =";A(I)\NEXT I
1960 PRINT\PRINT\PRINT "T 0 =";T0\PRINT "T 1 =";T1\PRINT "T 2 =";T2
1970 PRINT "T 3 =";T2+(I3-I2)*LY*SZ
1980 PRINT\PRINT\PRINT
1990 PRINT "DO YOU WANT TO GRAPH THE EXPERIMENTAL WAVEFORM AND THE FIT ";
```

```
2000 INPUT S$
2010 IF S$="N" THEN 420
2020 PRINT\PRINT "MOMENT PLEASE ";
2030 FOR I=0 TO I0-1\WY(I)=0\NEXT I
2040 FOR I=I0 TO 51'\GOSUB 2280\NEXT I
2050 SY=SZ\HY$=HZ$\ Y$=VZ$
2060 B$=A$&"F"
2070 PAGE\WAIT 700\GRAPH Z\DISPLAY Y
2080 SMOVE 0,0
2090 FOR I=1 TO M
2100 PRINT "      A";I;"  =";A(I);
2110 NEXT I
2120 SMOVE 450,/80\PRINT B$;
2130 WAIT
2140 GOTO S1 OF 2200,2200,2150
2150 PAGE\WAIT 700
2160 GRAPH Z-Y
2170 SMOVE 130,780
2180 PRINT "RESIDUAL DIFFERENCE:   WAVEFORM  ";A$;"  MINUS  FIT"
2190 WAIT
2200 PAGE\WAIT 700
2210 GOTO S1 OF 500,500,430
2220 RETURN
2230 PRINT\PRINT
2240 PRINT "DO YOU WANT TO FIT ANOTHER WAVEFORM ";
2250 INPUT S$
2260 IF S$="Y" THEN GOTO 120
2270 END
2280 REM FUNCTION TO BE FIT
2290 IF I<I2 THEN 2320
2300 X=T2-TO+LY*SZ*(I-I2)
2310 GOTO 2330
2320 X=SZ*(I-I0)
2330 ONERR NOWARN
2340 WY(I)=A(1)*(EXP(-A(2)*X)-EXP(-A(3)*X))
2350 ONERR
2360 RETURN
2370 REM GRADIENT AND FUNCTIONAL MATRIX
2380 ONERR NOWARN
2390 F=0
2400 C=0
2410 FOR I=I1 TO I3
2420 IF I>I2 THEN 2450
2430 X=(I-I0)*SZ
2440 GOTO 2460
2450 X=T2-TO+LY*SZ*(I-I2)
2460 G=EXP(-A(2)*X)
2470 H=EXP(-A(3)*X)
2480 GH=G-H
2490 P=A(1)*GH
2500 Q=P-WZ(I)
2510 PQ=P+Q
2520 R=A(1)*X
2530 SG=X*G
2540 SH=X*H
2550 F(1)=F(1)+Q*GH
2560 F(2)=F(2)-Q*R*G
2570 F(3)=F(3)+Q*R*H
2580 C(1,1)=C(1,1)+GH*GH
2590 C(1,2)=C(1,2)-PQ*SG
2600 C(1,3)=C(1,3)+PQ*SH
2610 C(2,2)=C(2,2)+(A(1)*G+Q)*R*SG
2620 C(2,3)=C(2,3)-R*R*G*H
2630 C(3,3)=C(3,3)+(A(1)*H-Q)*R*SH
2640 NEXT I
2650 FOR I=2 TO M\FOR J=1 TO I-1\C(I,J)=C(J,I)\NEXT J\NEXT I
2660 ONERR
2670 RETURN
```